IN-07
9932
P. 279

NASA Contractor Report 189106 – Vol-1

Stratified Charge Rotary Engine Critical Technology Enablement Volume I

C.E. Irion and R.E. Mount
Rotary Power International, Inc.
Wood-Ridge, New Jersey

(NASA-CR-189106-Vol-1) STRATIFIED CHARGE ROTARY ENGINE CRITICAL TECHNOLOGY ENABLEMENT, VOLUME 1 Final Report, Feb. 1990 - 1992 (Rotary Power International) 279 p

N94-34231

Unclas

G3/07 0009982

August 1992

Prepared for
Lewis Research Center
Under Contract NAS3–25945



National Aeronautics and
Space Administration

TABLE OF CONTENTS

1.0	Introduction	3
2.0	Executive Summary	7
3.0	Performance	21
	3.1 Research Rig Engine/Critical Component Testing	23
	3.2 New/Improved Computational Fluid Dynamics (CFD) Codes	47
4.0	Critical Technologies	95
	4.1 Advanced Fuel Injection Systems	99
	4.2 Reduced Friction/Improved Tribology/Sealing	151
	4.3 Lightweight/Low Conductivity Parts	189
	4.4 Catalytic Surfaces	201
	4.5 Reference Engine Design	213
5.0	Airframe/Mission Model	243
6.0	Controls System Model	263
7.0	Turbomachinery	271
8.0	University Coordination	295
9.0	Conclusions and Recommendations	299
10.0	Listing of Appendices	303

1.0 INTRODUCTION

1.0 INTRODUCTION

A final report is provided for Contract NAS3-25945. The effort was conducted during the period of Feb 1990 through 1992. This contractual effort was the third phase in an overall consecutive contracts, multi-phase program (1983-1991) addressing Stratified Charge Rotary Engine technology enablement. The NASA long-range, overall program objectives are to establish the technology base for an advanced aircraft engine for the mid 1990's and beyond.

Phase III focused on critical technologies identified in the earlier phases while also further identifying and experimentally addressing the most critical technologies. The overall NASA effort has involved in-house efforts, small industry contracts and University grants in addition to the major industry effort with John Deere Technologies International, Inc. and earlier Curtiss-Wright Corporation.

As previously stated, NASA's objectives are to establish (through basic research) the technology base for a multi fuel, non-gasoline dependent, efficient general aviation aircraft engine. With this technology base, industry can then consider initiation of a full scale development and FAA certification program, thereby bringing the technology to the general aviation industry. Phases I, II and III are reviewed in Reference 1.

During Phase III, significant progress was achieved including:

- o Demonstration of 5 HP/CU IN (230 Kw/ℓ) power density
- o Demonstration of 0.375 Lbs/BHP-HR (228 Grs/Kw-HR) specific fuel consumption at cruise power using Jet-A fuel.
- o Correlation between experimental test results and advanced, high speed computational fluid dynamics.

During the contract, a business decision by Deere & Co. to terminate its involvement with rotary engines and focus on its core agricultural business forced a re-direction of the program and a reduction in scope. The technology advancement was thereby restricted to a degree since some configurations of rotor and rotor housing were defined but not tested. These factors are discussed more fully in Section 2.0.

Reference 1 "NASA's Rotary Engine Technology Enablement Program -- 1983 thorugh 1991", E.A. Willis and J.J. McFadden, SAE 920311, Feb 24-28, 1992

2.0 EXECUTIVE SUMMARY

PRECEDING PAGE BLANK NOT FILMED

2.0 EXECUTIVE SUMMARY

NASA Contract No. NAS3-25945, entitled "Stratified Charge Rotary Engine Critical Technology Enablement-Phase III" was a continuation of research work conducted in prior contracts NAS3-23056 and NAS3-24628 (Phases I and II, respectively).

As summarized in Figure No. l, the NASA primary objectives for this effort are aimed at establishing a technology base through basic research which can ultimately lead to a new, advanced multi-fuel capability engine for the General Aviation industry.

During the Phase III effort, significant progress was achieved in the areas of power density and specific fuel consumption. These achievements are illustrated graphically over the 1988 to 1991 timeframe in Figure Nos. 2 and 3.

o Figure No. 2

Maximum power demonstration (with Jet-A fuel) at 400HP (300Kw) meeting the original goal of 5HP/cu. in. (230Kw/ℓ) and demonstrating long range potential. These tests were conducted with the 1007R single rotor research engine (200HP (150Kw) level) with appropriate correction to the twin rotor, 2013R engine basis.

o Figure No. 3

Brake specific fuel consumption (with Jet-A fuel) at 0.375 Lbs/BHP-Hr (228g/Kwh) at cruise conditions. These tests were conducted on the 1007R single rotor research engine with appropriate correction to the twin rotor, 2013R engine basis and, it should be noted that the testing related to BSFC was independent of testing for power output. That is, no one discrete configuration performed both power and BSFC achievements.

The original goal, based upon completion of the originally planned full Phase III program was 0.355 Lbs/BHP-Hr (216g/Kwh). With the decision by Deere and Company to terminate its involvement with rotary engines (September 1990), a re-planned program was directed by NASA for completion of testing in late 1991 vs. June 1992. In the redirected program, a goal of 0.375 Lbs/BHP-Hr (228g/Kwh) was established for 1991. This goal was achieved.

PRECEDING PAGE BLANK NOT FILMED

PAGE 6 INTENTIONALLY BLANK

2.1 GENERAL BACKGROUND

Early studies directed by NASA Lewis Research Center identified the Stratified Charge Rotary Engine as the leading candidate for an advanced, non-aviation gasoline dependent general aviation engine for the mid-1990's and beyond time- frame, Reference 2. An industry-wide fuels conference conducted by NASA Lewis Research Center noted the ever-increasing limitations in the availability of high octane aviation fuels. An engine capable of operating with Jet-A fuel combined with low cost and high efficiency was deemed necessary. The Stratified Charge Rotary Engine can meet these requirements.

Figure No. 4 depicts the basic operating cycle for the Stratified Charge Rotary Engine, utilizing a pilot injector located in close proximity to a spark plug and a separate main injector.

Figure No. 5 presents an enlarged view of the basic injection-ignition geometry. The pilot injector provides a small quantity of fuel (less than 5% of the total fuel flow) and maintains a constant volume per stroke. A stoichiometric mixture is created at the spark plug-pilot injector region for spark ignitable conditions inde- pendent of fuel type. A wide variation in fuel flow as a function of load demand can then be introduced by the main injector into the pilot initiated combustion. This separation of main injector and pilot injector permits optimization of condi- tions in the light-off zone.

Figure No. 6 presents a general arrangement of a two rotor, Stratified Charge Rotary Aircraft Engine based upon the early NASA studies. This general configuration was used in studies conducted by Cessna and Beech under NASA Lewis Research Center's direction to investigate aircraft performance and operating cost characteristics.

2.2 PHASE I CONTRACT

The Phase I Contract NAS3-23056 was conducted during the period of 1983-1985 initially by Curtiss-Wright Corporation (through January 1984) and subsequently by the Rotary Engine Division of John Deere Technologies International, Inc.

During Phase I, a high performance single rotor research rig engine was designed, procured and check-out tested. The research rig engine was designed for 200BHP (150Kw) at speeds up to 9600RPM and peak internal pressures of up to 1400psi (9653kPa), Reference 3. Basic performance and multi-fuel operation was demonstrated.

2.3 PHASE II CONTRACT

The Phase II Contract NAS3-24628 utilized the research rig engine as a vehicle for examining component technologies. An advanced electronically controlled fuel injection system was procured and tested. Power output of 4.3HP/cu. in. (194Kw/ℓ)

was demonstrated exceeding the contract objectives of 4.0HP/cu. in. (180Kw/ℓ). Subsequently, a revised long range goal of 5HP/cu. in. (230Kw/ℓ) was established as an objective. A fuel consumption at cruise of 0.42 Lbs/BHP-HR (256 Grs/Kw-HR) was achieved on Jet-A, diesel and aviation gasoline fuels. During the Phase II effort, Computational Fluid Dynamics (CFD) studies were utilized extensively at John Deere Technologies International, Inc. and at NASA supporting contractors and grantees to guide the improved fuel economy thrust.

During the Phase II effort, discussions between NASA, JDTI, Inc. and Naval Air Development Center, Warminster, PA resulted in USN participation in the technology enablement efforts. This activity involved preparation of an engine performance model and design of a twin rotor core power section aimed at 250BHP (188Kw) at 66,000 Ft. (20km) altitude.

2.4 PHASE III CONTRACT

The Phase III Contract NAS3-25945 was awarded to JDTI, Inc. on 19 January 1990.

The program was comprised of five major tasks with appropriate sub-tasks. Figure No. 7 presents the Work Breakdown Structure.

A number of industry and university participants were involved in the overall program as reflected in Figure No. 8, Program Team.

The program addressed critical technology enablement in the areas of advanced, higher speed Computational Fluid Dynamics (CFD) analyses via three-dimensional combustion modeling; airframe mission modeling; design of a reference engine; friction reduction; improved tribology/sealing methods; control system modeling; lightweight/low conductivity parts; catalytic surfaces; advanced fuel injection and an extensive effort to define the turbomachinery system including the consideration of turbo-compounding.

As previously noted, with an announcement by Deere and Company in September 1990 of a desire to terminate its involvement with rotary engines, a re-directed program was outlined by NASA LeRC for October 1991 completion of testing (vs. the original contract end date of June 1992). Figure No. 9 presents the guidelines for the re-directed effort.

As outlined in the Section 1.0 Introduction, and in the initial portion of this summary, significant progress was achieved in the power density and efficiency regimes during the Phase III program. However, as noted, the power and BSFC capabilities have not been combined into a single, optimized configuration. Also, as a result of the program curtailment, some designs of rotor, rotor housing, porting variations, lightweight rotors and sealing/tribology were defined and procured but not tested. Further work would be required to conduct this optimization and to demonstrate overall performance (full range operability) in an engine suitable for aircraft

installation (i.e., twin rotor engine with appropriate accessories and controls including turbomachinery).

STRATIFIED CHARGE ROTARY ENGINE
CRITICAL TECHNOLOGY ENABLEMENT

NASA OBJECTIVES

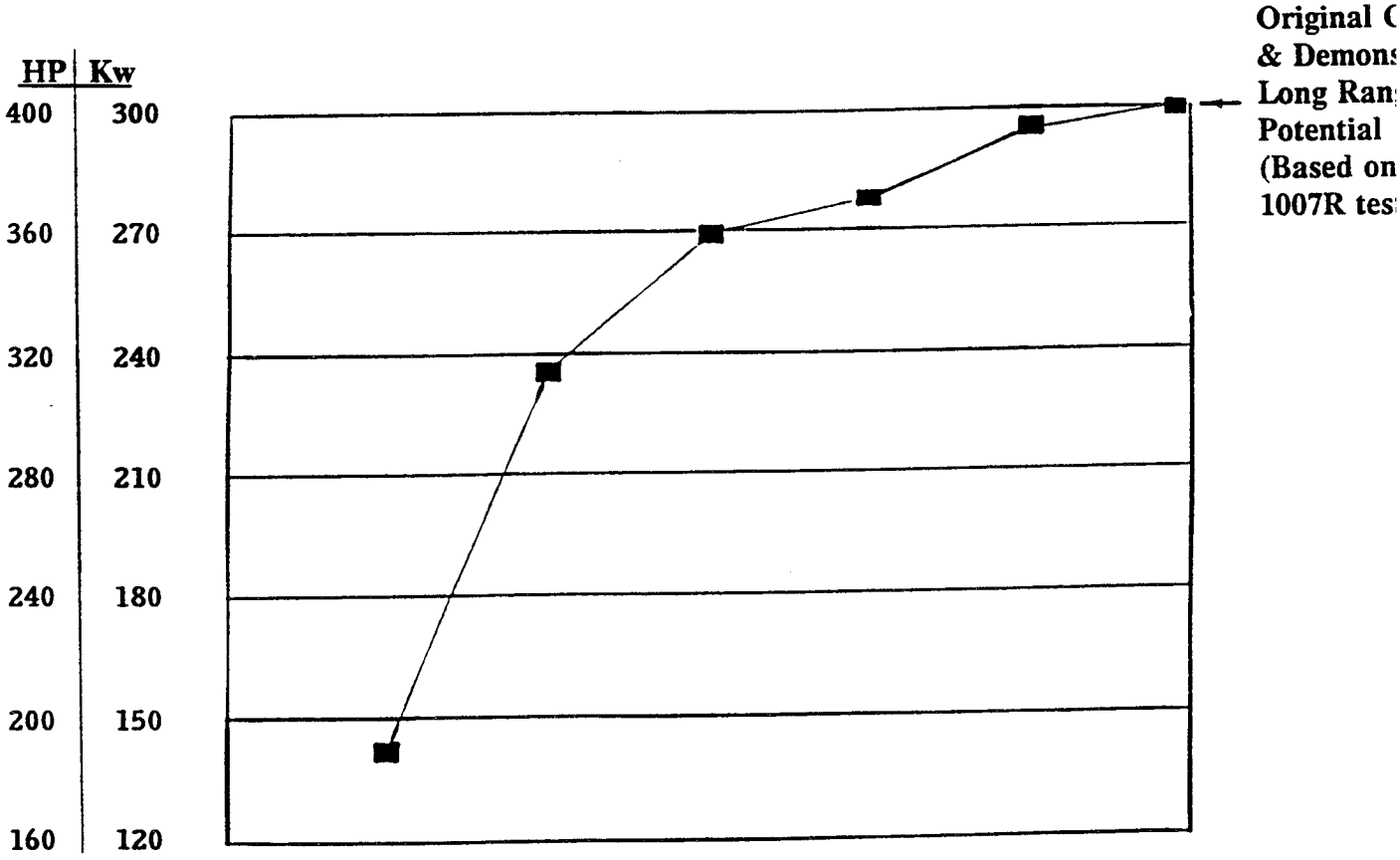
- MULTIFUEL CAPABILITY, INCLUDING CIVIL AND MILITARY JET FUEL AND DF-2
- BRAKE SPECIFIC FUEL CONSUMPTION (BSFC) AT CRUISE OF 0.355 LBS/BHP-HR (216 GRS/Kw-HR)
- POWER DENSITY OF 5 HP/CU. IN. (230 Kw/ℓ)
- TIME BETWEEN OVERHAULS (TBO) OF 2000 HOURS
- ALTITUDE CAPABILITY: UP TO 33,000 FT. (10 KM) CRUISE
- MODULAR DESIGN (FAMILY OF ENGINES CONCEPT)
- MANUFACTURING COST COMPETITIVE WITH COMPARABLE RECIPROCATING ENGINES

Figure No. 1

NASA SCRE CRITICAL TECHNOLOGY ENABLEMENT

MAXIMUM POWER

2013R SCORE 70 ENGINE



PROGRESS WITH TIME - 1988/1991

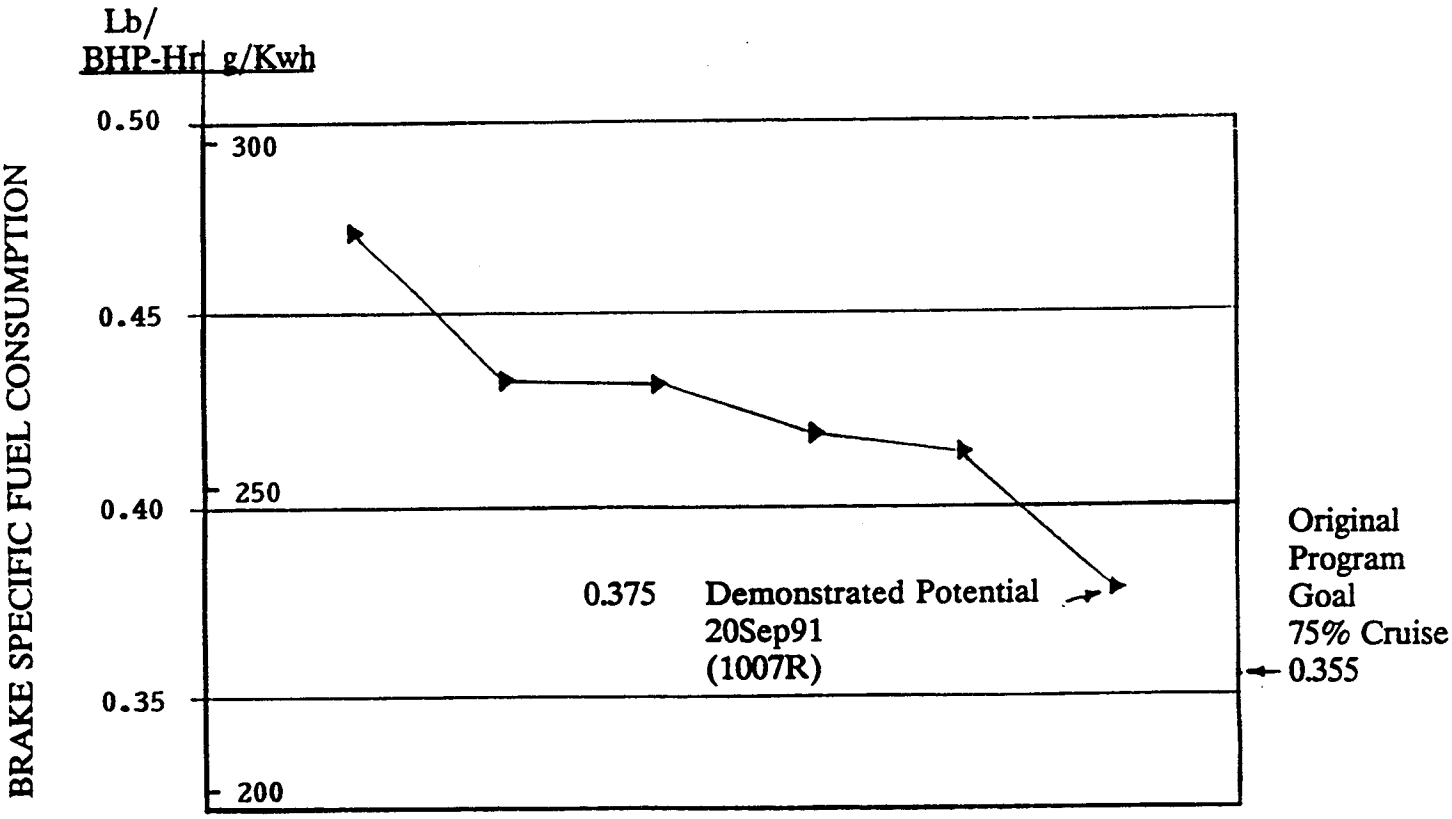
Figure No. 2

ORIGINAL PAGE IS
OF POOR QUALITY

NASA SCRE CRITICAL TECHNOLOGY ENABLEMENT

BRAKE SPECIFIC FUEL CONSUMPTION

2013R SCORE 70 ENGINE



PROGRESS WITH TIME - 1988/1991

Figure No. 3

OPERATING CYCLE, STRATIFIED CHARGE ROTARY ENGINE

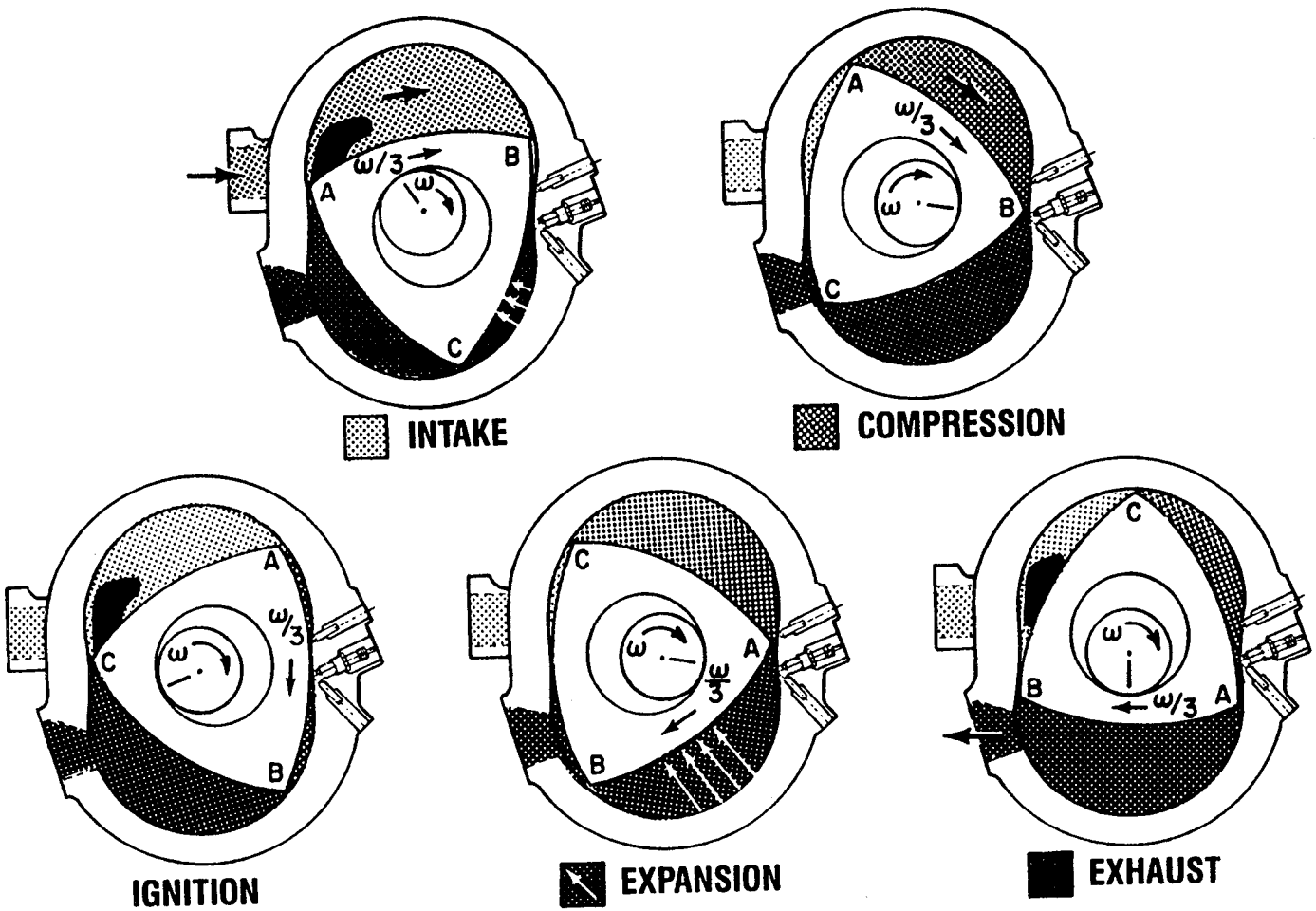


Figure No. 4

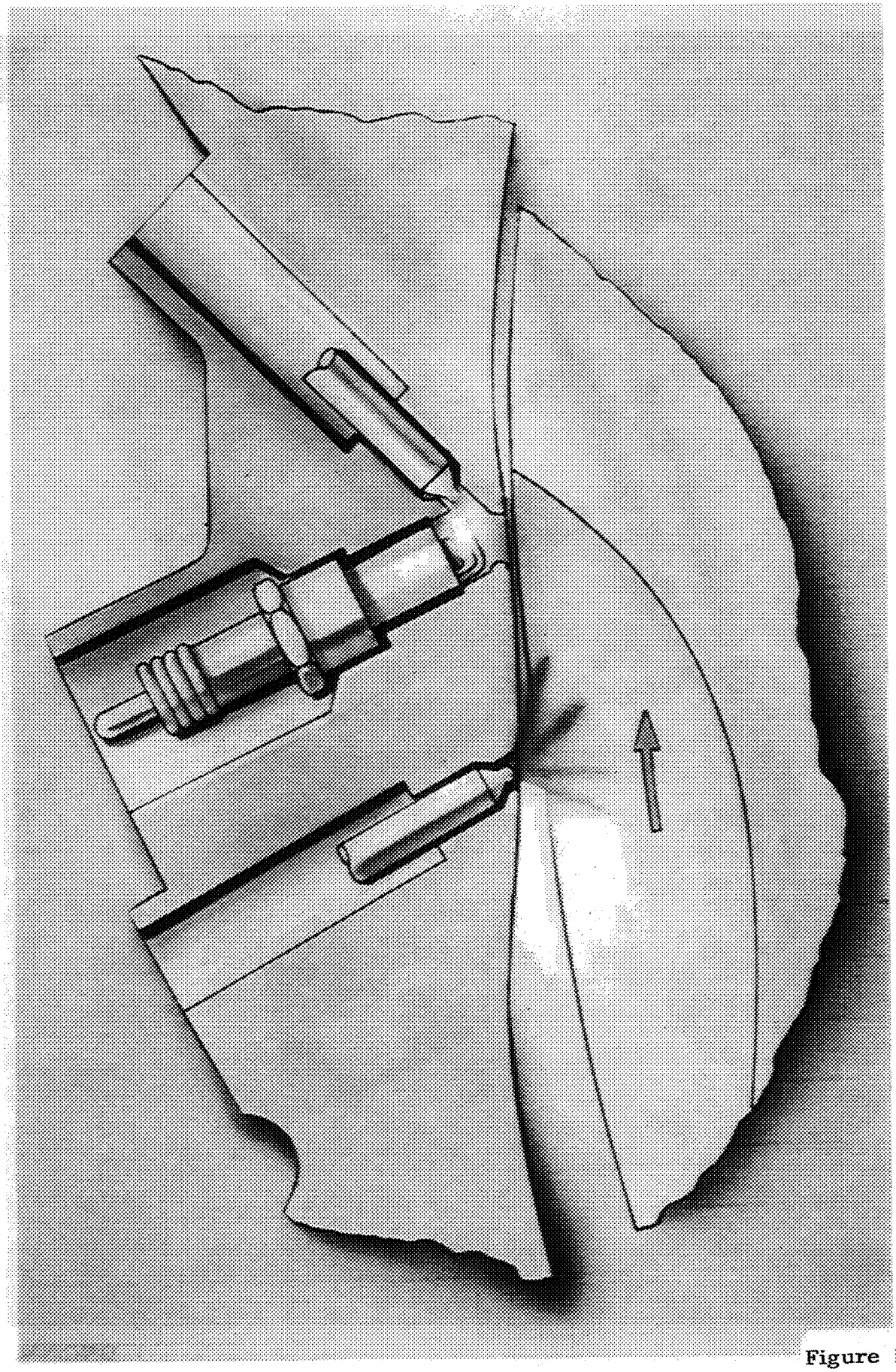
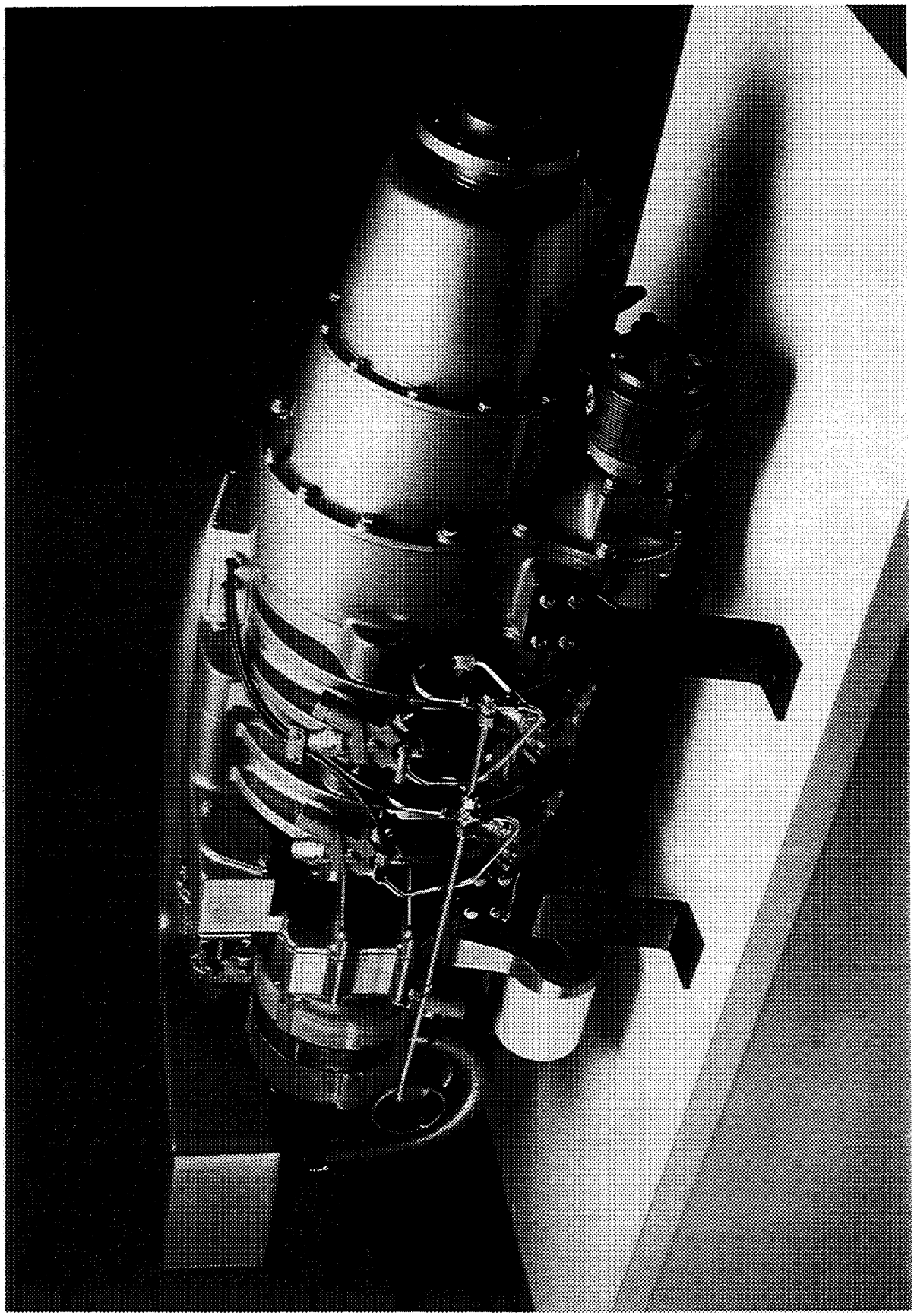


Figure No. 5



2013R AVIATION ENGINE

ORIGINAL PAGE IS
OF POOR QUALITY

Figure No. 6

STRATIFIED CHARGE ROTARY ENGINE CRITICAL TECHNOLOGY ENABLEMENT

WORK BREAKDOWN STRUCTURE

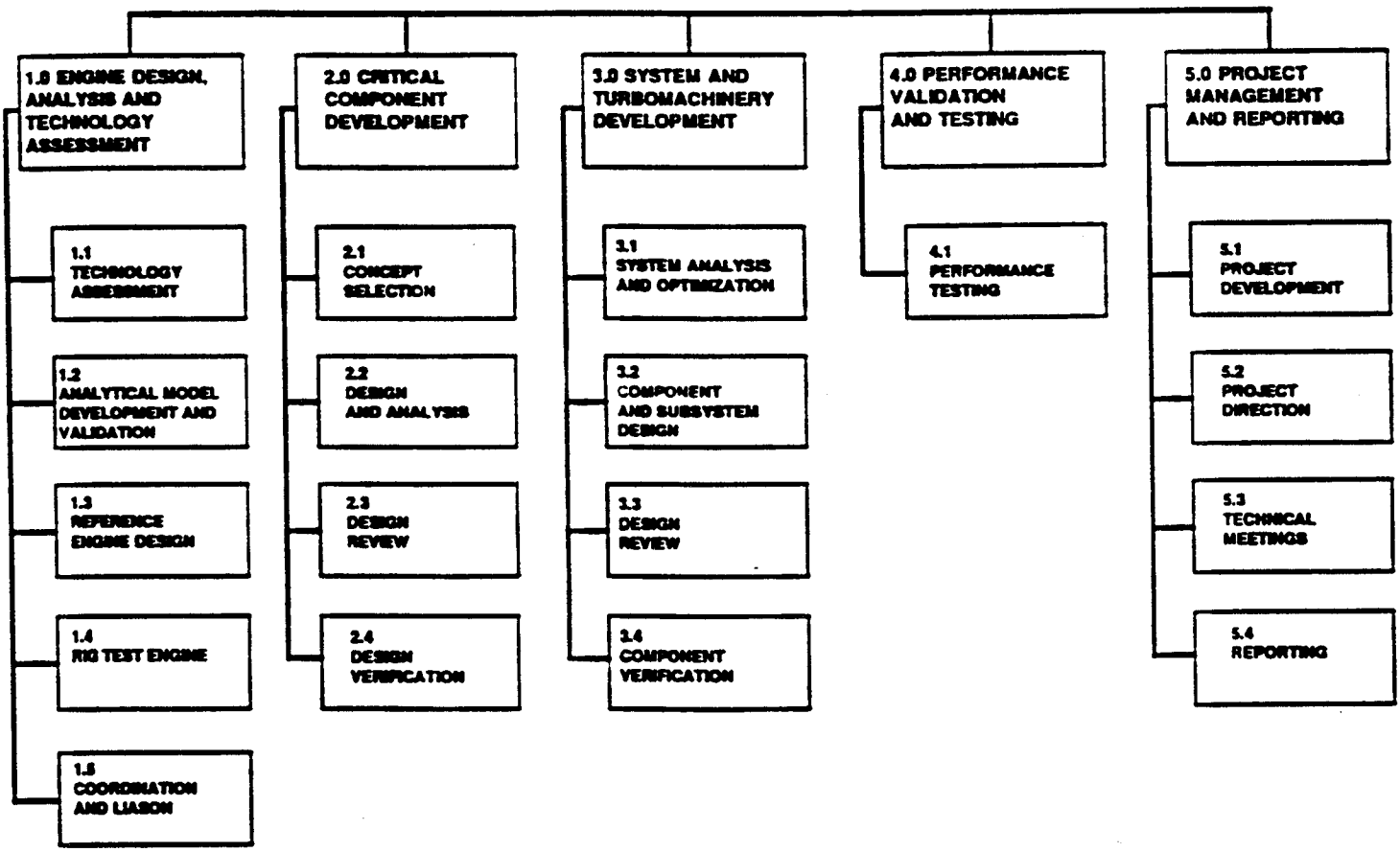
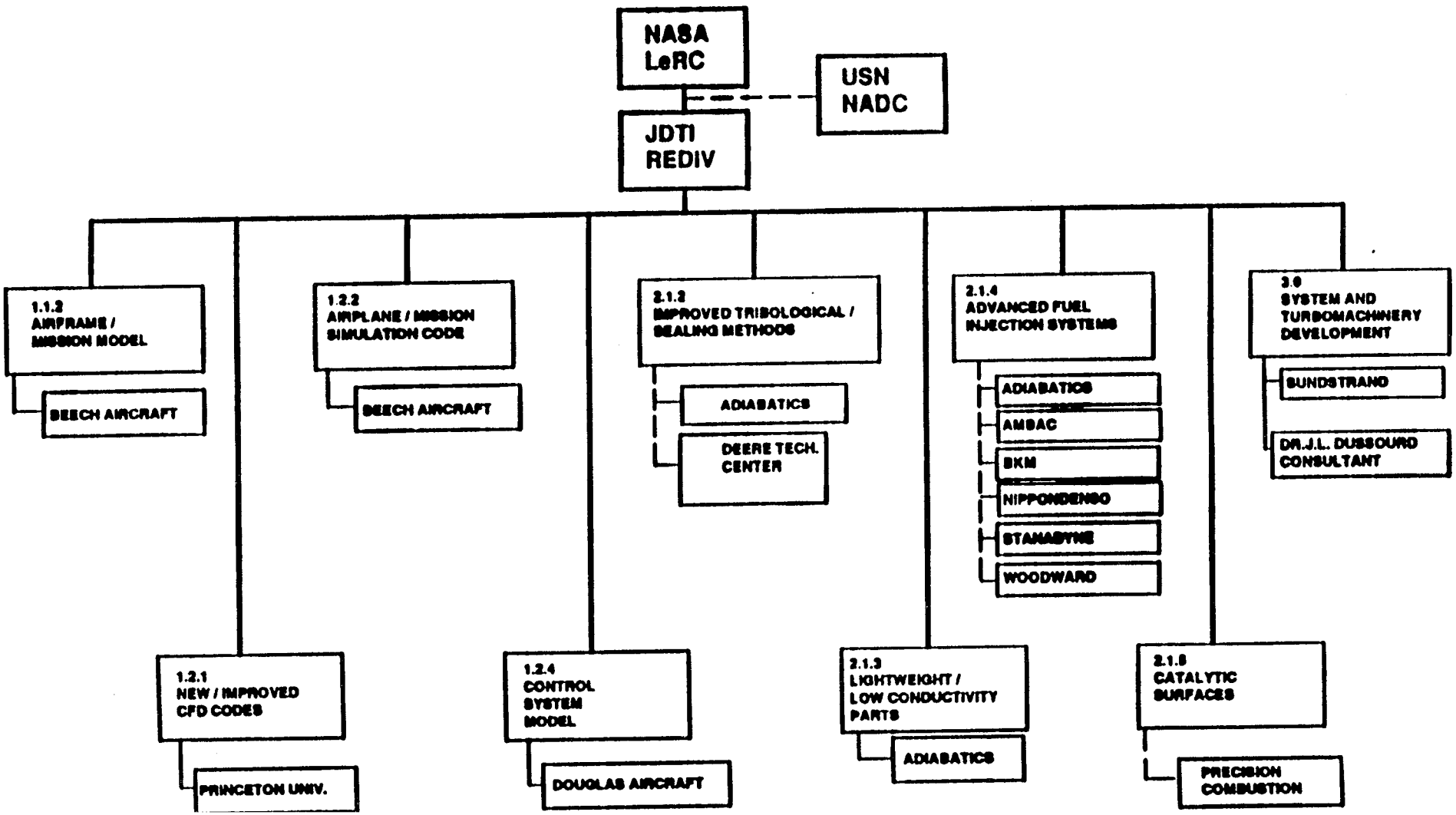


Figure No. 7

STRATIFIED CHARGE ROTARY ENGINE CRITICAL TECHNOLOGY ENABLEMENT

PROGRAM TEAM



STRATIFIED CHARGE ROTARY ENGINE CRITICAL TECHNOLOGY ENABLEMENT

RE-DIRECTION OF CONTRACT NAS3-25945

GUIDELINES

- COMPLETE ALL TESTING BY OCTOBER 31, 1991 (LETTER REQUEST/NASA)
- FOCUS ON BSFC (TARGET 0.375 LBS/BHP-HR (228G/KWH), 1991
- CONTINUE COMBUSTION MODELING CFD WORK
- CONTINUE SINGLE ROTOR RESEARCH RIG ENGINE TESTING
- CONTINUE PERFORMANCE MODELING EFFORT
- CONTINUE LIGHTWEIGHT ROTOR PROCUREMENT
- CONTINUE SELECTED TRIBOLOGY/SEALING/REDUCED FRICTION EFFORTS
- CONTINUE SBIR AND UNIVERSITY COORDINATION
- TERMINATE ALL TURBOMACHINERY WORK
- TERMINATE ALL CONTROLS SYSTEM MODELING WORK
- MODIFIED/REDUCED FUEL INJECTION EFFORT

Figure No. 9

3.0 PERFORMANCE

PRECEDING PAGE BLANK NOT FILMED

3.1 NASA RESEARCH RIG ENGINE/CRITICAL COMPONENT TESTING

PRECEDING PAGE BLANK NOT FILMED

INTRODUCTION

The NASA 1007R Research Rig Engine provides an engine power section test bed for performance and critical component testing. The rig engine design simultaneously provides the capability to perform single rotor engine performance testing while retaining the capability of rapid engine configuration changes. A total of twelve separate rig engine builds were completed for the performance and combustion development portions of the NASA Phase III contract.

The NASA Rig Engine, described by the basic bill of material NJ11950, is comprised of a mainshaft assembly and rotor as the major rotating assemblies. The two end housings encapsulating the rotor housing and two end housing covers are equipped with mainshaft journal bearings to allow the sustained high load and high speed operation required in the rig engine program. A cross section of the rig engine is shown in Figure 1.

The rotor housing assembly includes the fuel delivery and ignition components. Fuel delivery to the combustion chamber is accomplished with two fuel injection nozzles, the main and pilot nozzles. The pilot nozzle, which shares a chamber with the single 12mm spark plug (ignitor), delivers approximately 5% of the total fuel flow at full load. By spraying the pilot fuel charge into the cavity shared with the ignitor fuel ignition is achieved. The ignited fuel then enters the main combustion chamber. The remaining 95% of the fuel flow is injected into the combustion chamber and rotor pocket by the main fuel injection nozzle. The ignited pilot fuel charge then ignites the main fuel charge. The base configuration of the rotor housing fuel injection nozzles, and rotor pocket at top center location are shown in Figure 2.

The rig engine core power section is augmented by a high speed gearbox (reference drawing LS34003) which drives the fuel injection system, and other engine accessories such as turbomachinery and oil metering systems. The fuel injection pump and turbomachinery configurations comprise an element of the power section performance development program.

Engine testing was performed primarily in test cell WX20-6, using an electric dynamometer for engine load and speed control. The engine and dynamometer are linked by a speed reduction gearbox due to dynamometer speed limitations. The driveline configuration is shown in Figure 3.

OBJECTIVE

The Research Rig Engine program focused on three primary goals set forth in the technical proposal:

PRECEDING PAGE BLANK NOT FILMED

PAGE 24 INTENTIONALLY BLANK

1. To demonstrate a brake specific fuel consumption (bsfc) of 0.355 lbs/hp-hr (216 g/kwh) at optimum cruise condition above 50% maximum power. It should be noted that the redirection of the program as discussed in Section 2.0 Executive Summary resulted in a 1991 target of 0.375 lb./hp/hr (228 g/kwh). This target was demonstrated.

2. To demonstrate 200 brake horsepower (bhp) from the 0.7 liter displacement research rig, or a specific power of 5 horsepower per cubic inch. This was achieved.

3. To validate the Computational Fluid Dynamics (CFD) predictions for combustion development and reduction of engine bsfc. Validation and correllation of analytical with experimental results was achieved.

TECHNICAL APPROACH

Demonstrating the specific power of 5 horsepower per cubic inch with the research rig engine focused on the evaluation of fuel injection system and turbocharger configurations to achieve the desired power level.

The goal of achieving a bsfc of 0.375 lbs/hp-hr (228 g/kwh)and validating the CFD predictions were closely linked. Concepts for engine combustion development and reducing engine bsfc were derived from the CFD analysis. The CFD program was used to predict engine hardware modifications which would reduce engine bsfc by improving engine combustion characteristics. A series of discrete engine configuration modifications intended to reduce engine bsfc were then prepared. (Development of the engine configurations from the CFD code is described in the section titled New/Improved CFD Codes.) Rationale for the modifications were drawn both from the CFD predictions and from analysis of prior Phase II engine performance test results.

The engine configurations developed for demonstrating the power density goals and for reduction of engine bsfc were the following:

- Power density demonstration
- Dual orifice pilot
- Dual ignitor rotor housing
- Porting/timing rotor housing
- Catalytic rotor
- Leading rectangular pocket rotor
- Leading standard pocket rotor
- Dual pocket rotor

Numerous engine builds of different configuration engines were involved in the performance and combustion development testing of the NASA rsearch engine. A tabulation of the key engine configuration components segregated by engine test concept is provided in Table I.

RESULTS

POWER DENSITY DEMONSTRATION

Demonstration of the power density goal of 5 hp /cu. in. (230 kw/ℓ) entailed two engine builds of the essentially standard rig engine configuration, and variation on engine accessories to meet the performance goal of 200 (150 kw) horsepower. Fuel injection pumps capable of operating at engine speeds up to 8500 rpm were defined and procured. Numerous high fuel flow capability fuel injection nozzles with non-shadowing fuel sprays were defined and procured. Turbochargers capable of providing the requisite airflows and withstanding turbine inlet temperatures exceeding 1800°F were prepared for the test.

The NASA rig engine demonstrated an observed power output of 197 (148 kw) horsepower at 8400 rpm. When adjusted for friction losses in the test cell speed reduction gearbox the engine output meets the NASA performance goal of 200 horsepower (150kw) from the 0.7 liter rig engine. The power output was obtained at 8400 rpm and an engine load of 227 (1.56 mPa) psi bmep. Engine combustion pressures did not exceed 1200 psi (8.27 mPa).

Further details of engine performance and hardware development are provided in Reference 1.

DUAL ORIFICE PILOT

The dual orifice pilot nozzle demonstrated perhaps the most significant bsfc performance gains of all the configurations tested. Reductions in engine bsfc of 4.3% observed at 4400 rpm were directly attributable to the dual orifice pilot modifications. Minimal hardware changes to the research rig engine design provided the observed performance improvement.

The dual orifice pilot nozzle and the attendant modifications to the pilot/ignitor cavity were tested in two engine builds, engine 0705-1 and engine 0704-10. The two engine configurations differed in significant features such as compression ratio and other performance related features. However, the performance improvements identified in both engines were of equal significance.

The dual orifice pilot engine 0705-1 demonstrated a reduction in observed brake specific fuel consumption of 4.3% at 4400 rpm. The best performance of the 7.5:1 compression ration (CR) engine 0705-1 was at 5500 rpm. An observed bsfc of 0.422 lbs/hp-hr (257 g/kwh) was obtained at 98 brake horsepower (73.5 kw) and 5500 rpm. Detailed engine test performance results for Engine 0705-1 are provided in Reference 2.

Testing of the Dual Orifice Pilot in Engine 0705-1 encountered numerous difficulties in achieving hardware durability. The Dual Orifice Pilot demonstrated superior fuel ignition but suffered poor hardware durability in the first engine build 0705-1. The poor durability was due to high temperatures generated within the pilot-ignitor cavity. The high temperatures caused carboning of the fuel injection nozzle tips and severe erosion of the spark plug electrodes. Analysis of the nozzle durability problem and the development of a fuel system to improve Dual Orifice Pilot performance are provided in Reference 3. The changes developed were incorporated in the second Dual Orifice Pilot Engine 0704-10.

Engine 0704-10 demonstrated the reduction in engine bsfc achieved with a combination of performance related improvements and the dual orifice pilot nozzle. Engine 0704-10 with an 8.5:1 CR demonstrated an observed bsfc of 0.398 lbs/hp-hr (242 g/kwh) at 169 psi (1.164 mPa) bmep and 5500 rpm, or 95 horsepower (71kw). The bsfc performance of Engine 0704-10 meets the September 1991 bsfc goal of 0.375 lbs/hp-hr (228g/kwh) when adjusted for engine friction differences. An observed bsfc below 0.41 lbs/hp-hr (249 g/kwh) was demonstrated between 145 psi (0.999 mPa) and 180 psi (1.24 mPa) bmep at 6000 rpm, or 89-110 hp (67-83 kw). Further details of the engine test results are provided in Reference 4.

DUAL IGNITOR

The dual ignitor engine provided two ignition sources in the combustion chamber. A trailing, trochoid-surface mounted ignitor was incorporated to supplement the standard pilot ignitor. The engine was further modified to provide main nozzle light-off fuel sprays directing fuel to the trochoid ignitor.

The final configuration of the dual ignitor engine, tested in Engine 0704-8, allowed successful demonstration of a dominant trochoid ignitor combustion contribution. A 7.5% reduction in observed bsfc was provided by the trochoid ignitor at 130 psi bmep (0.896 mPa) and 6000 rpm, or 80 bhp (60kw). The best observed bsfc was 0.455 lbs/hp-hr (277 g/kwh) at 131 psi (0.902 mPa) bmep and 6000 rpm. Further discussion of the performance results for the four dual ignitor engines is provided in References 5 and 6.

Additional reductions in bsfc at higher loads were limited in the dual ignitor engine by the onset of combustion instability. Combustion analysis of engine operation with the dual igniter was undertaken to further examine the combustion instability phenomena observed. Three references discussed in the following paragraphs examine different aspects of the observed instability.

The first analysis effort focused on identifying the cause and the effect of the combustion instability observed in the dual igniter engine. The instability is attributed to auto ignition of the Jet-A fuel being burned. The auto ignition of the fuel is attributed to the rapid combustion pressure rise generated by the dual igniter engine configuration. Combustion cycle analysis indicated that the combustion instability and spikes did not detract from the

engine work output. The combustion instability and spikes were concluded to be detrimental primarily due to the high variability in engine output and peak combustion pressures generated. The rapid combustion pressure rise in particular appeared to affect the apex seal sealing effectiveness. The complete analysis is provided in Reference 7.

The second analysis effort compared the effectiveness of fuel lightoff for two configurations of trochoid mounted spark plugs; and the effect of increasing engine intake air temperatures on engine combustion. The analysis concluded that an electrode type spark plug resulted in far less cycle to cycle variability (indicated by misfires) than the surface gap type spark plug. The increased intake air temperature appears to have resulted in faster combustion, somewhat higher peak pressures and greater instability in the combustion pressure traces. The analysis is provided in further detail in Reference 8.

The third analysis examined in detail the effect of fuel octane rating on the combustion instability observed in the dual igniter engines. The combustion instability was effectively eliminated while operating on high octane fuel (gasoline). This demonstration appeared to confirm the hypothesis that auto ignition of the Jet A fuel was responsible for the combustion instability. Further discussion is provided in Reference 9.

PORTING/TIMING ENGINE

The Porting and Timing engine was designed to evaluate the effects of variable intake port flow area and variable intake opening and closing times on engine performance. The standard rotor housing and the variable porting/timing rotor housing are shown in Figure 4. Inserts (not shown) were designed for the Porting/Timing rotor housing which provided selective opening and closing times and port flow areas within the enlarged port areas evident in Figure 4. The rotor housing for Engine 0704-9 was originally intended to provide both variable intake and variable exhaust ports. However, errors in the rotor housing casting process prevented incorporating the variable exhaust ports. A salvage rework provided an exhaust port area enlarged by 33% compared to the standard exhaust port. The Porting/Timing rotor Housing shown in Figure 4 was completed after testing of Engine 0704-9.

The rotor housing tested in Engine 0704-9 provided three variations of intake flow areas and intake port opening/closing timings. The three intake port variants provided were the standard rig engine flow area and opening/closing timings, a 42% larger intake port with early opening and late closing, and a standard flow area with late opening and late closing timings.

All three variants were tested with the enlarged exhaust port described above. New intake and exhaust manifolds were provided to match the enlarged intake and exhaust flow areas.

Performance testing of the porting/timing Engine 0704-9 indicates that the standard intake port area and timing provides the lowest engine bsfc, and that a 3% reduction in bsfc was attributable to the enlarged exhaust port flow area. The Engine 0704-9 demonstrated an observed bsfc of 0.447 lbs/hp-hr (272 g/kwh) at 6000 rpm and 180 psi (1.24 mPa) bmep. The bsfc performance of the three intake ports appeared to converge at high engine loads.

The clear reduction in bsfc demonstrated in Engine 0704-9 indicates the need to further investigate the effects of intake and exhaust porting and timing. Comprehensive performance testing of the variable intake and exhaust port rotor housing is strongly recommended. More detailed discussion of the performance results of Engine 0704-9 are provided in Reference 10.

CATALYTIC ROTOR

The catalytic rotor engine test was intended to establish the potential for catalytic surfaces to improve combustion rates and improve engine operating efficiency. The catalytic coating is intended to promote combustion of fuel in close proximity to the rotor face and pocket. The catalytic coating, by promoting the oxidation process, is intended to reduce fuel ignition delay and promote combustion stability at lower temperatures than would be required for non-catalytic surfaces.

The catalytic coating is a proprietary coating developed and applied by Precision Combustion (reference SAE paper 890326). The catalytic coating was applied over a thermal barrier coating intended to increase the rotor surface temperature. The thermal barrier coating was tested in the NASA Phase II engine test program.

The catalytic rotor engine 0705-2 demonstrated a best observed bsfc of 0.427 lbs/hp-hr (260 g/Kwh) at 165 psi (1.137 mPa) bmep and 6000 rpm. Engine output is 100 bhp (75 kw) or 50% cruise power at the above speed and load.

A reduction in engine brake specific fuel consumption due to the catalytic coating applied to the rotor flank and pocket was not observed. The catalytic rotor engine performance was essentially identical to the thermal barrier rotor without the catalytic coating. Additional performance results are described in detail in Reference 11.

ROTOR COMBUSTION POCKET DEVELOPMENT

The CFD analysis produced four proposed variants of rotor combustion pocket shapes. The combustion pocket shape changes were predicted by CFD to increase gas recirculation within the rotor pocket during the compression and combustion phases of the engine cycle. Increased gas circulation was predicted to improve fuel-air mixing and to increase combustion rates.

The different pocket shapes proposed are shown in Figures 5 and 6. Figure 5 shows cross-sections of the standard pocket, the leading standard pocket, the leading re-entrant pocket and the leading rectangular pocket. The re-entrant pocket was not produced due to concerns for hardware durability from the formation of 'hot spots' at the thin cross-sectional areas created by the re-entrant shape. The leading rectangular pocket was a compromise design intended to emulate the characteristic behavior of a 'true' re-entrant pocket.

Figure 6 is a photograph of the four rotor pocket configurations which have been manufactured. Three of the pocket designs, the standard pocket, the leading standard pocket, and the leading rectangular pocket, were engine tested. The fourth, the dual pocket design, was not engine tested due to the foreshortening of the NASA contract effort.

Details of the hardware configurations and engine test results for the three combustion development rotor pockets are provided in the following sections.

LEADING RECTANGULAR POCKET ROTOR

The leading rectangular pocket rotor was predicted by CFD to increase gas recirculation and diffusivity and hence improve fuel and air mixing in the rotor pocket. Both the recirculation and diffusivity are to be driven by the squish flow from the trailing flank of the rotor. The rotor was modified to relocate the pocket to the leading flank of the rotor. The rotor pocket is roughly rectangular in shape as shown in Figure 5. To accommodate the relocated rotor pocket, an After Top Center (ATC) Main rotor housing was developed. The ATC Main housing featured relocated main and pilot fuel injectors and ignitor to correspond to the location of the leading rectangular rotor pocket when the engine is at top center. The location of the injectors and ignitors was derived from initial optimization studies using CFD. The 8.5.1 compression ratio Leading Rectangular (LR) pocket rotor and ATC Main rotor housing were tested in Engine 0707-1.

Performance of the LR pocket rotor demonstrated a slight penalty in observed bsfc but was limited in engine load capability by a pressure wave phenomena. An observed bsfc of 0.481 lbs/hp-hr (293 g/kwr) was demonstrated at 115 psi (0.792 mPa) bmep and 4400 rpm. This bsfc indicates a 1.5% increase compared to the 'standard' NASA rig engine configuration. Engine load capability was limited due to the presence of a pressure wave in the combustion chamber which generated conditions exceeding hardware design pressure limits.

Operating at 115 psi (0.792 mPa) bmep and 4400 rpm the combustion pressure in Engine 0707-1 was 44% higher than the comparable standard rig engine. A combustion pressure of 1600 psi (11.02 mPa) was observed at 6000 rpm and 112 psi (0.772 mPa) bmep. Detailed performance test results for the leading rectangular pocket rotor engine 0707-1 are provided in Reference 12.

The pressure wave phenomena was approximated using additional CFD analysis. The additional analysis indicates the pressure wave results from the rapid combustion generated by the leading rectangular pocket rotor. Further details of the analysis are provided in Reference 13. Additional study is required before final conclusions can be provided.

LEADING STANDARD POCKET ROTOR

The leading standard pocket rotor was predicted by CFD to increase diffusivity and hence fuel and air mixing in the rotor pocket. The diffusivity is predicted by CFD to be driven by the squish flow from the trailing flank of the rotor.

The leading standard pocket rotor provides a pocket shape identical to the standard rotor pocket relocated towards the leading flank. The leading standard pocket rotor was tested with the ATC Main rotor housing developed for use with the leading rectangular pocket rotor. The 8.5:1 compression ratio leading standard pocket rotor and ATC Main rotor housing were tested in Engine 0707-2.

The leading standard pocket rotor demonstrated an observed brake specific fuel consumption of 0.439 lbs/hp-hr (267 g/kwh) at 204 psi (1.405 mPa) bmep and 4400 rpm. A limited test duration of nine hours did not allow sufficient time for extensive performance optimization.

Performance of the leading standard rotor pocket indicated a 1.5% increase in observed bsfc relative to the standard location pocket rotor at 160 psi (1.102 mPa) bmep and 4400 rpm.

The leading standard pocket rotor engine 0707-2 demonstrated significant difficulty operating at speeds above 4400 rpm. A high frequency of engine misfire at engine speeds above 4400 rpm was encountered. The high rate of misfires prevented obtaining acceptable performance at speeds above 4400 rpm. An engine modification to reduce the misfire rate, such as the dual orifice pilot would appear to be required.

Additional details of performance tests of the leading standard pocket rotor engine 0707-2 are provided in Reference 14.

DUAL POCKET ROTOR (AND ROTOR HOUSING)

The dual pocket rotor design features two rotor pockets located symmetrically around the rotor flank center. The two pockets form separate combustion "chambers" for each of the trochoid lobes located on opposite sides of the rotor housing minor axis. Each pocket provides a separate main fuel injection nozzle and ignitor. The separate main fuel nozzles provide independent fuel injection timing and fuel flow for the two rotor pockets. The two rotor pockets are designed with equal displacements and yield an overall engine compression ratio of 8.4:1.

Two configurations of rotor housings were designed for use with the dual pocket rotor. The first design provided a single main fuel injection nozzle and trochoid surface mounted ignitor for each rotor pocket. The second, and preferred configuration, provides a separate pilot nozzle and pilot/ignitor cavity in addition to the main fuel injection nozzle for each rotor pocket. The pilot nozzle and ignitor cavity were added to address concerns regarding possible difficulties establishing stable fuel ignition and combustion in each pocket without the standard pilot ignition capability.

The dual pocket rotor and the first rotor housing with the main nozzle/ignitor configuration are available in machined hardware for testing. The second rotor housing featuring the pilot nozzle ignitor combination for fuel ignition is available in casting form but requires finish machining before testing could proceed.

CONCLUSIONS

1. The NASA single rotor rig engine demonstrated the power density of five horsepower per cubic inch (230 kw/ℓ), or 200 horsepower (150 kw) from 0.7 liter displacement, as set forth in the NASA Phase III technical proposal.

2. The NASA single rotor rig engine demonstrated the September 1991 brake specific fuel consumption goal (bsfc) of 0.375 lbs/hp-hr (228 g/kwr) when adjusted for engine friction differences. Achievement of the bsfc goal is based upon an observed bsfc of 0.398 lbs/hp-hr (242 g/kwr) at 169 psi (1.164 mPa) brake mean effective pressure (bmep) and 5500 rpm demonstrated in Engine 0704-10.

3. The NASA single rotor rig Engine 0704-10 demonstrated an observed bsfc below 0.41 lbs/hp-hr (249 g/kwr) between 145 psi (0.999) mPa) and 180 psi (1.240 mPa) bmep at 6000 rpm. An equivalent expression of this performance is an observed bsfc of 0.41 lbs/hp-hr or better between 45% and 55% cruise powers.

4. The configuration of Engine 0704-10 appears to provide the best near term configuration of the NASA rig engine. The significant features of Engine 0704-10 include the modified dual orifice pilot nozzle and pilot/ignitor cavity, an 8.4:1 compression ratio, and an enlarged exhaust port.

5. The dual orifice pilot nozzle configuration appears to provide the capability to extend the successful lean operating limit of the SCORE 70 engine.

6. The Nippondenso/Ambac type 9mm dual orifice pilot nozzles, used in Engine 0704-10, appear to provide superior performance and durability characteristics than the Stanadyne 5mm dual orifice pilot nozzles used in Engine 0705-1.

7. The dual ignitor engine configuration appears to require a redesign to overcome the combustion instability observed while operating on Jet A fuel. The redesign should address the load limitation encountered when operating with lightoff spray angles greater than 75 degrees. Spray angles greater than 75 degrees were required to obtain a trochoid ignitor combustion contribution. A complete reconfiguration to reverse lightoff spray direction and to relocate the trochoid ignitor correspondingly may be required. Additional CFD analysis may indicate the best development direction for the dual ignitor concept.

8. The leading rectangular pocket rotor appears to provide a significant increase in the engine combustion rate. Additional development is required to eliminate or mitigate the combustion pressure wave observed and to establish optimum engine configuration and performance.

9. The leading standard pocket rotor demonstrated a slight performance penalty relative to the standard rig engine during the limited amount of testing completed. Optimization of nozzle spray patterns and/or nozzle locations may be required to achieve the performance potential of the leading standard pocket rotor. Fuel lightoff performance problems at engine speeds above 4500 rpm must be addressed before further engine testing can fully explore the leading standard pocket rotor performance potential.

RECOMMENDATIONS

1. The NASA reference engine design should incorporate the major performance design features of the rig Engine 0704-10. The significant features include the modified pilot ignitor cavity, the 9mm pilot nozzle tips, an 8.4:1 compression ratio, and an enlarged exhaust port. Further performance testing is strongly recommended to examine engine performance at 7250 rpm and above, and to more clearly identify optimum engine F:A ratios, turbo-charger requirements, nozzle spray configurations, and fuel injection pump configuration.

2. The porting/timing engine configuration (reference decision number 12875NJ) should be tested. The effects of exhaust port opening and closing, and exhaust port flow area were demonstrated in Engine 0704-10 to be critical to engine performance. Test and analysis of the effects of exhaust port opening and closing, exhaust port flow area, and the interaction of these changes with the same variables of intake porting and timing, may provide additional performance improvements. Analysis and testing of intake plenum volumes and intake manifold tract lengths may be required to accommodate the broad range of engine speed operation encountered in this engine application.

3. Further development of the leading rectangular pocket rotor should work to eliminate the combustion pressure wave phenomena and to optimize the engine configuration. Modifications to the pressure relief slot appear to be required to prevent propagation of the combustion pressure to the trailing flank. Concepts which prevent this propagation should be analyzed and tested. Other alternatives include modifying the pocket to extend across the minor axis (by ramping the pocket trailing wall) to relieve pressure in the trailing flank. Optimization of the engine configuration should also address identifying nozzle spray configurations optimized for the rectangular pocket, and establishing reliable pilot fuel lightoff. The dual orifice pilot configuration is recommended as the best available means of providing this improvement.

4. The leading standard pocket rotor requires additional testing to identify avenues of continued development. Modifications to address the pilot lightoff difficulties

encountered with this configuration are required. The dual orifice pilot appears to be a likely method of improving the fuel lightoff performance.

LIST OF REFERENCES

1. "Power Density Performance Demonstration, Engine 0704-4 and 0704-5", C.R. Shoemaker, December 1991

2. "Performance Test of Dual Orifice Pilot Injection Nozzle, Engine 0705-1", C.R. Shoemaker, 5 March 1991

3. "Investigation into Changes in Engine Light-Off Performance using the 2 Orifice "Rabbit Ear" Pilot Configuration", A. Meyer, 30 Apr. 1991

4. "Demonstration of BSFC Capability for NASA 1007R Rig Engine, Engine 0704-10", C.R. Shoemaker, 20 November 1991

5. "Performance Test of Modified Dual Ignitor Engine, Engine Builds 0704-7, 0704-8 and 0705-3", C.R. Shoemaker, 4 October 1991

6. "Performance Test of Modified Dual Ignitor Engine, Engine Builds 0704-7, 0704-8, and 0705-3", C.R. Shoemaker, 4 October 1991

7. "Analysis of Experimental Pressure Traces from the Dual Ignitor Engine (Engine Build #0704-8)", J. Abraham and P. Epstein, 26 July 1991

8. Memo; J. Abraham to C. Irion, Subject: "Analysis of Experimental Pressure Traces from the Dual Ignitor Engine Build #070503 and Build #0704-8", 6 Aug. 91.

9. Memo; J. Abraham T. C. Irion, Subject: "Analysis of Experimental Pressure Traces from the Dual Igniter Engine #0705-3", 27 Aug. 91.

10. "Performance Test of Porting/Timing Engine 0704-9", A.E. Meyer, 4 December 1991

11. "Engine 0705-2, Performance Test of Catalytic Surface, Thermal Barrier Rotor", C.R. Shoemaker, 15 July 1991

12. "Performance Test of Leading Rectangular Pocket Rotor, Engine 0707-1", C.R. Shoemaker, 26 November 1991

13. Memo: J. Abraham to C. Shoemaker, Subject: "Correlation of Experimental and Analytical Results of Leading Rectangular Pocket", 6 Dec 1991

14. "Performance Test of Leading Standard Pocket Rotor, Engine 0707-2", C.R. Shoemaker and P. Dimpelfeld, 1 December 1991.

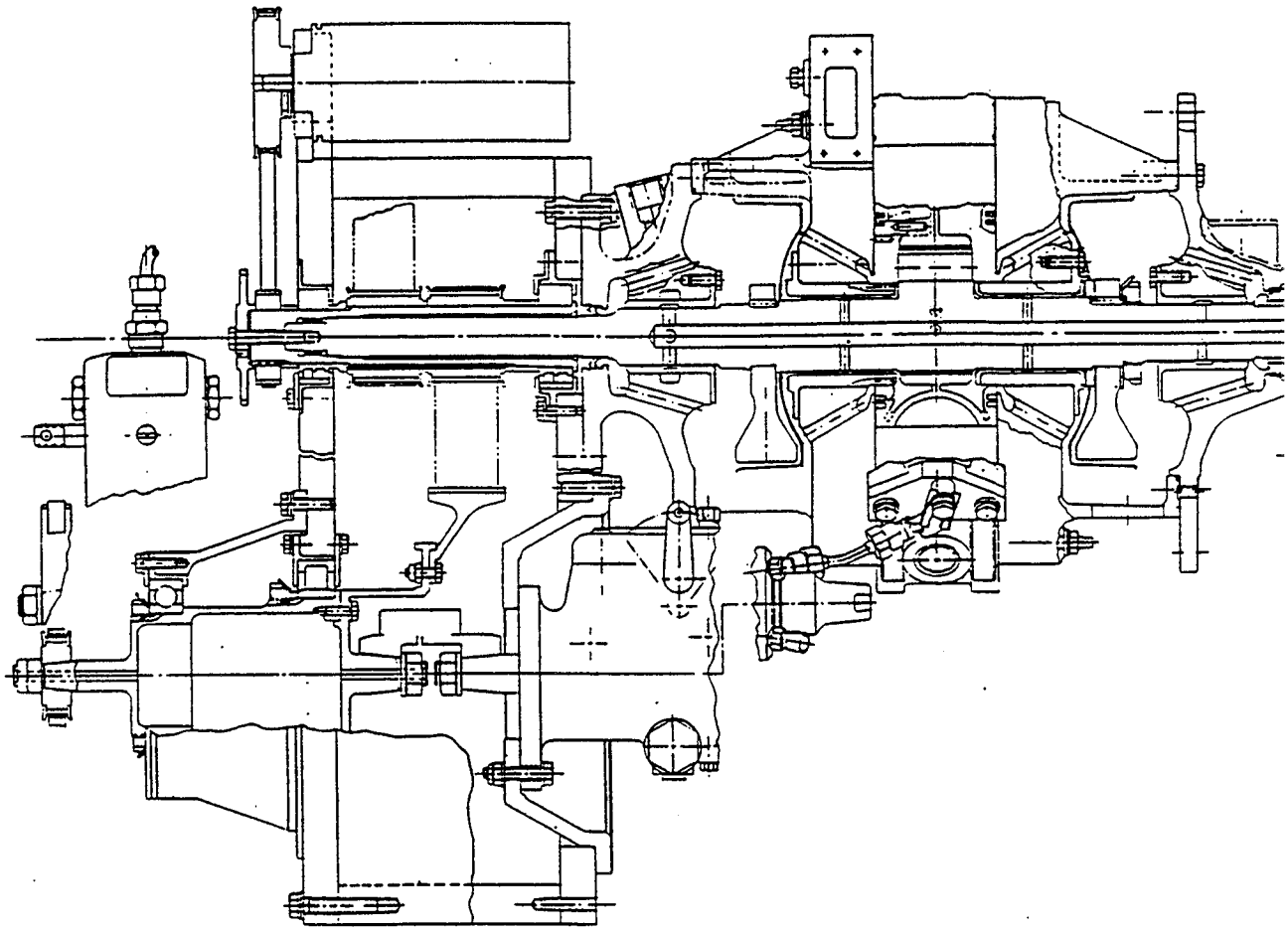


Figure 1. NASA SINGLE-ROTOR RIG ENGINE

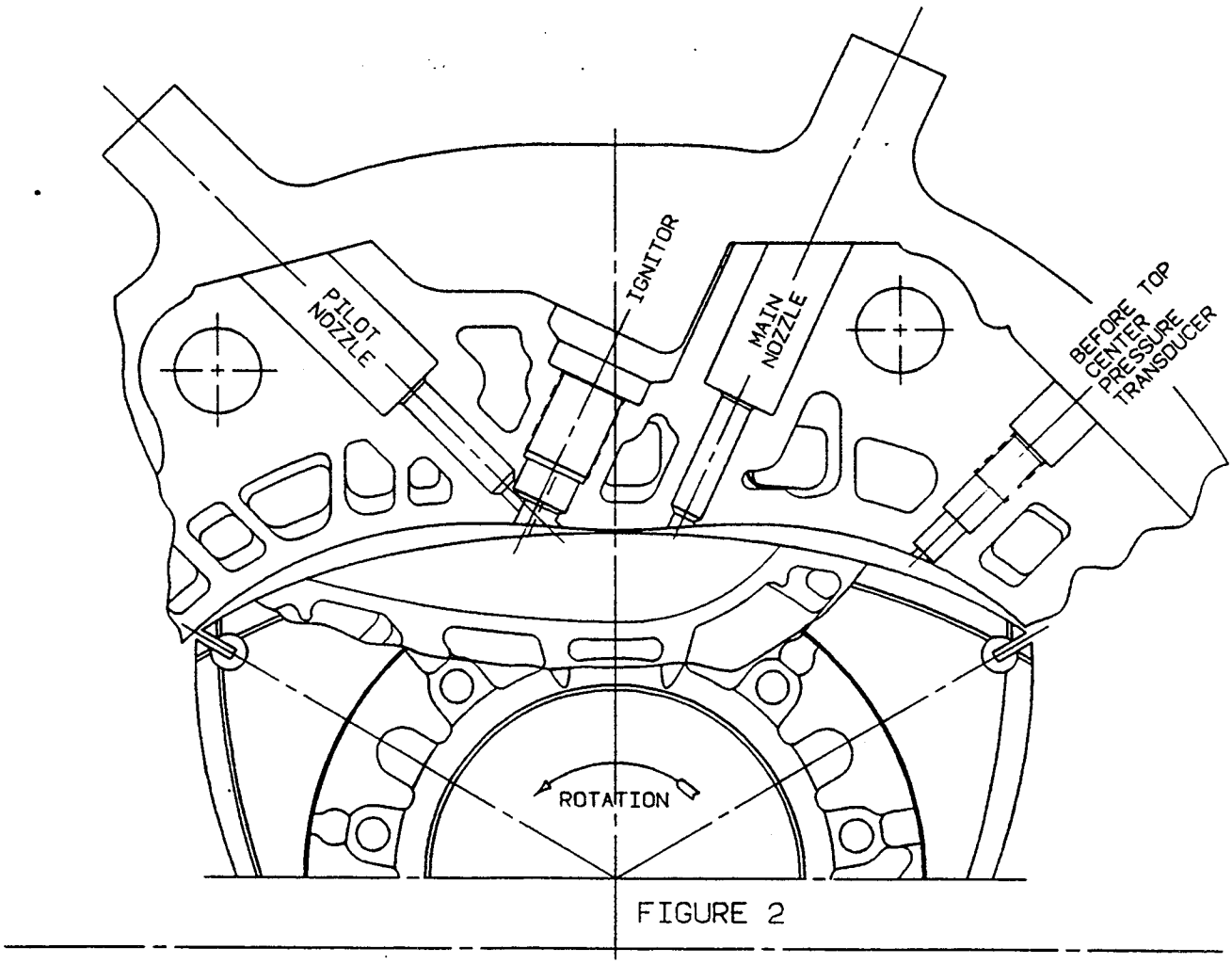


FIGURE 2

CROSS SECTION OF STANDARD RIG ENGINE AT TOP CENTER POSITION

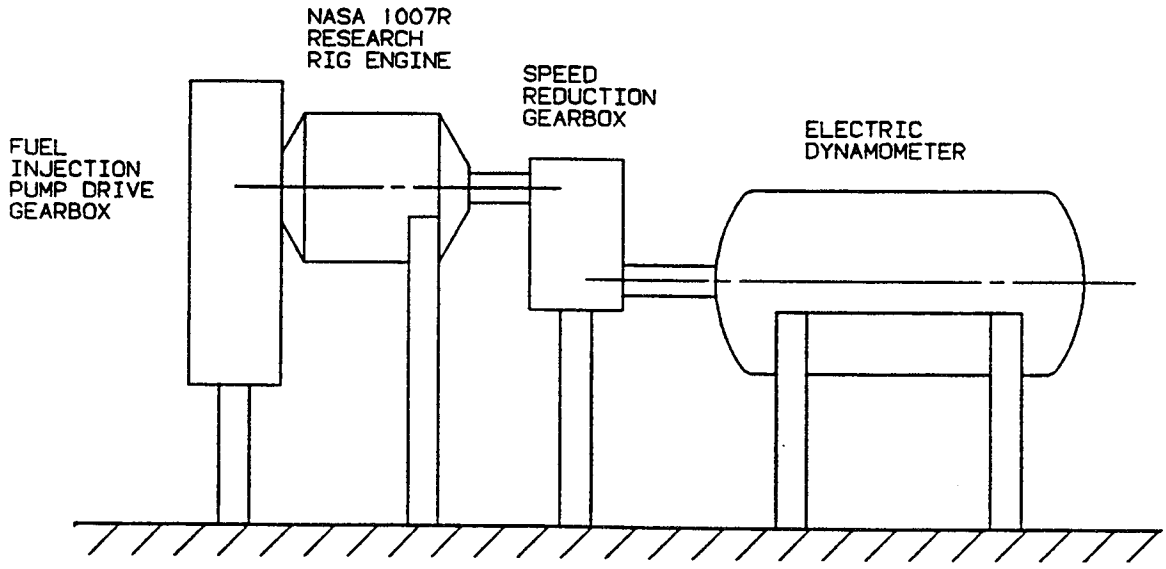


FIGURE 3

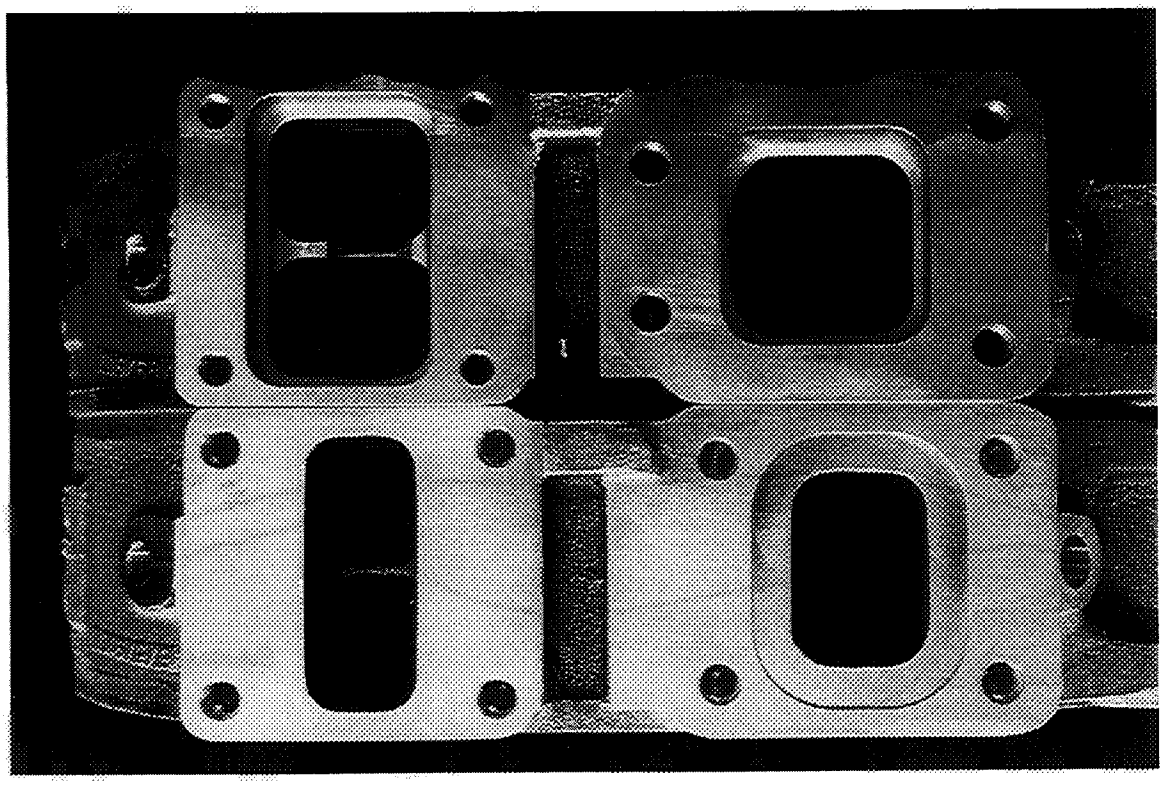
ENGINE AND DYNAMOMETER
DRIVELINE-WX20-6

TABLE I
NASA 1007R RIG ENGINE CONFIGURATIONS

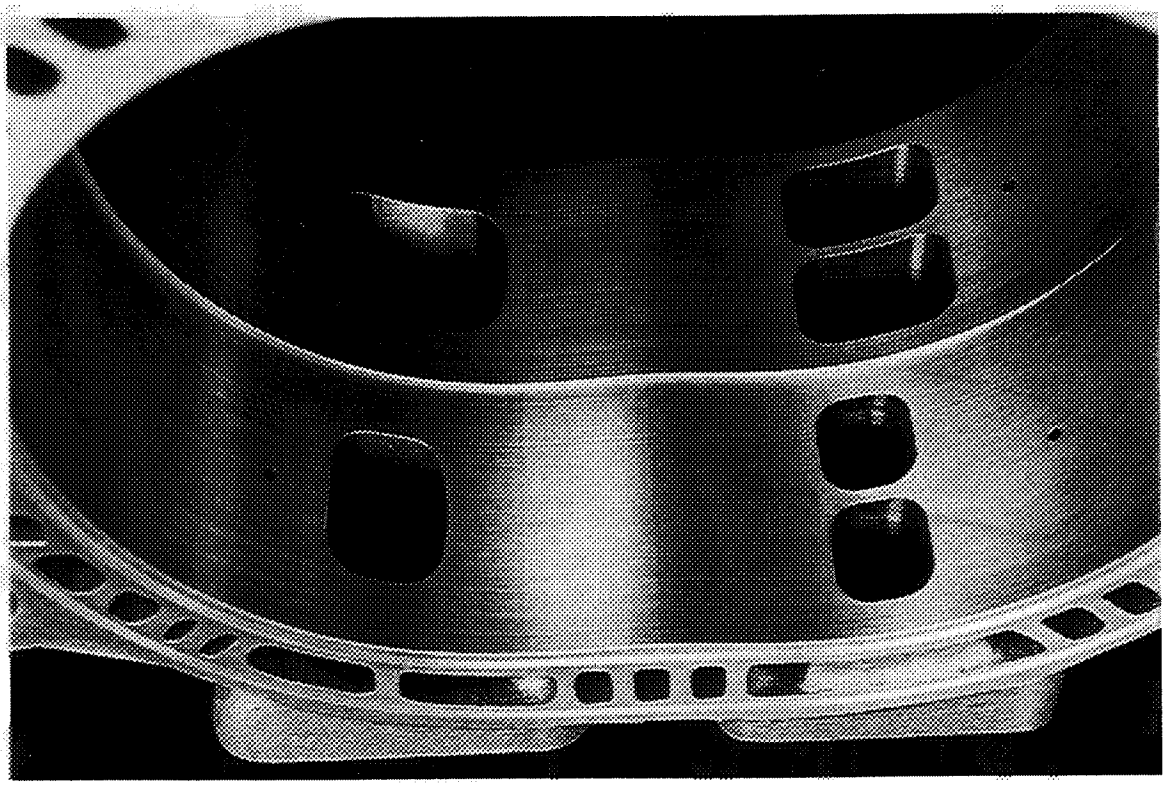
ENGINE TEST CONCEPT	POWER DENSITY DEMONSTRATION 200 HP		DUAL ORIFICE PILOT NOZZLE		DUAL IGNITOR		
ENGINE NUMBER	0704-4	0704-5	0705-1	0704-10	0704-6	0704-8	0705-3
Housing Rotor	210001	070X00118N1	070X00024A	070X00237A	NR10290	NR10290 (REWORK)	070X00267A
Rotor Assy.	NR10246N2	NR10246N2	NR10246N2	NR10246N2	NR10246N2	NR10246N2	NR10246N2
Rotor Compression Ratio	NJ12419N2 7.5:1	NJ12419N2 7.5:1	NJ12419N2 7.5:1	NJ12419N2 8.5:1	NJ12419N2 7.5:1	NJ12419N2 7.5:1	NJ12419N2 7.5:1
Rotor Bearing	210008N2	210008N2	210008N2	210008N2	NJ12462	NJ12462	NJ12462
Crankshaft	NJ11488	NJ11488	NJ11488	NJ11488	NJ11488	NJ11488	NJ11488
Apex Seals	ES10470	ES10470	NJ12463	NJ12463	NJ12463	NJ12463	NJ12463
Side Seals	NJ11154N2 Lap Butt	NJ11138N3 Lap Butt	210112N2 Lap Butt	NJ11138N3 Lap Butt	NJ11138N3 Lap Butt	NJ11138N3 Lap Butt	NJ11138N3 Lap Butt
Pilot FI Nozzle	210028N	210028N	070X0009,10,11A	NJ11961N156, N157,N158	210028N	210028N	210028N
Main FI Nozzle	210028N	210028N	210028N	210028N	NJ12394N	NJ12394N	NJ12394N
Turbocharger Turbine Housing	T04B/T04E 1.3 A/R	T04B 1.3 A/R	T04E 0.81 A/R	T04E 0.68 A/R	T04E 0.81 A/R	T04E 0.81 A/R	T04E 0.81 A/R
Spark Plug Plug Diameter	A5YC 12mm	A5YC 12mm	A5YC 12mm	C53YC 14mm	A5YC/NJ12564 12mm/10mm	A5YC/NJ12564 12mm/10mm	A5YC/A5YC 12mm/12mm
Manifold, Intake	210074	210074	210074	070X00159A	210074	210074	210074
Manifold, Exhaust	210075	210075	210075	NJ13005	210075	210075	210075

TABLE I (CONTINUED)

ENGINE TEST CONCEPT	CATALYTIC ROTOR	VARIABLE AREA PORT TIMING	LEADING RECTANGULAR POCKET ROTOR/ATC MAIN ROTOR HOUSING	LEADING STANDARD POCKET ROTOR/ ATC MAIN ROTOR HOUSING	DUAL POCKET ROTOR
ENGINE NUMBER	0705-2	0704-9	0707-1	0707-2	NOT TESTED
Housing Rotor	070X00118N1	070X00228A	NR10527	NR10527	NJ12997
Rotor Assy.	NR10246N2	NR10495	NR10514	NR10510	NR10512
Rotor Compression Ratio	NJ10071 8.4:1	NJ12522 7.5:1	NJ12975 8.5:1	NJ12960 8.5:1	NJ12964 8.5:1
Rotor Bearing	NJ12462	NJ12462	NJ12437	NJ12437	NJ12437
Crankshaft	NJ11488	NJ11488	070X00209A	070X00209A	T.B.D.
Apex Seals	NJ12463	NJ12463	070X00252AN1	070X00252AN1	NJ12463
Side Seals	NJ11138N3 Lap Butt	NJ11138N3 Lap Butt	070X00147AN3 Butt Butt	070X00147AN3 Butt Butt	NJ12958N3 Butt Butt
Pilot FI Nozzle	210028N	NR10139N4	210028N	210028N	n/a
Main FI Nozzle	210028N	210028N	210028N	210028N	070X00246AN, 070X00247AN
Turbocharger Turbine Housing	T04E 0.81 A/R	T04E 0.68 A/R	T04E 0.68 A/R	T04E 0.68 A/R	T.B.D. T.B.D.
Spark Plug Plug Diameter	A5YC 12mm	C63YC 4mm	RA6HC 12mm	RA6HC 14mm	T.B.D.
Manifold, Intake Intake Inserts	210074	070X00159A NJ12586,588,589	210074	210074	210074
Manifold, Exhaust	210075	NJ13005	210075	210075	210075



COMPARISON OF PORT OPENINGS OF STANDARD (BOTTOM) AND VARIABLE PORT/TIMING (TOP) ROTOR HOUSINGS



FRONT: STANDARD REAR: VARIABLE PORT/TIMING

TROCHOID PENETRATIONS OF STANDARD AND PORT/TIMING ROTOR HOUSINGS. NOTE THE AVAILABLE VARIATIONS IN PORT CLOSING AND OPENING POSITIONS OF INTAKE AND EXHAUST PORTS. ROTATION IS FROM LEFT TO RIGHT.

FIGURE 4

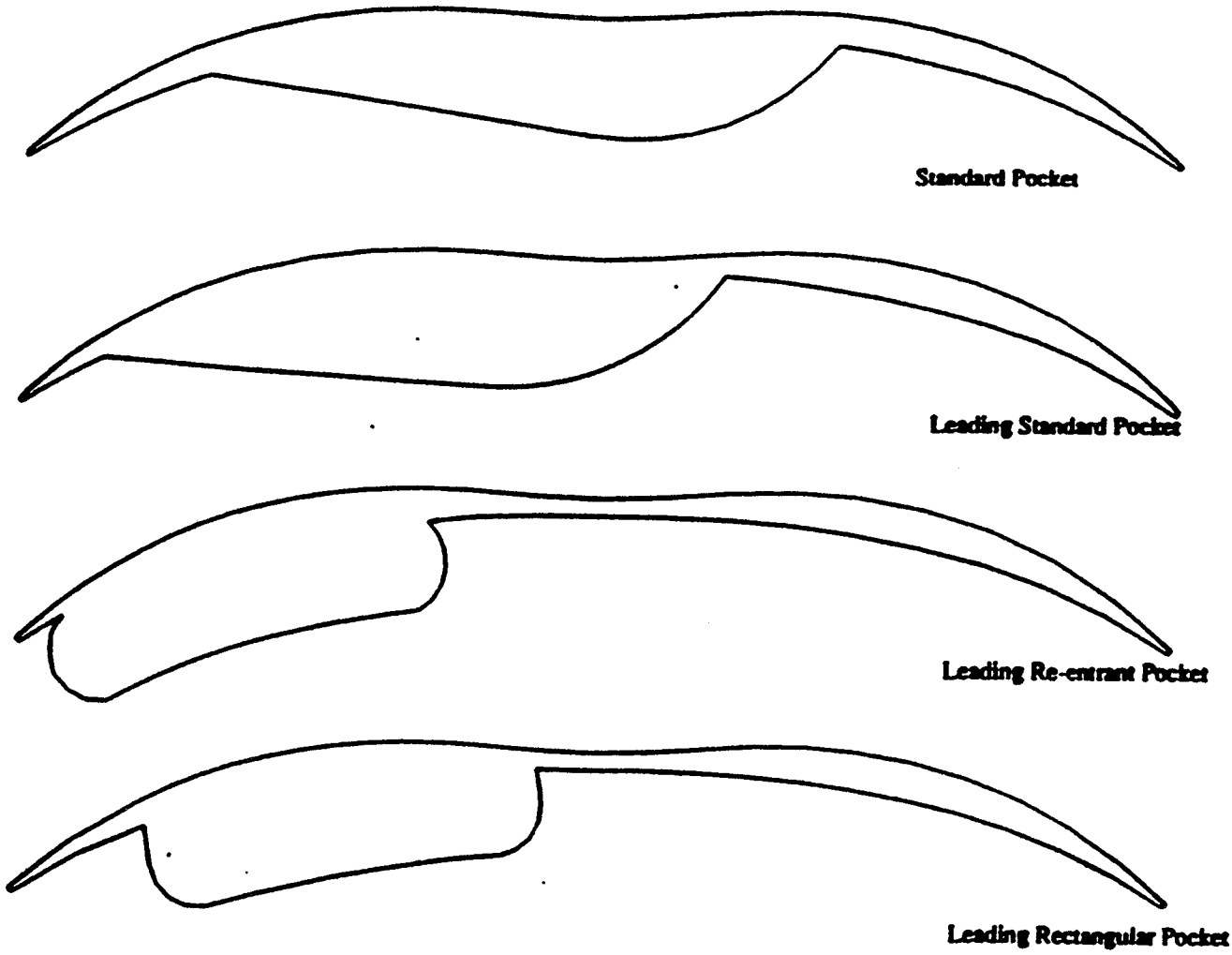
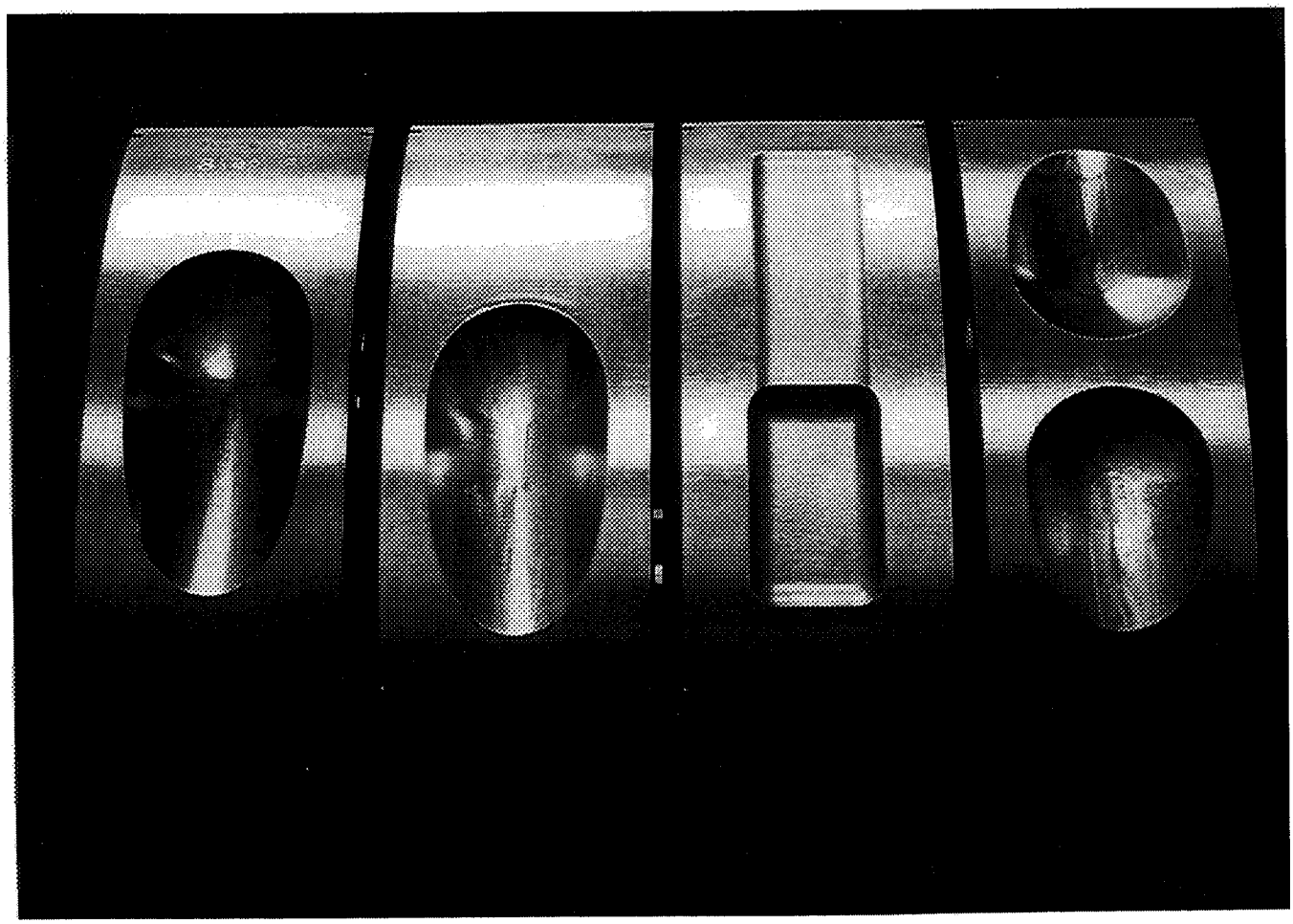


FIGURE 5:

SECTIONS THROUGH THE MIDPLANE FOR FOUR POCKET GEOMETRIES



COMBUSTION DEVELOPMENT ROTOR POCKETS

FROM LEFT TO RIGHT: STANDARD ROTOR POCKET; LEADING STANDARD ROTOR POCKET; LEADING RECTANGULAR ROTOR POCKET; DUAL POCKET. ALL ROTORS SHOWN ARE 8.4:1 COMPRESSION RATIO.

FIGURE 6

3.2 NEW/IMPROVED COMPUTATIONAL FLUID DYNAMICS (CFD) CODES

PRECEDING PAGE BLANK NOT FILMED

INTRODUCTION

During the past decade Computational Fluid Dynamics (CFD) has evolved into a powerful tool to investigate physical problems. This evolution has been spurred by advances in computer hardware and software and by the development of more fundamentally based physical submodels.

During the past five years the techniques of CFD have been applied to stratified-charge rotary engine combustion. References 1-7 describe various aspects of the development and application of CFD to stratified-charge rotary engine combustion.

OBJECTIVES

The objectives of the work described in this section were:

1. To improve the CFD code so as to make them faster and more accurate;

2. To develop graphics visualization tools to enable the results to be examined and interpreted;

3. To use the tools developed in 1. and 2. above to optimize the stratified-charge rotary engine; and

4. To couple the three-dimensional CFD code and a structural analysis code to obtain better estimates of heat fluxes.

TECHNICAL APPROACH

The tasks which would fulfill the objectives 1. and 2. above were subcontracted to Princeton University while John Deere concentrated on the tasks which would fulfill the objectives listed as 3. and 4. above. The scope of the original subcontract to Princeton was changed in October 1990 because of changes in John Deere's rotary engine program. The change involved reductions in cost and duration by about 30%. As part of the agreement leading to this reduction, 'Improvements to Submodels' in section 3.1.2.3 of the statement of work was not done. Reference 7 describes the work done at John Deere to fulfill objective 4. Reference 8 is a report which describes the work done at Princeton to fulfill objective 1. Reference 9 is a report which describes the work done at Princeton to fulfill objective 2.

In order to fulfill objective 3 above, the following approach was taken. Through computations made during the period 1988-89 modifications to the main injector and pilot injector spray patterns and to the pilot cavity location had been suggested. These suggestions had been partially implemented in hardware and shown to improve performance. Initial computations

PRECEDING PAGE BLANK NOT FILMED

PAGE 48 INTENTIONALLY BLANK

had also been made with a two igniter configuration. References 10-12 describe the analysis of the test data from the dual igniter configuration. During the period of the work reported here, additional computations were made for a two igniter configuration. An additional focus of the work was on changes to the geometry of the engine. Exploratory work was done to assess the feasibility of using air-assist injectors and to assess the effect of injection rates on engine performance with the objective of optimizing engine efficiency.

A STARDENT mini-supercomputer (Model 3000) purchased for the program and a slower STARDENT (Model 1500) were used to perform the computations. The STARDENT 3000 was used exclusively to make computations for this contract.

RESULTS

NOTE TO READER: Complete graphical illustrations in support of these analytical, iterative evaluations and discussion is provided in Volume II Appendix A. Some examples are included in this section for reference and are noted by an asterisk. However, for the complete association of illustrations and text (too volumnious to be included here) the reader is referred to Volume II Appendix A, "New/Improved Computational Fluid Dynamics (CFD) Codes/ Detailed Illustrations".

POCKET GEOMETRY

Depth of Pocket

The first set of computations were made with pockets of different depths. Figs. 1 (a)*-(c) show three such pockets. Fig.2* shows the computed pressure in the chamber for the three pockets respectively as a function of crank angle. It may be seen that the deeper and more compact pocket results in the fastest burning. However, from a practical point of view, a limit on increasing the depth of the pocket exists because of possible interference with the bearing. The alternate approach of increasing the K-factor (i.e. R/e ratio) was also considered. However, in order to obtain the same displacement with an increased K-factor the size of the engine has to be increased. If the size were to be kept the same, the increased efficiency on account of the increased depth of the pocket would not offset the reduced power on account of reduced displacement. Hence the next step was to consider relocating the pocket along the face of the rotor so that interference with the bearing could be avoided when the depth of the pocket was increased.

B. Relocated Pockets

Computations were made with the standard (baseline) pocket relocated circumferentially along the face of the rotor towards the leading edge and towards the trailing edge. In the case of the leading pocket the standard pocket was shifted toward the leading edge by 5 degrees whereas in the case of the trailing pocket the pocket was shifted toward the trailing edge by 10 degrees. (The angle of shift refers to the arc that defines the rotor surface).

Figs. 3(a)*-(e), 4(a)-(e), and 5(a)-(e) show the diffusivity contour lines in the plane of symmetry at different crank angles around top-center (TC=1170 degrees) for the standard, the leading and the trailing pockets respectively. Figs. 3(a), 4(a) and 5(a) show that at 1140 degrees (30 BTC) most of the air in the leading and standard pockets has a diffusivity between 40 and 60 cm2/s and most of the air in the trailing pocket has a diffusivity between 20 and 40 cm2/s. Figs. 3(b), 4(b), and 5(b) show that at 1155 degrees (15 BTC) most of the air in the trailing and standard pockets has a diffusivity between 40 and 60 cm2/s, but most of the air in the leading pocket has a diffusivity above 40 cm2/s and significant amounts are above 60 and 80 cm2/s. Figs. 3(c), 4(c), and 5(c) show that at 1170 degrees (TC) the leading and trailing pockets are each similar to what they were at 1155 degrees, but the standard pocket has become similar to the leading pocket. Figs. 3(d), 4(d), and 5(d) show that at 1185 degrees (15 ATC) the standard and trailing pockets are each similar to what they were at 1170 degrees, but the leading pocket has a smooth distribution of diffusivity from 20 to 200 cm2/s. Figs. 3(e), 4(e), and 5(e) show that at 1200 degrees (30 ATC) the trailing pocket has not changed much, the leading and standard pockets have increased in average diffusivity. Throughout this interval the trailing pocket was significantly lower in diffusivity than the other two pockets, and the leading pocket was most often higher than the standard pocket. Also the diffusivity was generally highest in the region of the deepest part of the pocket where the fuel is injected.

Figs. 3(f)*-(j), 4(f)-(j) and 5(f)-(j) show the velocity fields in the plane of symmetry and in a plane above the rotor surface at different crank angles beginning at top center. Figs. 4(g) shows that beginning at 1185 degrees there is a recirculation set up in the leading pocket aligned with the symmetry plane of the rotor. It grows stronger through the rest of the calculation (Figs. 4(h)-(j)). In both the leading and standard pockets there is a weak recirculation above the pocket in the plane of the rotor surface (Figs. 3(h)-(j) and 4(h)-(j)). With the trailing pocket the flow reverses on the leading flank of the rotor (Figs. 5(f)-(j)).

Figs. 3(k)*, 4(k) and 5(k) are plots of the pressure along the rotor at different crank angles. With the leading pocket at 1185 and 1200 degrees the pressure on the trailing flank of the rotor is about 5 atm higher than the pressure on the leading flank (Fig. 4(h)). With the standard pocket the largest difference is only 2 atm (Fig. 3(h)). This difference is reflected in the higher velocities with the leading pocket. The trailing pocket shows a large dip in pressure at the leading edge of the pocket at 1155 degrees (Fig. 5(h)).This might be an effect of the narrow clearance between the rotor and housing at this time and might explain the reversed velocities seen on the leading flank.

Both the higher diffusivity and the recirculation are driven by the squish flow from the trailing flank of the rotor. The leading pocket increases the velocity of this flow both by having more mass above the trailing flank and by remaining close to the dip in the housing for a longer time than either of the other pockets. These computations with relocated pockets suggested that moving the pocket toward the leading edge would be helpful and moving it toward the trailing flank harmful.

Subsequent to these studies two parallel paths of study, both of which were logical steps from above , were undertaken. The first path focused on a leading pocket and on attempts to obtain recirculation in the pocket at earlier crank angles than with the leading standard pocket. Since the pocket was leading, the depth of the pocket could also be increased to utilize the advantages noted earlier with deep pockets. However these series of leading pockets had certain disadvantages. The long narrow trailing flank resulted in a higher compression pressure as the gas trapped by the minor axis and the rotor face on the trailing side would be compressed. Also as a result of this effect, the air trapped would not be utilized in the pocket for mixing with air- an effect which would be detrimental to performance at higher loads when the fuel air ratio would become very rich. The second path of study, pursued in parallel with the above, attempted to overcome some of these disadvantages. In addition it incorporated positive features from the use of dual injectors, another concept which had been explored.

Dual Injectors

This concept originated with efforts to obtain higher power with the standard pocket configuration. A single main injector would be limited in its capacity to provide sufficient fuel to the engine over a certain duration and distribute the fuel uniformly with the pocket. Hence two separate injectors were considered. Figs. 6*,7*-10 show liquid fuel distribution within the pocket at different crank angles. Notice that each one of the two injectors has a four hole pattern. The first injector (indicated at I1) begins injection at about 1035 CA. The second injector begins injection at about 1050 CA. Fig. 11* shows a typical vaporized fuel-air distribution in the pocket at 15 CA BTC. Pockets of richer-than-flammable mixtures are absent. Figs. 12-13* show the temperature contour lines 15 crank angle degrees before top-center and at top-center respectively. These figures indicate that burning is fairly rapid. However the shape of the pocket with the leading part shallower than the trailing part was not a good match for two main injectors. Hence such a change in injection strategy required a change to the pocket geometry as well, whereby the shallower part of the pocket (i.e. towards the leading edge) had to be increased in depth to reduce wall wetting. Such an increase in depth results in significant reduction in compression ratio. The compression ratio may be increased to its original value by including a hump in the center of the pocket- in principle creating two separate pockets, one for each injector. Fig. 14 (a)*-(b)* show the cross-sections of such a geometry. I1 and I2 and S1 and S2 indicate locations of the two injectors and spark plugs respectively. Figs. 15 (a)*-(f) show the computed velocity flowfield at the indicated crankangles. Figs. 15 (a)-(d) show the velocity with respect to the housing

and Figs. 15 (e)-(f) show the velocity with respect to the rotor. Fig. 15 (f) shows that at top-center there is a significant relative velocity with respect to the rotor generated by the squish which in turn results in a high level of turbulence as indicated by the diffusivity contour lines on Figs. 16(a)-(b). Notice that this geometry is still not very practical since the surfaces have sharp corners.

This restricted the cooling of the rotor. In addition there were physical limitations to placing two injectors and two spark plugs in the vicinity of the minor axis. With the considerations above and others discussed in the section on 'relocated pockets' earlier, a dual pocket concept was pursued.

The Dual Pocket Rotor

Fig. 17* shows a sketch of a 'dual pocket' rotor. Notice that there is a spark plug and injector on the leading side located downstream of the pilot cavity on the standard engine and a spark plug and injector located upstream of the pilot cavity location. Figs. 18 (a,b*-e*)-(h) show the computed flowfield at several crank angles for this pocket. 1080 CA is top-center. Rotation is counterclockwise on all figures. F/A denotes fuel/air mixture contours, T the temperature, D the diffusivity and v the velocity. Injection in the leading pocket starts at about 50 CA BTDC and ignition at about 25 CA BTDC. It may be observed from fig. 18 (b) that the squish flow into the leading pocket generates high diffusivity which results in fast vaporization and mixing of the vaporized fuel with the air. Combustion in the leading pocket is complete by 1125 CA. Injection in the trailing pocket starts at about 10 CA BTC and ignition at about 10 CA ATC. Combustion in both pockets is complete by about 1140 CA. The timings are different for the two pockets so as to obtain positive torque on account of combustion from both pockets. Fig. 19* shows typical computed pressures in the leading and trailing pockets with and without combustion. It may be seen that there are significant differences in the magnitude of the pressures in the two pockets at a given crank angle. The magnitude of the differences would depend on the position of the pockets and ignition timings, parameters which were explored in the study.

In order to provide guidance for optimization calculations of the two-pocket configuration with the 3-D model a zero-dimensional model which analyses the two-pocket configuration was also developed. The model was used to study the effect of spark timings, crank-angles at which combustion pressures in the two pockets peak, and to a lesser extent the location of the pockets and injection timings.

Fig. 20 (a)-(d) show the computed flowfield results for a case where the trailing pocket is moved closer to the trailing edge. In general, the cases where the pocket is moved away from the trailing edge appears to offer greater flexibility in injection and ignition timings.

Computations were also made with the dual pocket configuration at compression ratios of 8.5 and 7.5. At a compression ratio of 8.5 the indicated efficiencies were about 3% better

at 6000 rpm and at an imep of 190 psi (1.309 mPa) relative to the results at a compression ratio of 7.5. Optimization computations were also done for the dual-pocket rotor configuration at different loads and with different timings to identify the best strategy for varying loads and timings. It appeared from the computations that the best efficiencies are obtained when at relatively high load (about 200 PSI (1.378 mPa) IMEP), 25% of the fuel is injected into the trailing pocket and 75% into the leading pocket. As the load was reduced, the quantity of fuel injected into the trailing pocket is kept constant and the fuel quantity injected into the leading pocket reduced till the quantities of fuel injected into both pockets are about the same. At lighter loads the quantity of fuel injected into the trailing pocket should be reduced while keeping the quantity of fuel injected into the leading pocket a constant.

Fig.21 shows the computed flowfield at top-center for the dual-pocket configuration. Fig.22 (a)* shows the computed pressures in the leading and trailing pockets at high load (about 200 PSI IMEP (1.378 mPa)) when 25% of the total fuel is injected into the trailing pocket and 75% of the the fuel is injected into the leading pocket. Fig.22 (b) shows the computed pressures in the pockets when the load is reduced by keeping the fuel quantity injected into the trailing pocket the same as in (a) but reducing the quantity injected into the leading pocket so that it is 50% of what it would be in (a). Fig. 22(c) shows the computed pressures when the fuel quantity injected into the leading pocket is 25% of what it would be at high load i.e in (a). It may be seen that this strategy also keeps the peak pressures in the pockets within 1400 PSI (9.646 mPa). A set of computations have also been done to assess the effect on efficiency and peak pressures of injection and spark timings. Fig. 23(a) shows the computed pressures in the pockets when the injection and spark timings of the trailing pocket are adjusted to obtain 5% to 95% mass burned fraction in the trailing pocket from 0 CA ATC to 30 CA ATC. Figs. 23(b), 23(c) and 23(d) show the pressures when this burned mass fraction is obtained in the trailing pocket between 20 to 55 CA ATC, 50 to 75 CA ATC and 60 to 95 CA ATC respectively. The best efficiency is obtained for (c) though in this case the peak pressure in the trailing pocket is above 1500 PSI (10.335 mPa).

Computations were also made for the dual-pocket configuration where the volumes of the two pockets were varied. In these computations the volumes of the two pockets which were kept equal in the design version was varied in relation to each other. In general, the computations show that increasing the volume of the leading pocket and reducing the volume of the trailing pocket appear to result in better efficiency. There is a limit on the maximum possible depth of the leading pocket because of structural considerations. A configuration where the volume of the leading pocket is about twice the volume of the trailing pocket has shown the highest efficiency of the different cases computed. This is because in the leading pocket recirculation is generated which in turn results in better fuel-air mixing and faster burning. The limiting case of using only a leading pocket is also being studied in relation to the dual-pocket configuration. While this pocket results in somewhat similar efficiency to the dual-pocket configuration there may be a limit to the maximum load that could be obtained with the pocket.

at 6000 rpm and at an imep of 190 psi (1.309 mPa) relative to the results at a compression ratio of 7.5. Optimization computations were also done for the dual-pocket rotor configuration at different loads and with different timings to identify the best strategy for varying loads and timings. It appeared from the computations that the best efficiencies are obtained when at relatively high load (about 200 PSI (1.378 mPa) IMEP), 25% of the fuel is injected into the trailing pocket and 75% into the leading pocket. As the load was reduced, the quantity of fuel injected into the trailing pocket is kept constant and the fuel quantity injected into the leading pocket reduced till the quantities of fuel injected into both pockets are about the same. At lighter loads the quantity of fuel injected into the trailing pocket should be reduced while keeping the quantity of fuel injected into the leading pocket a constant.

Fig.21 shows the computed flowfield at top-center for the dual-pocket configuration. Fig.22 (a)* shows the computed pressures in the leading and trailing pockets at high load (about 200 PSI IMEP (1.378 mPa)) when 25% of the total fuel is injected into the trailing pocket and 75% of the the fuel is injected into the leading pocket. Fig.22 (b) shows the computed pressures in the pockets when the load is reduced by keeping the fuel quantity injected into the trailing pocket the same as in (a) but reducing the quantity injected into the leading pocket so that it is 50% of what it would be in (a). Fig. 22(c) shows the computed pressures when the fuel quantity injected into the leading pocket is 25% of what it would be at high load i.e in (a). It may be seen that this strategy also keeps the peak pressures in the pockets within 1400 PSI (9.646 mPa). A set of computations have also been done to assess the effect on efficiency and peak pressures of injection and spark timings. Fig. 23(a) shows the computed pressures in the pockets when the injection and spark timings of the trailing pocket are adjusted to obtain 5% to 95% mass burned fraction in the trailing pocket from 0 CA ATC to 30 CA ATC. Figs. 23(b), 23(c) and 23(d) show the pressures when this burned mass fraction is obtained in the trailing pocket between 20 to 55 CA ATC, 50 to 75 CA ATC and 60 to 95 CA ATC respectively. The best efficiency is obtained for (c) though in this case the peak pressure in the trailing pocket is above 1500 PSI (10.335 mPa).

Computations were also made for the dual-pocket configuration where the volumes of the two pockets were varied. In these computations the volumes of the two pockets which were kept equal in the design version was varied in relation to each other. In general, the computations show that increasing the volume of the leading pocket and reducing the volume of the trailing pocket appear to result in better efficiency. There is a limit on the maximum possible depth of the leading pocket because of structural considerations. A configuration where the volume of the leading pocket is about twice the volume of the trailing pocket has shown the highest efficiency of the different cases computed. This is because in the leading pocket recirculation is generated which in turn results in better fuel-air mixing and faster burning. The limiting case of using only a leading pocket is also being studied in relation to the dual-pocket configuration. While this pocket results in somewhat similar efficiency to the dual-pocket configuration there may be a limit to the maximum load that could be obtained with the pocket.

Figs. 24(a)*-(e) show the computed velocity flowfield in a case where the leading pocket has about twice the volume of the trailing pocket. It may be seen that recirculation appears in the leading pocket about 5 CA before top- center. This recirculation persists after top-center but disappears at about 60 CA after top-center. The trailing pocket does not show any recirculation. Figs. 25(a)-(e) show the computed velocity flowfield in a case where the trailing pocket has about twice the volume of the leading pocket. Though recirculation appears in the leading pocket past top-center, this is neither sustained nor significant. Figs. 26(a, c*, d) and 27(a)-(c) show the liquid particle and fuel-air distribution in the pockets for the cases corresponding to Fig.25 and Fig.24 above respectively. It may be seen that in the case where the leading pocket has less volume (Fig.26) there is significant impingement on the wall and the vaporized fuel-air mixture in the leading pocket is rapidly carried towards the leading edge.

Figs.28 (a)*-(c) and 29 (a)-(c) show computed velocity,liquid particle and fuel-air distribution for two cases with only leading pockets but with somewhat different geometries. Since the pocket volume is less that the dual- pocket volume the quantity of fuel injected is also less and the maximum load that can be obtained is less than with the dual pocket configuration. It may be seen from the figures that there is significant recirculation and mixing in these cases. The differences in pocket geometries do not appear to affect these conclusions.

Computations were also done with aymmetrically located injectors. These computations were done because of design limitations in installing all the injectors and spark plugs along the symmetry plane. The computations indicated that small asymmetries (say, about 2-3 mm) did not significantly affect performance. However computations indicated that larger displacements in the location of the injector tip from the symmetry plane would result in asymmetric distribution of liquid fuel and vaporized fuel, a condition that would be made worse by the nature of the flowfield.

Fig. 30* shows the computed velocity, liquid fuel and vaporized fuel distribution in the chamber when the injector tip is located on the symmetry plane. Fig. 30(a) shows the results in the symmetry plane and Fig. 30(b) is a top 3-D view. The distributions of liquid fuel and vaporized fuel are almost symmetric - the slight asymmetry arising from the effects of turbulence. The velocity flowfield on the downstream side of the leading pocket may be seen to be divergent out of the pocket. Fig. 31 shows the computed velocity, liquid fuel and vaporized fuel distribution in the chamber when the injector tip is located about 1 cm away from the symmetry plane. Because of the divergent nature of the flowfield, the vaporized fuel is carried even further away from the symmetry plane. Hence the flowfield is noticeably asymmetric. Fig.30 shows that for the symmetrically located injector there is better utilization of the air on the downstream side of the leading pocket than on the upstream side. This situation could be improved by changing spray patterns and spray angles, a possibility limited at present by the tilt of the injector. Fig.32 shows a cross-section of the dual pocket housing.

As pointed out earlier optimum combustion in the dual-pocket configuration would generate a significant pressure differential of 600 psi (4.134 mPa) peak differential at high loads

between the leading and trailing pockets. These pressure differentials arise because injection and ignition timings in the two pockets are independently controlled to obtain maximum work output from each individual pocket. Fig. 32* shows the dual pocket rotor housing. Fig.33* shows the pressure in the chamber at different crank angles around Top-Center for an operating condition of 6000 rpm and an imep of about 220 psi (1515 kPa). These pressure differentials would result in high gear loads. Rotor gear loads for this configuration operating under this condition have been made and found to be about 14220 N (about 3200 lbf). The gear will be unable to withstand such high loads for sustained periods of time. Hence initial testing of the rotor would have to be done at moderate loads (less than 750 KPa imep) where the pressure differentials could be restricted to be less than 2000 kPa. Additional optimization computations are being made for this pocket, in particular, under conditions where the pressure differential is less than about 2000 Kpa.

ADDITIONAL COMPUTATIONS

Effect of Injection Rates

It is believed that fuel injection rates are an important parameter affecting engine performance. Computations were done with different injection rates to assess this effect. Fig.34* shows two measured injection rates. They are for an Accumulator Unit Injector (AUI) and for a Stanadyne model DM pump. In previous engine tests the Stanadyne DM pump had given better performance. It may be seen from Fig.34 that the rate of fuel injection is greater at the start of injection for the AUI system than for the DM pump. This results in greater vaporization and the formation of richer mixtures at the start of injection with the AUI system. Figs. 35 (a)* and (b) show the prescribed injection velocities in the computations for the AUI and DM pumps respectively. These are approximations to the typical measured rates. Figs.36 (a)* and (b) show the injected (_____) and vaporized (------) mass of fuel in the chamber as a function of crank angle for the AUI and DM pumps respectively. The relatively fast initial injection rate of the AUI system results in the formation of smaller drops and hence faster vaporization relative to the DM system. Fig.37 (a) and (b) show the liquid drop and fuel-air distribution in the chamber 15 CA degrees after the start of injection for the AUI system and the DM system respectively. Figs.38 (a)* and (b)* show the lean,flammable and rich fractions of fuel in the chamber as functions of crank angle for the AUI and DM pumps respectively. The AUI system, because of faster vaporization, has significantly greater quantities of rich fractions of fuel relative to the DM pump system. Figs. 39(a)-(b) show temperature and fuel/air distribution in the chamber at 1145 CA and 1165 CA for the AUI system. It may be seen that because of the greater quantities of rich fraction of fuel present in the chamber, the flame gets quenched. Figs. 40 (a)- (h) show the temperature , fuel/air and liquid fuel distribution in the chamber at different crank angles for the DM pump system. In this case the flame is not quenched.

Further computations with injection rates were obtained with the objective of obtaining a rate shape which would be optimum. Fig.41* shows 5 different rates for total delivery during each injection event of about 60 mm3 of jet-A fuel and engine rpm of 6000. The maximum

amount of flammable fraction of fuel-air mixture in the chamber has been obtained with the trapezoidal rate shape, indicated as 'A' on Fig.41. This is somewhat better (by about 10%) than the results with the AMBAC pump, indicated as 'B' on Fig.41. Fig.42* is a plot of the fractions of lean,flammable and rich vaporized fuel-air mixture as a function of crank angle degrees for shape 'A'. Fig.43* and Fig.44* show similar plots for rate shapes 'B' and 'C' respectively. Rate 'C' which approximates the Nippondenso pump rate results in somewhat lesser quantity of flammable fuel than the Ambac pump rate shape 'B'. The computations indicate that the linear rates 'D' and 'E' give the least amount of flammable fractions. These differences in the quantity of flammable fuel should result in differences in indicated efficiency. The computations were made with the N43 spray patte

Computations were also made to assess the possible effects of variations in L/D ratios of nozzles on fuel-air distribution and performance. Such variations would influence the spray angles, penetration and drop sizes. Fig. 45 shows the vaporized and liquid fuel distribution for a reference case at different crank angles. Fig. 46 shows the vaporized and liquid fuel distribution for a case where the spray angle is increased by a factor of two from the reference case and the penetration is consequently halved. Fig. 47* shows the vaporized fraction of injected fuel, and lean,rich, and flammable fractions for the reference case and Fig. 48 for the modified case. It may be seen that the reduced penetration appears to be detrimental to engine performance. These computations indicated that significant variations of L/D ratios of nozzles would have noticeable effects on engine performance.

CONCLUSIONS

The accuracy and speed of a three-dimensional code which had been developed through the Deere-Princeton collaborative work during the period 1985-89 were improved through the use of new computational techniques such as ADI methods and Stone's strongly implicit algorithms. Graphics visualization tools which could be used to examine and interpret the results from the 3-D computations were developed. With these computational tools and the use of dedicated mini-supercomputers changes to engine geometry, injector/ignitor locations and injector/ignitor strategies were explored. Three new promising engine configurations were identified. Time constraints, imposed, in particular by Deere's decision to exit from the Rotary Engine business, prevented these concepts from being optimized computationally or experimentally for best performance.

RECOMMENDATIONS

The following are recommendations for future work:

1. Injector/ignitor locations, spray patterns and geometry should be optimized for the leading standard, leading rectangular and dual pocket configurations.

2. An extensive series of hardware tests should be carried out for these configurations. The test results should be used to correlate with the computed results. Additional computations should then be made to further optimize these configurations taking into account the test results. This is an important and necessary stage in the development process because the codes are tools which should be used to provide guidance for experimental work and not to obtain absolute numbers. In addition the present version of the code does not include submodels for physical processes such as autoignition, the details of normal ignition, cycle to cycle variablility, detonation nor has its accuracy been assessed for computing pressure waves. .R

3. Computations should be made to explore the sensitivity of computed results to variations in timings, ignition/injector locations, fuel/air ratios since it appears difficult to obtain correspondence between these parameters computationally and experimentally.

4. Additional concepts such as optimum injection rate profiles and air-assist injectors should be explored computationally and then experimentally as in step 2 above.

5. The code should be improved to handle autoignition, normal ignition and flows with and without combustion in cavities. Its accuracy in handling propagation of thin wave fronts should be assessed.

REFERENCES

1. Grasso, F., Wey,M.-J.,Bracco,F.V. and Abraham,J., "Three-Dimensional Computations of Flows in a Stratified-Charge Rotary Engine," SAE Paper No. 870409,SAE Trans.,Vol.96,1987.

2. Abraham,J.,Wey,M.-J. and Bracco,F.V.,"Pressure Non-Uniformity and Mixing Characteristics in Stratified-Charge Rotary Engine Combustion," SAE Paper No. 880624,SAE Trans.,Vol.97,1988.

3. Abraham,J. and Bracco,F.V.,"Comparisons of Computed and Measured Mean Velocity and Turbulence Intensity in a Motored Rotary Engine,"SAE Paper No. 881602,SAE Trans.,Vol.97,1988.

4. Abraham,J. and Bracco,F.V.,"Fuel-Air Mixing and Distribution in a Direct Injection Stratified-Charge Rotary Engine," SAE Paper No.890329, SAE Trans., Vol.98,1989.

5. Abraham,J. and Bracco,F.V.,"3-D Computations to Improve Combustion in a Stratified-Charge Rotary Engine Part II: A Better Spray Pattern for the Pilot Injector,"SAE Paper No.892057,SAE Trans.,Vol.98,1989.

6. Abraham,J. and Bracco,F.V.,"3-D Computations to Improve Combustion in a Stratified-Charge Rotary Engine Part III:Improved Ignition Strategies," to be presented at the SAE International Congress and Exposition, Detroit, February 1992.

7. Abraham,J.,Ramoth,D. and Mannisto,J.,"3-D Steady-State Wall Heat Fluxes and Thermal Analysis of a Stratified-Charge Rotary Engine,"SAE Paper No.910706, 1991.

8. a) A Fortran 77 Library for Postscript Plotting, by M.J. Andrews, Princeton University, August 1990.

   b) Notes on Animation, Princeton University, January 1991.

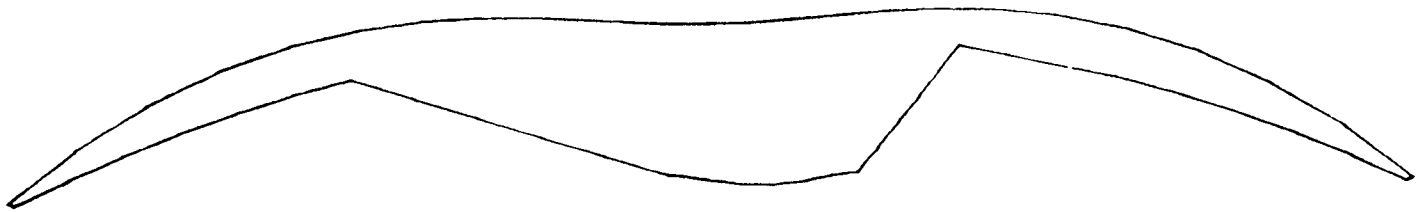
   c) Rotary Engine Design Using Three-Dimensional Displays as a Diagnostic Tool for Computer Simulations, by Anna Thornton, Princeton University, 1990.

9. Some Elements of REC-91: A 3-D Code for Flows, Sprays and Combustion in Reciprocating and Rotary Engine, by V.Magi and F.V. Bracco, Princeton University, September 1991.

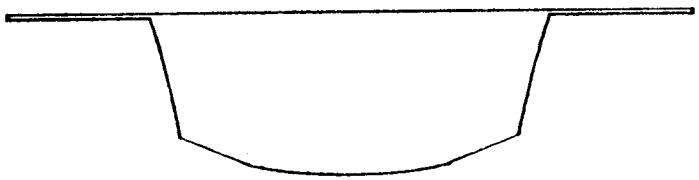
10. Abraham,J. and Epstein,P.,"Analysis of Experimental Pressure Traces from the Dual Igniter Engine (Engine Build #0704-8), Report prepared on 26 July 1991.

11. Abraham,J. and Epstein,P.,"Analysis of Experimental Pressure Traces from the Dual Igniter Engine Build #0705-3 and Build #0704-8," Report prepared on 06 August 1991.

12. Abraham,J. and Epstein,P.,"Analysis of Experimental Pressure Traces from the Dual Igniter Engine Build #0705-4," Report prepared on 27 August, 1991.



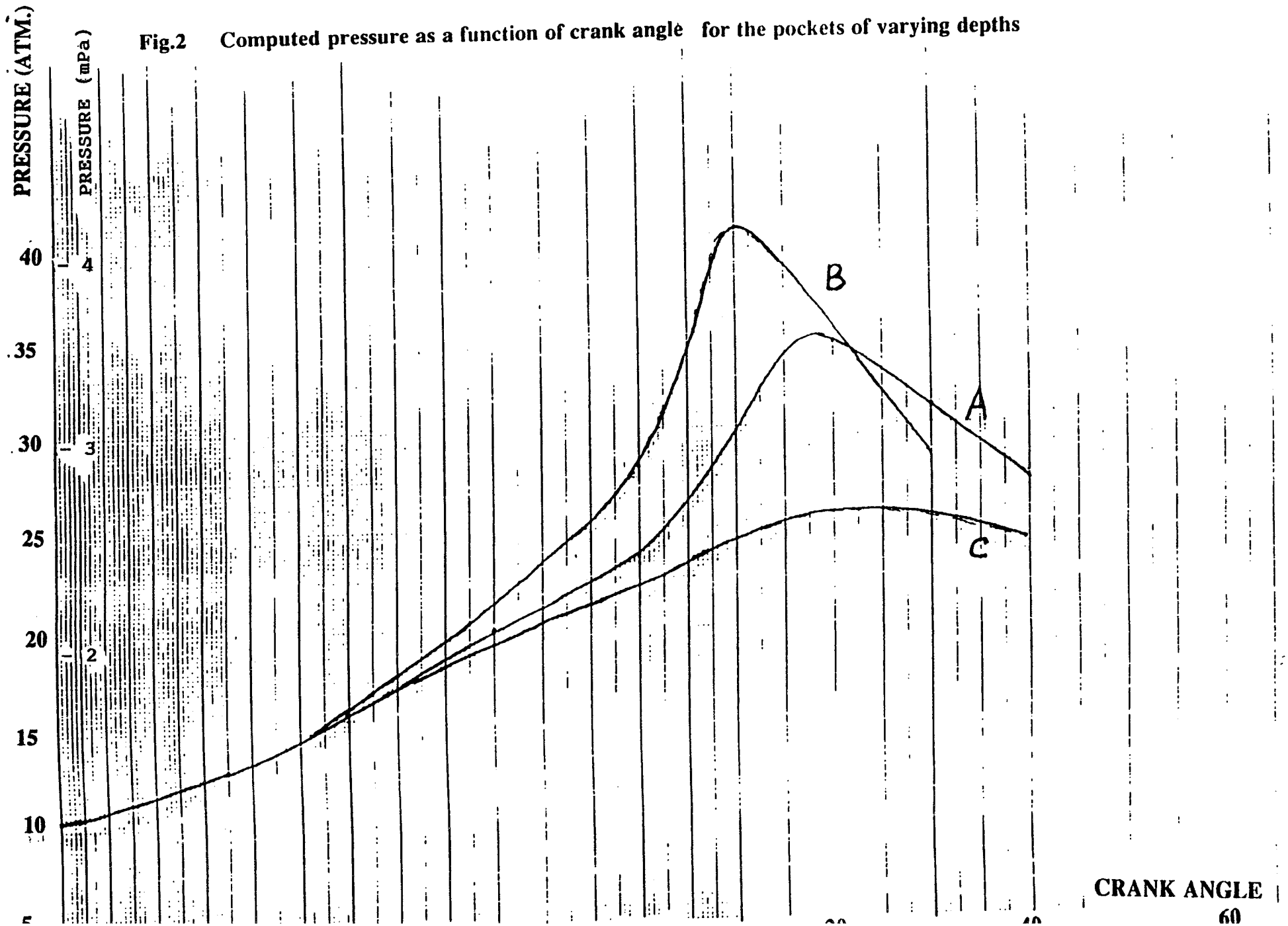
crank angle= 0.1
J= 7
T interval= 500.00K
H=4500.0000 : L=4500.0000

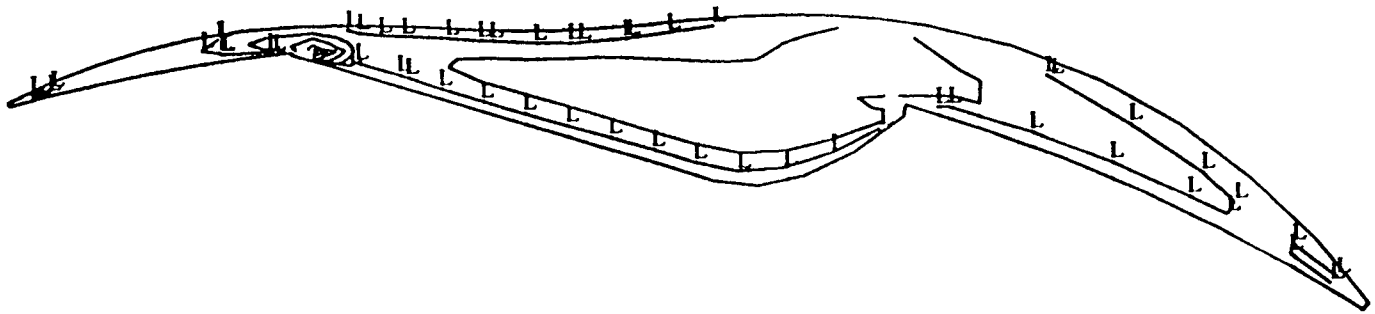


I=13
T interval= 500.00K
H=4500.0000 : L=4500.0000

Fig.1 (a) Cross-sections of standard pocket geometry

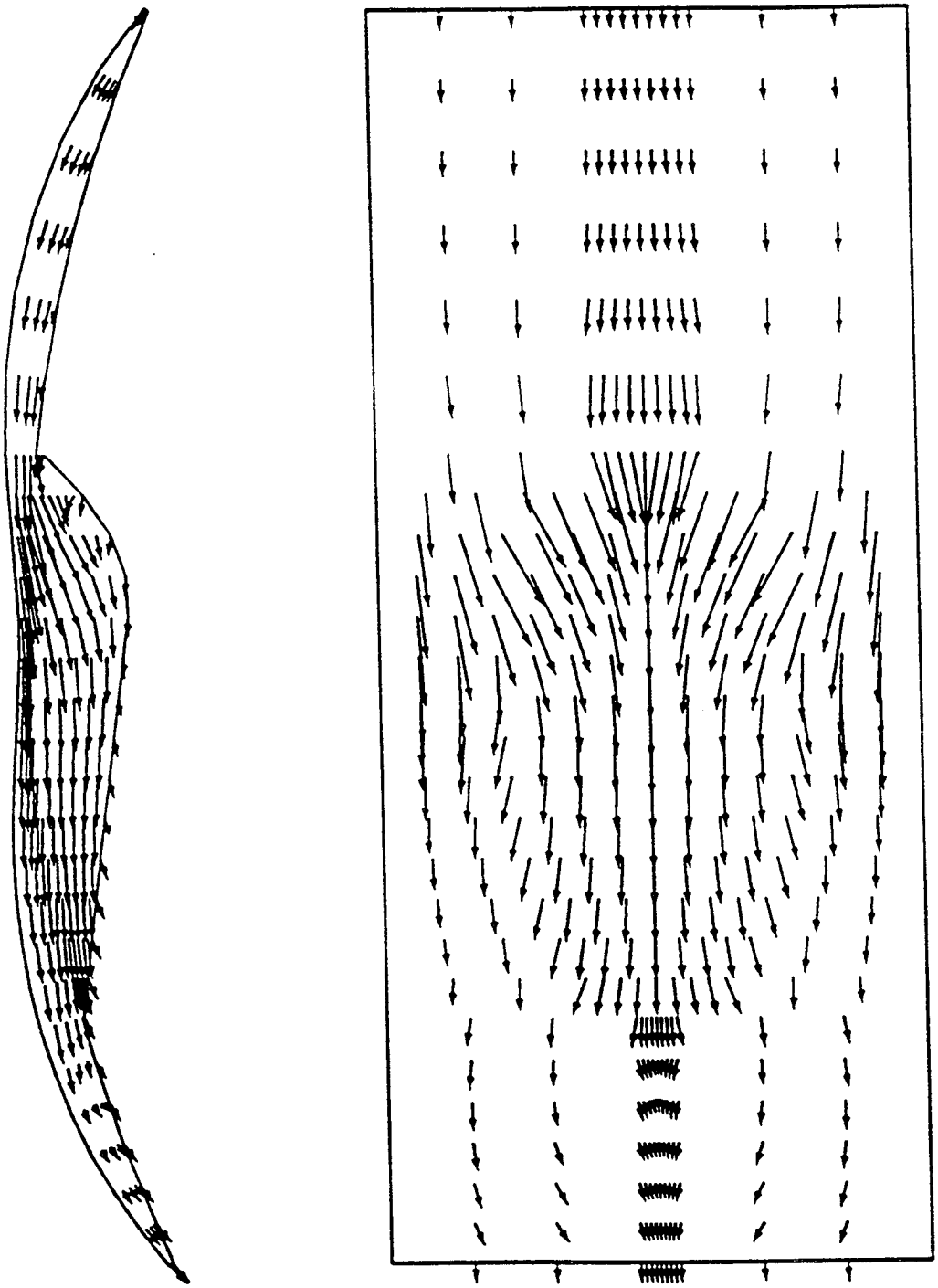
Fig.2 Computed pressure as a function of crank angle for the pockets of varying depths





DIFFUSIVITY, interval = 20.00 cm2/s
H = 200.0 ; L = 20.00
J = 7
crank angle = 1140.0

Fig. 3(a): Cross-section of combustion chamber along symmetry plane showing diffusivity contours at 1140 CA. for standard pocket rotor.



100 m/s

100 m/s

K = 8

crank angle = 1170.0

ORIGINAL PAGE IS
OF POOR QUALITY

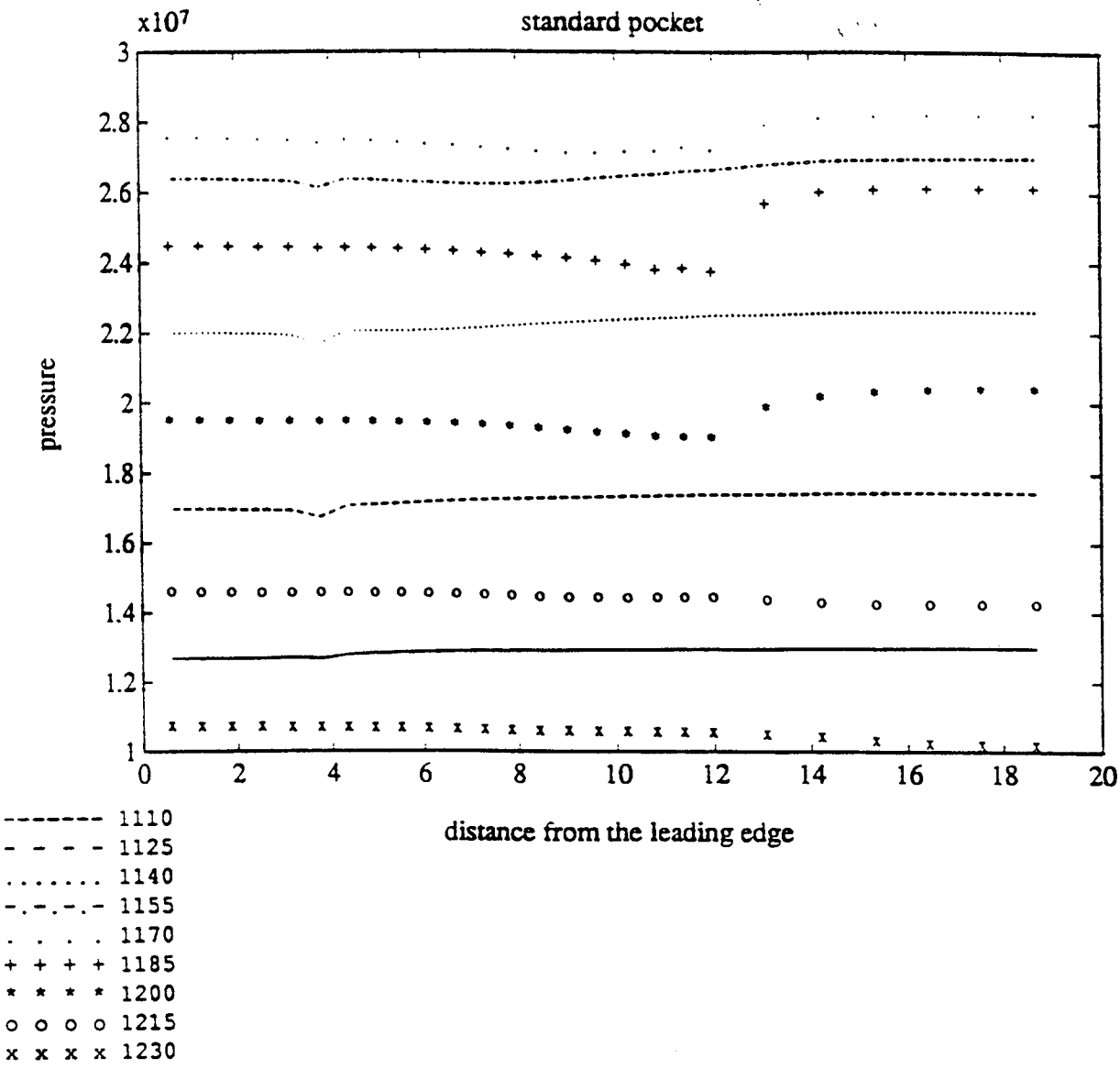


Fig. 3(k): Pressure along the rotor at different crank angles

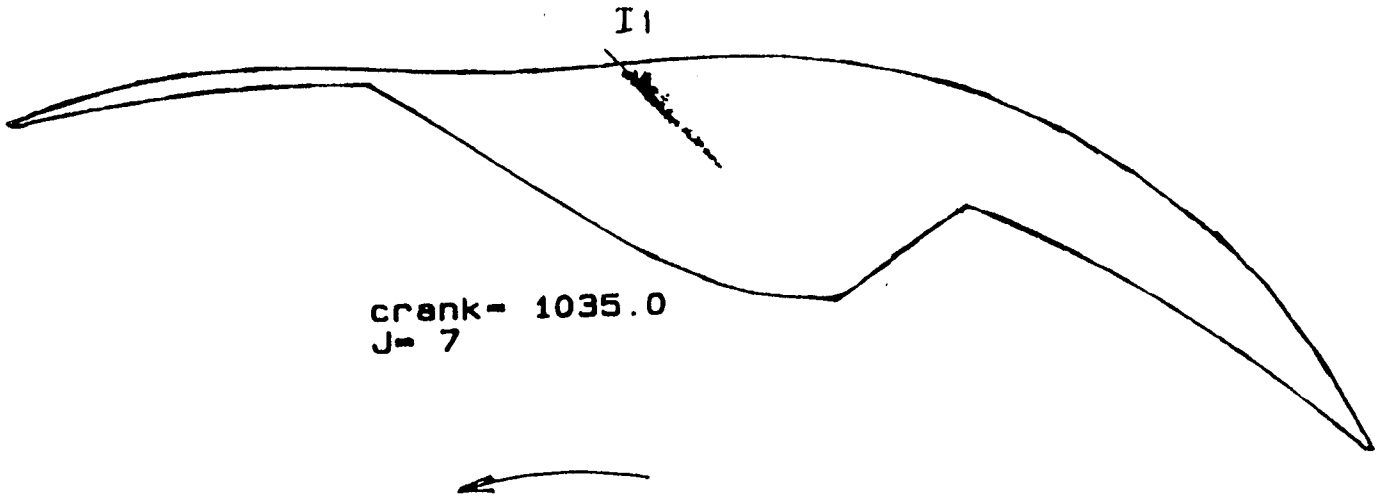


Fig. 6: Cross-section view of combustion chamber along symmetry plane showing liquid fuel distribution at 1035 CA (1080 is TC).

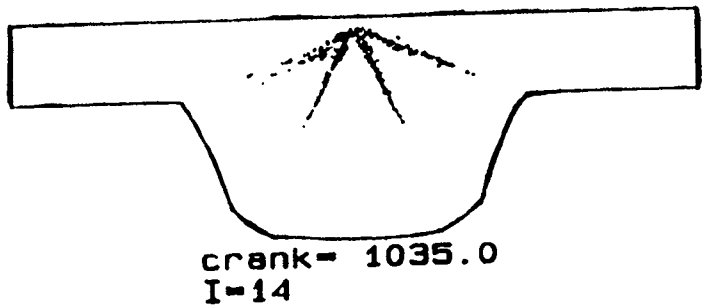


Fig. 7: Cross-section of combustion chamber showing liquid fuel distribution at 1035 CA. Injector has a 4-hole pattern.

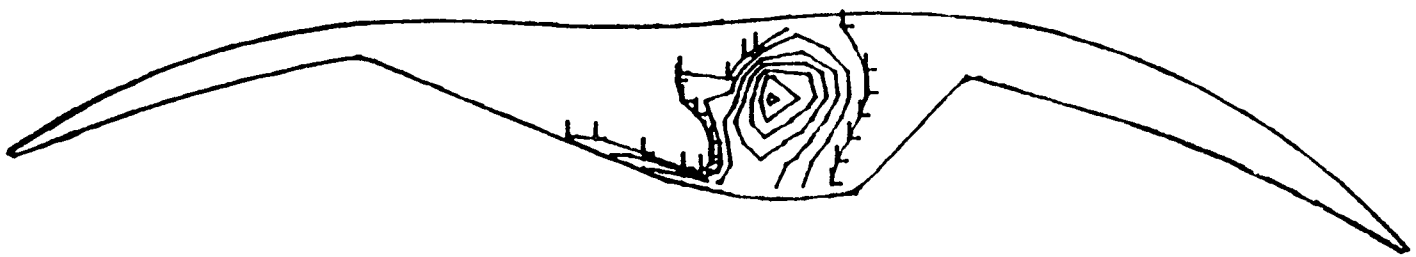


Fig. 11: Cross-section view of combustion chamber along symmetry plane showing vaporized fuel distribution at 1065.1 CA.

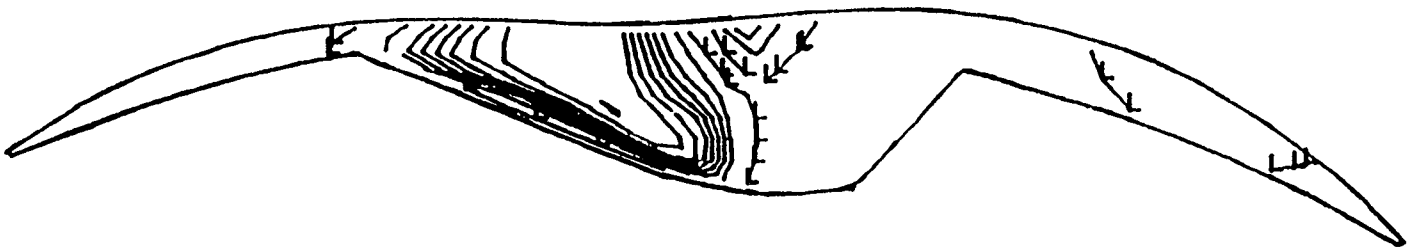


Fig. 12: Cross-section view of combustion chamber along symmetry plane showing temperature contours at 1065 CA.

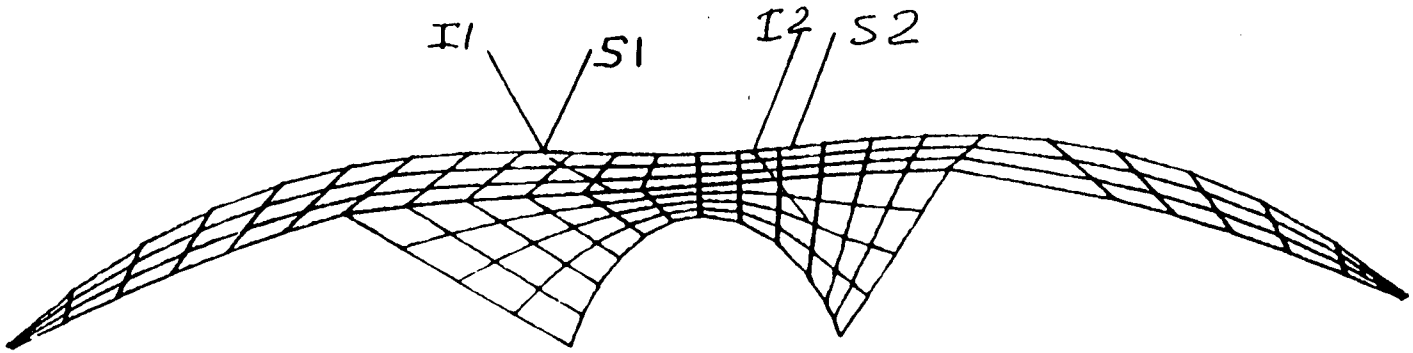
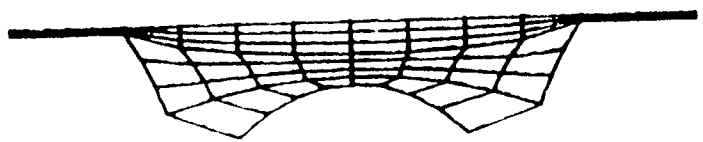


Fig. 14 (a): Cross-section view of combustion chamber along symmetry plane showing grid layout and locations of injectors and spark plugs.



CRANK= 27.000

I=13

Fig. 14 (b): Cross-section view of combustion chamber showing grid layout.

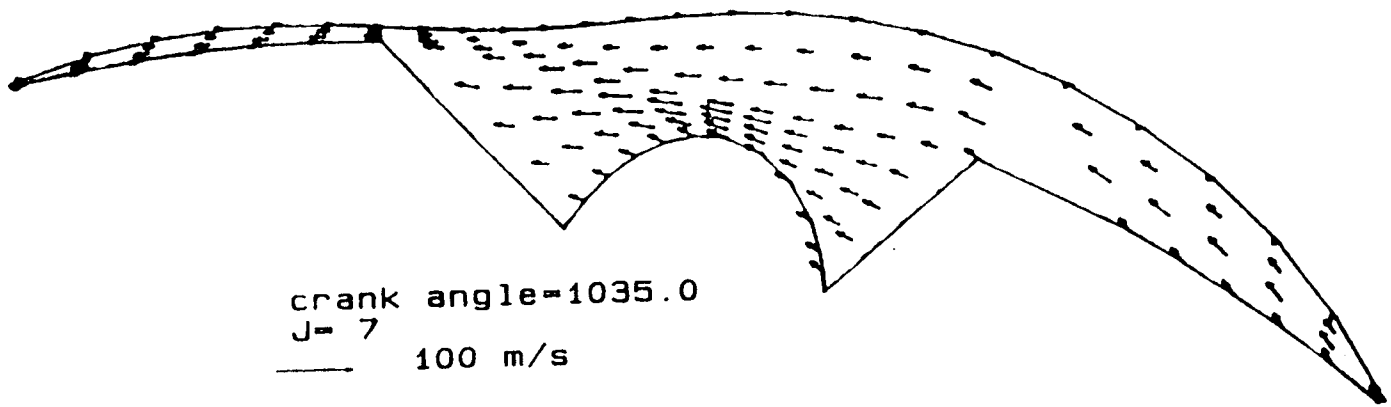


Fig. 15 (a): Cross-section view of combustion chamber along symmetry plane showing velocity vectors at 1035 CA.

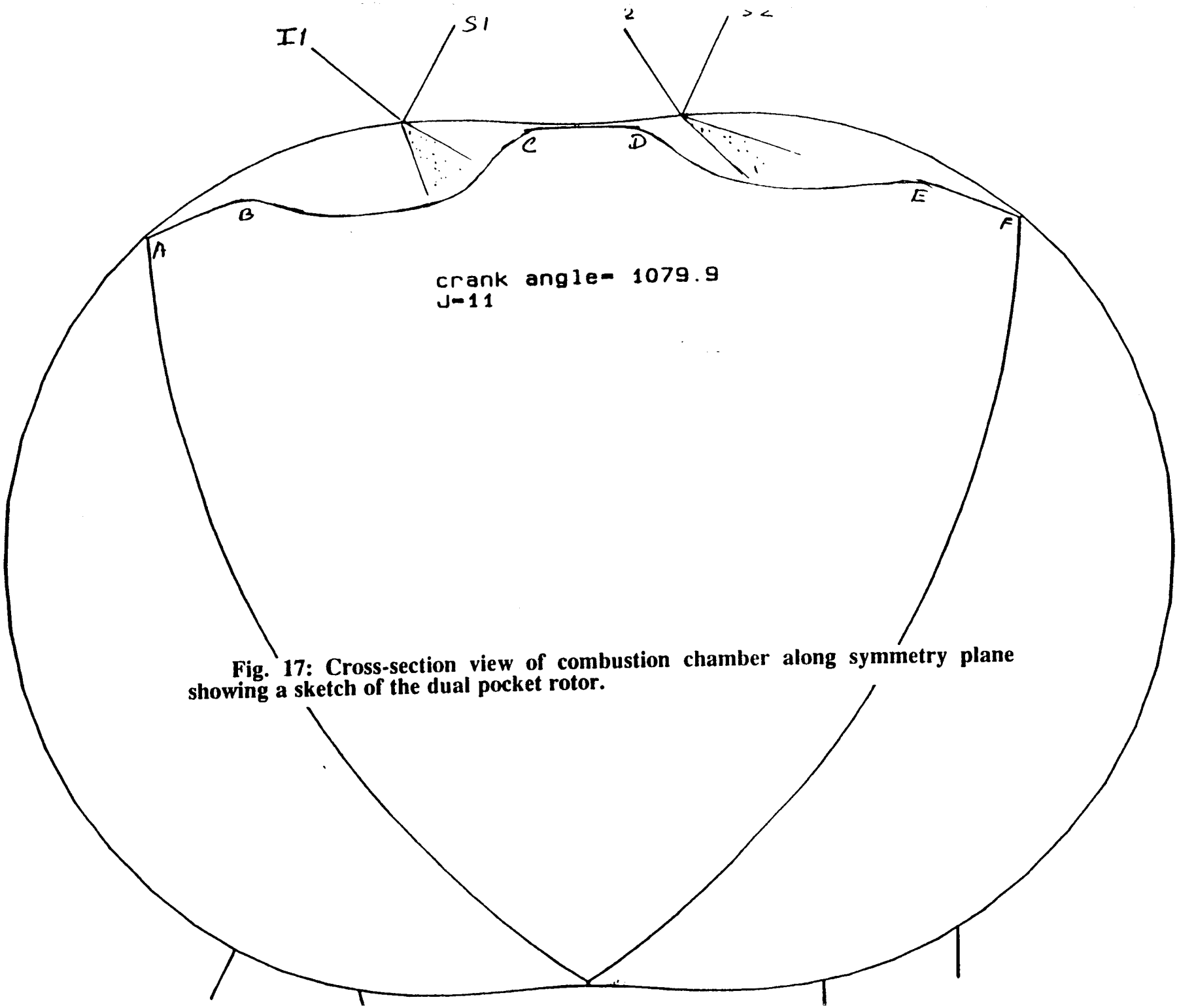


Fig. 17: Cross-section view of combustion chamber along symmetry plane showing a sketch of the dual pocket rotor.

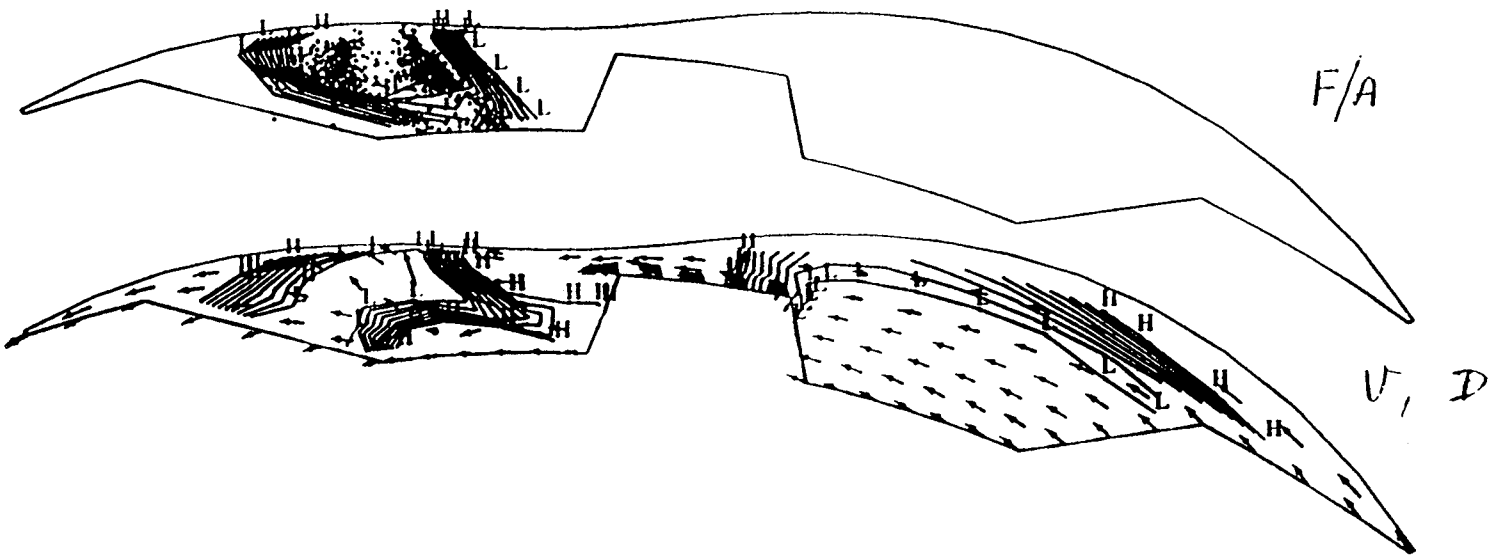
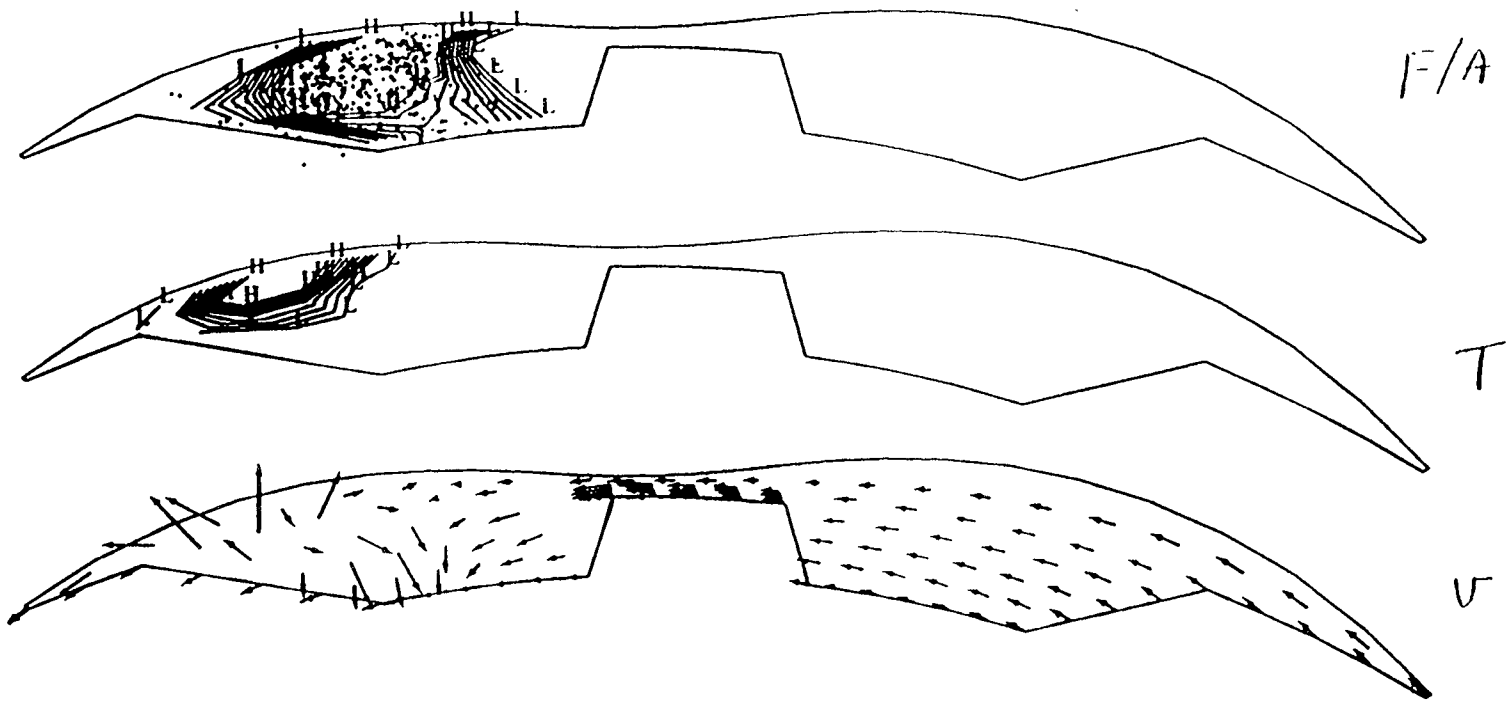


Fig. 18(b): Cross-section view of combustion chamber along symmetry plane showing liquid fuel and vaporized fuel distribution ,velocity vectors and diffusivity contours at 1050 CA.

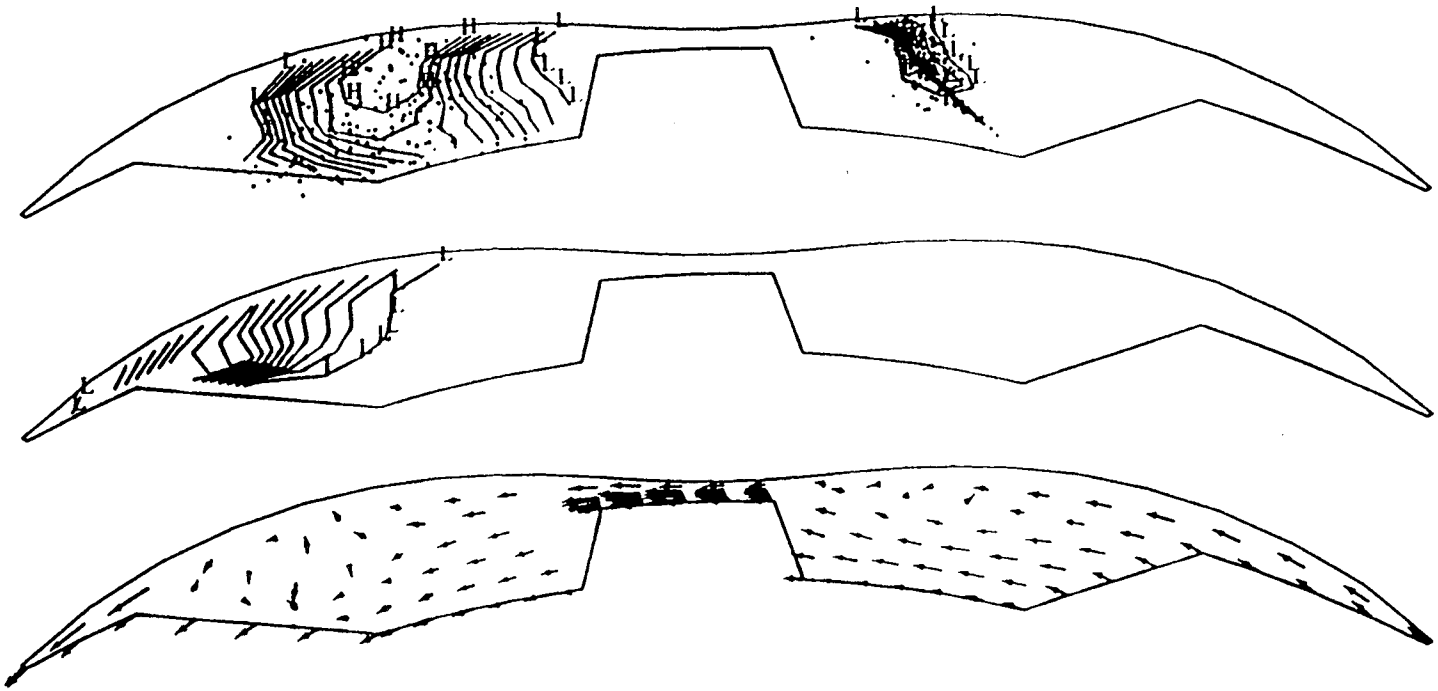
FUEL/AIR RATIO, interval = 0.1000E-01
H = .1200 ; L = .3000E-01
TEMPERATURE, interval = 155.6 K
H = 2100. ; L = 700.0
DIFFUSIVITY, interval = 55.56 cm2/s
H = 600.0 ; L = 100.0



FUEL/AIR RATIO, interval = 0.1000E-01
H = .1200 ; L = .3000E-01
TEMPERATURE, interval = 155.6 K
H = 2100. ; L = 700.0

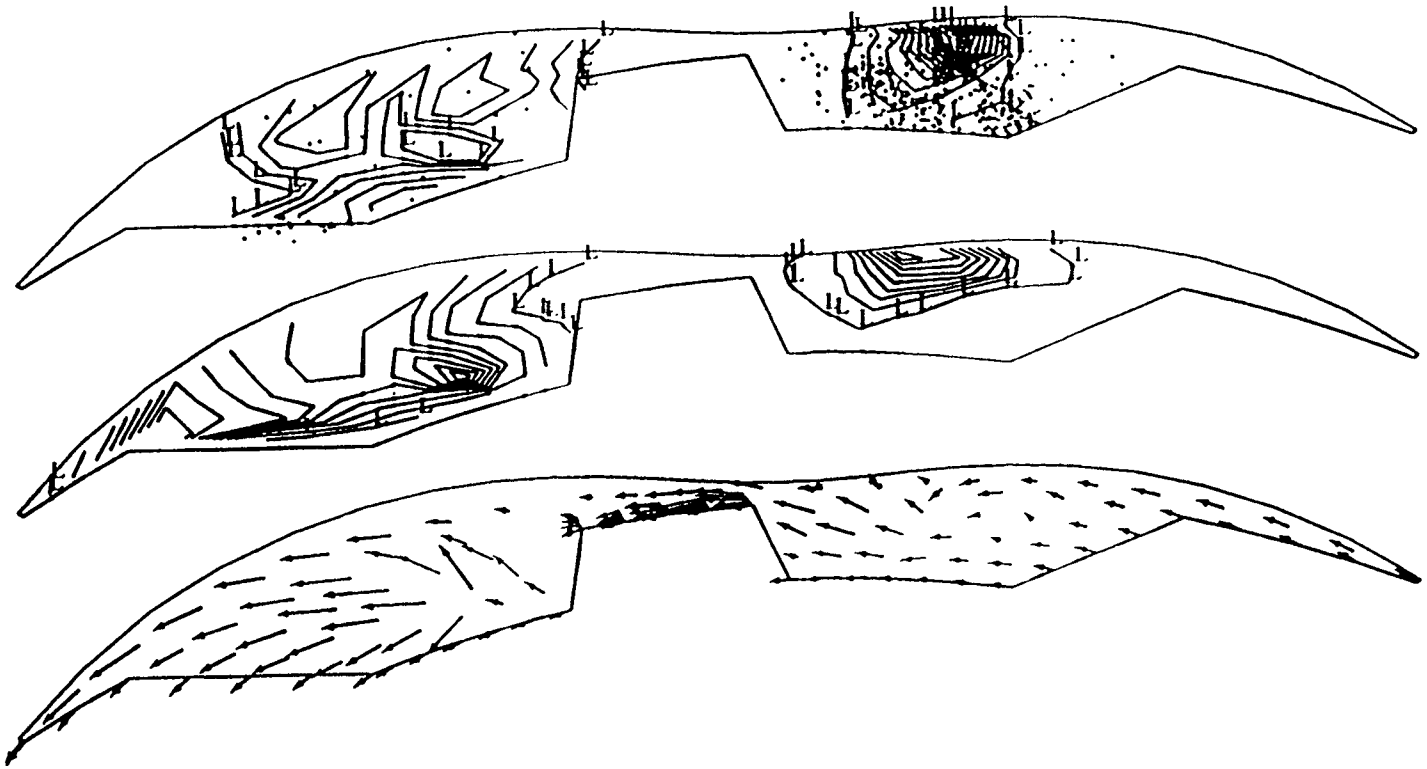
100 m/s
J = 7

Fig. 18(c): Cross-section view of combustion chamber along symmetry plane show-



FUEL/AIR RATIO, interval = 0.1000E-01
H = .1200 ; L = .3000E-01
TEMPERATURE, interval = 155.6 K
H = 2100. ; L = 700.0

100 m/s

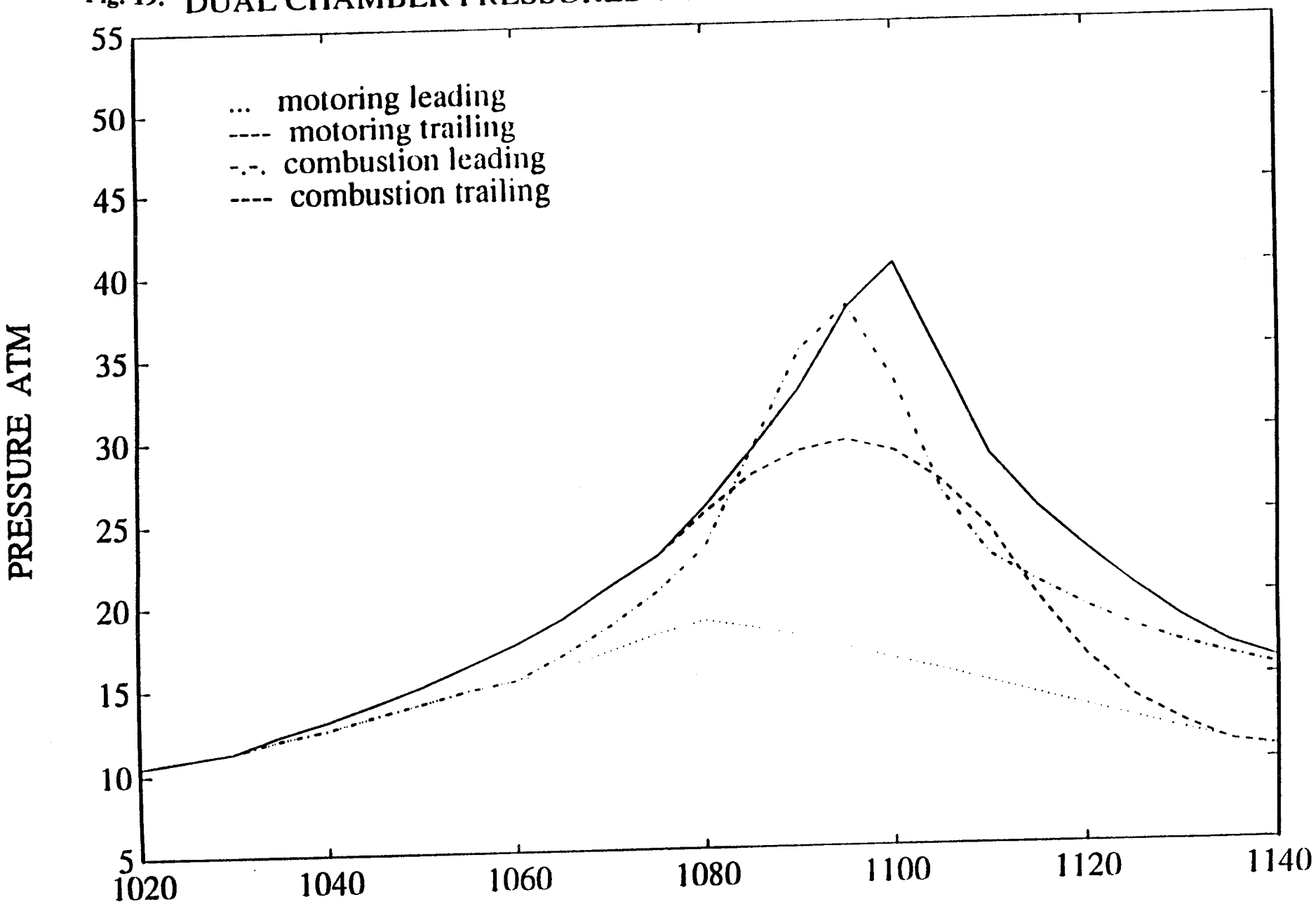


FUEL/AIR RATIO, interval = 0.1000E-01
H = .1200 ; L = .3000E-01
TEMPERATURE, interval = 155.6 K
H = 2100. ; L = 700.0

100 m/s
J = 7

Fig. 18(e): Cross-section view of combustion chamber along symmetry plane show-

Fig. 19: DUAL CHAMBER PRESSURES WITH AND WITHOUT COMBUSTION



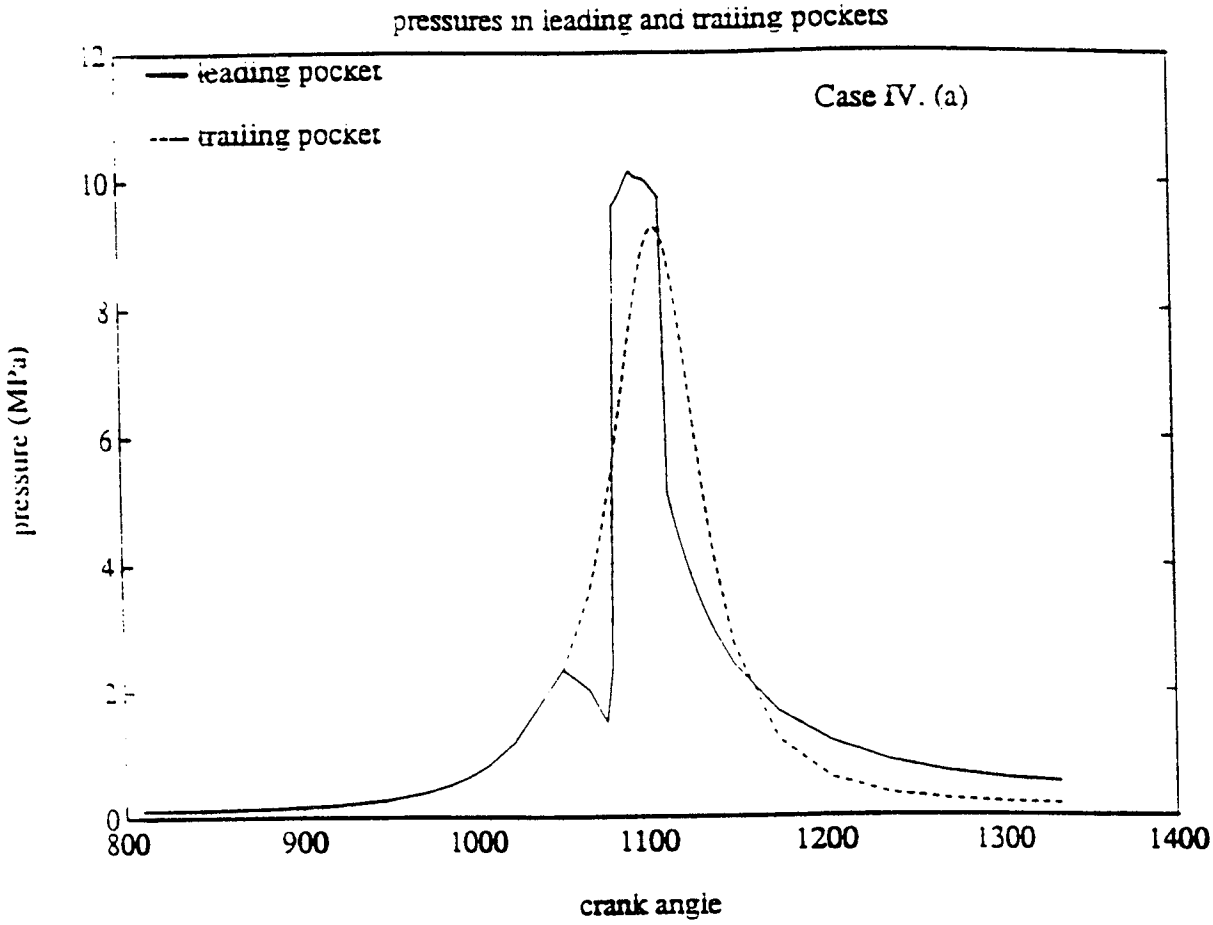
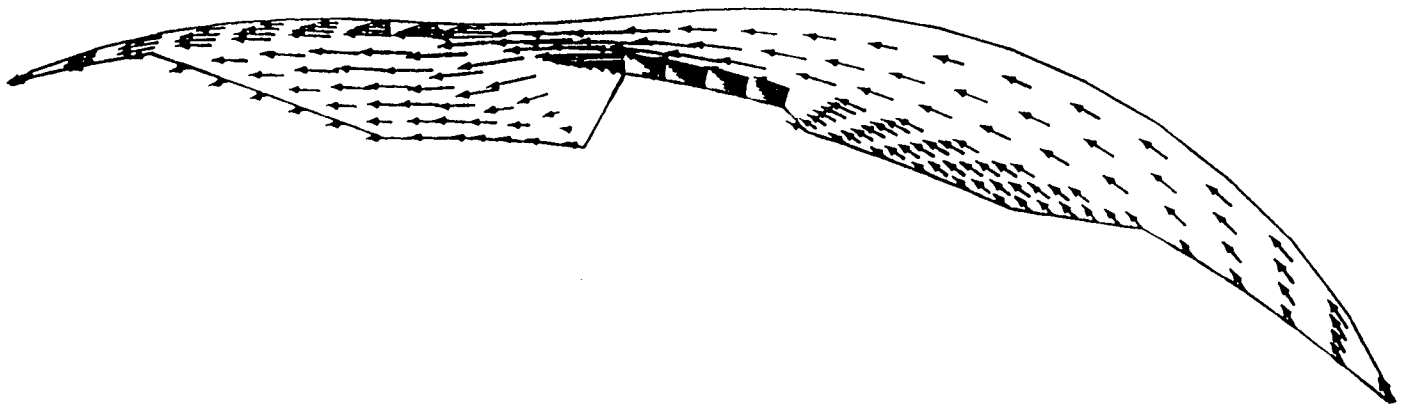


Fig. 22 (a): Computed pressures in the leading and the trailing pockets at high load (about 200 PSI IMEP) with 25% of fuel injected into trailing pocket and 75% of fuel injected into the leading pocket - Case (a)

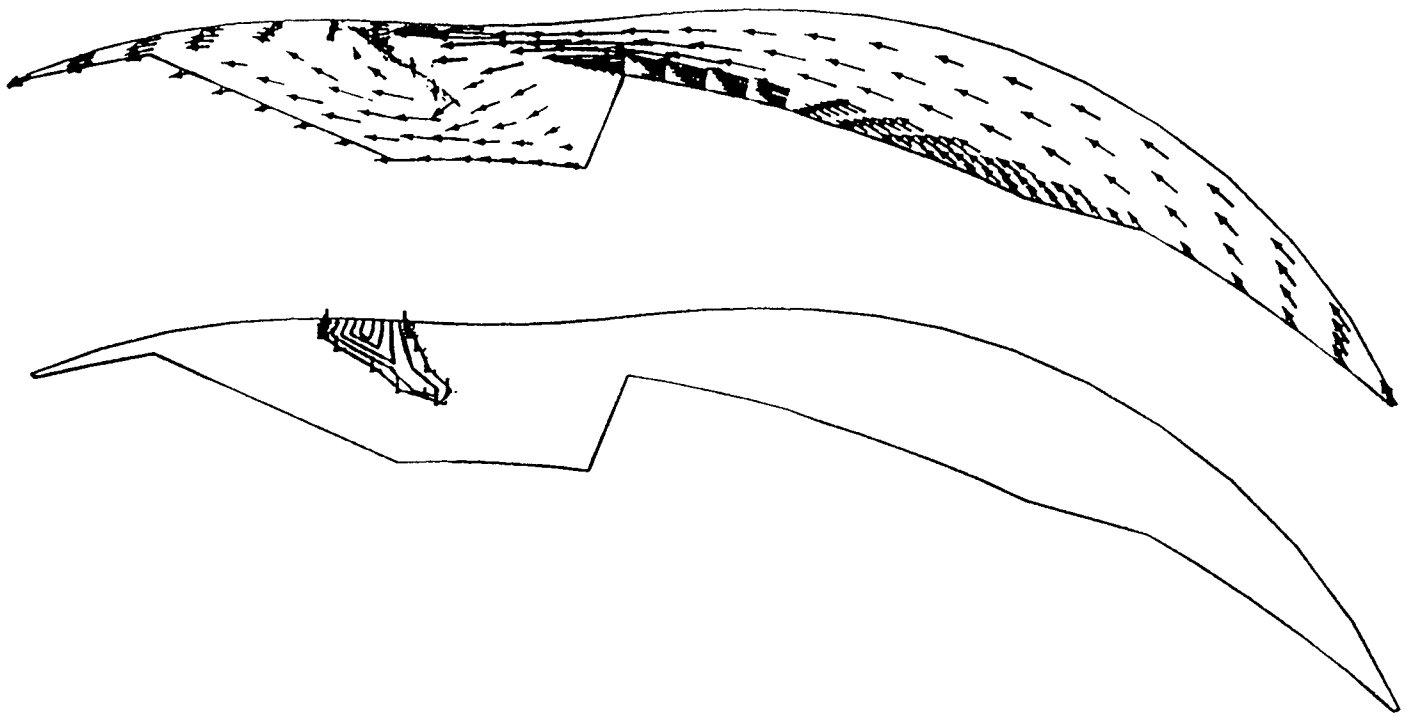


100 m/s
vertex limits of the region: (1, 7, 1) to (25, 7,11)

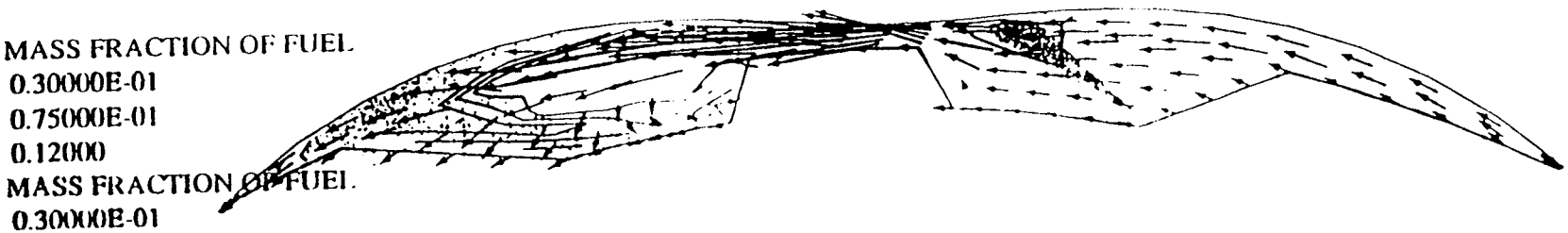


MASS FRACTION OF FUEL, interval = 0.18000E-01
H = 0.12000 ; L = 0.30000E-01
vertex limits of the region: (1, 7, 1) to (25, 7,11)
crank angle = 25.0

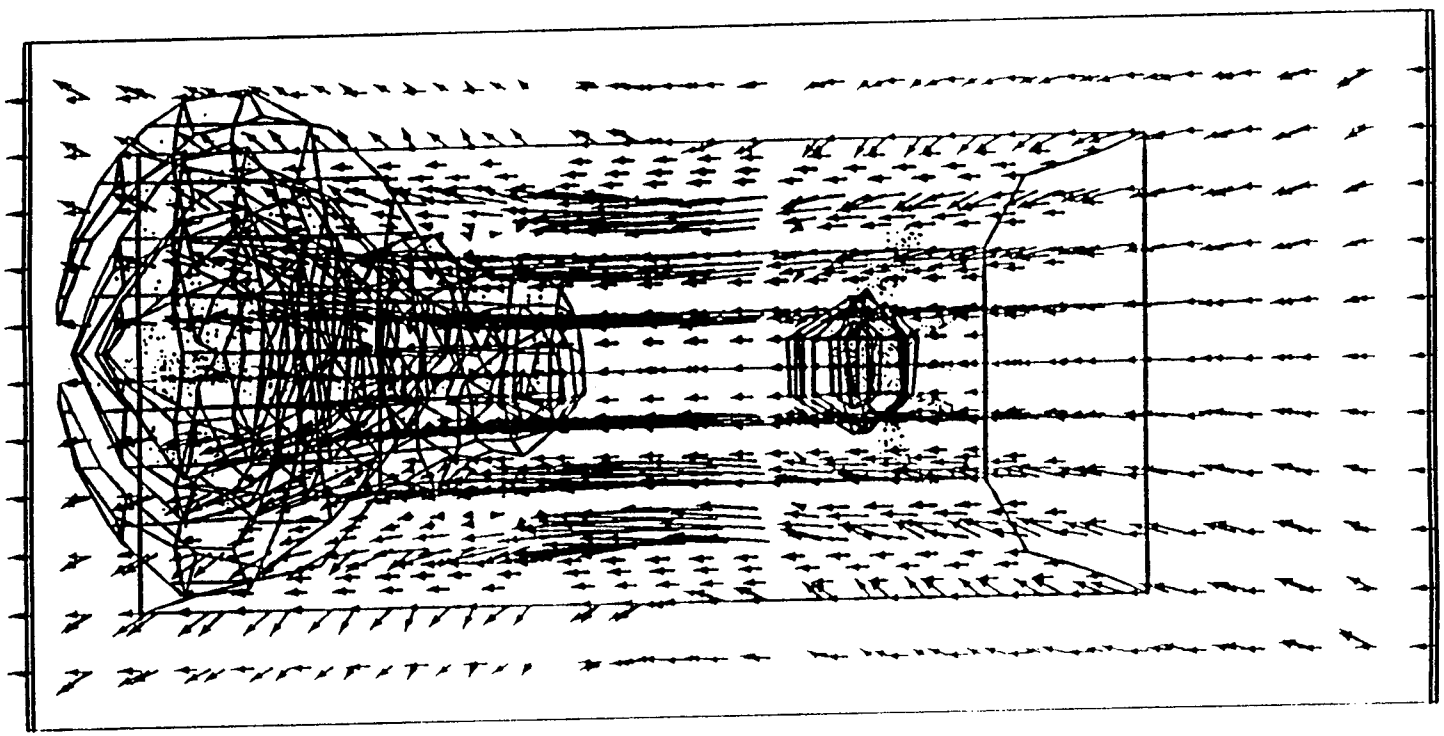
Fig.26(b): Particle and fuel/air distribution in the chamber at 1165 CA



100 m/s
MASS FRACTION OF FUEL, interval = 0.18000E-01
H = 0.12000 ; L = 0.30000E-01



(a)



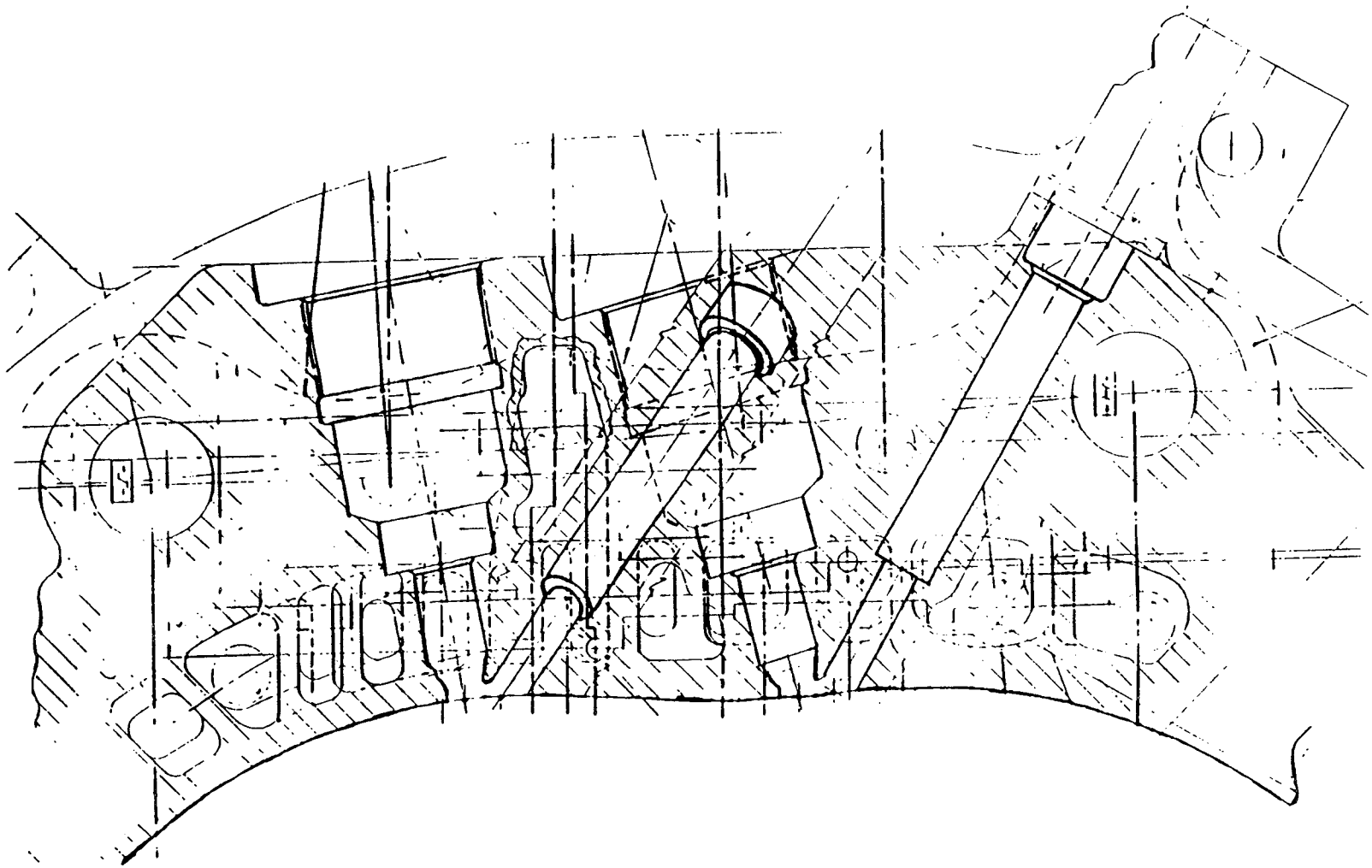
(b)

100 m/s

100 m/s

vertex limits of the region: (1, 1, 1) to (25,13, 8)

Fig.32 DUAL POCKET ROTOR HOUSING



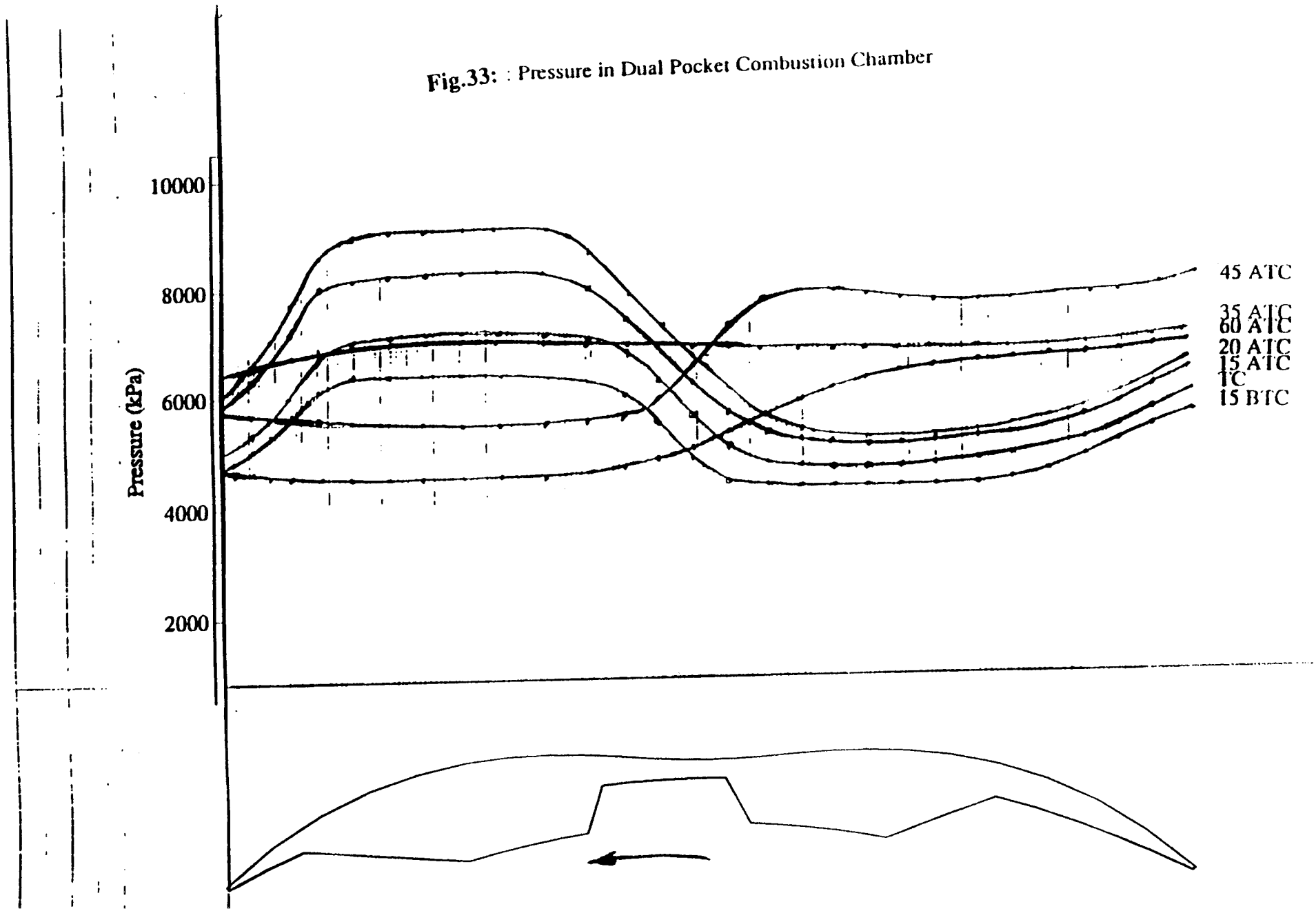
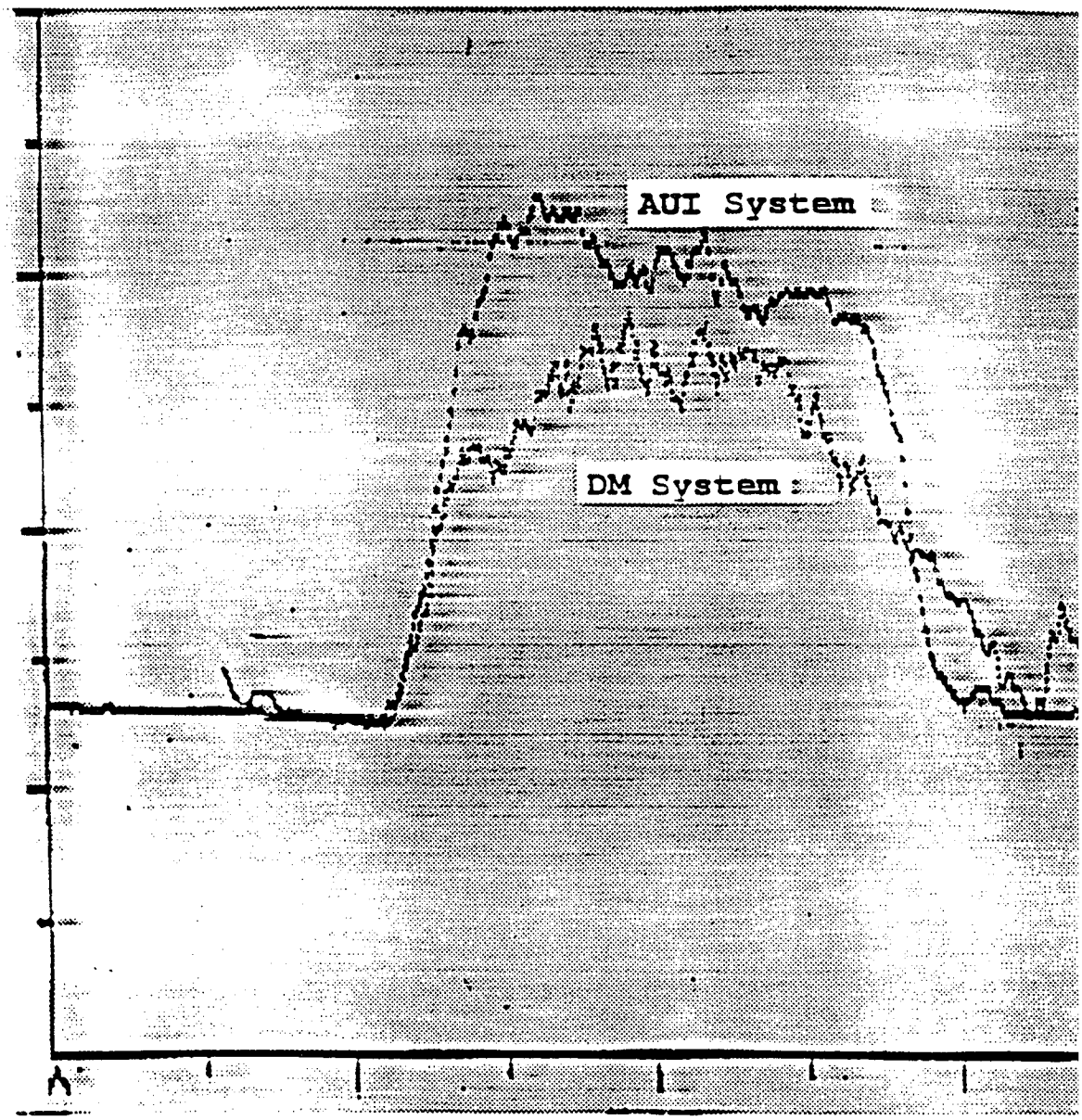


Fig.33: : Pressure in Dual Pocket Combustion Chamber

Fig.34 # Injection rate comparison

Stanadyne DM and AUI systems

8000 Rpm, 80 mm^3



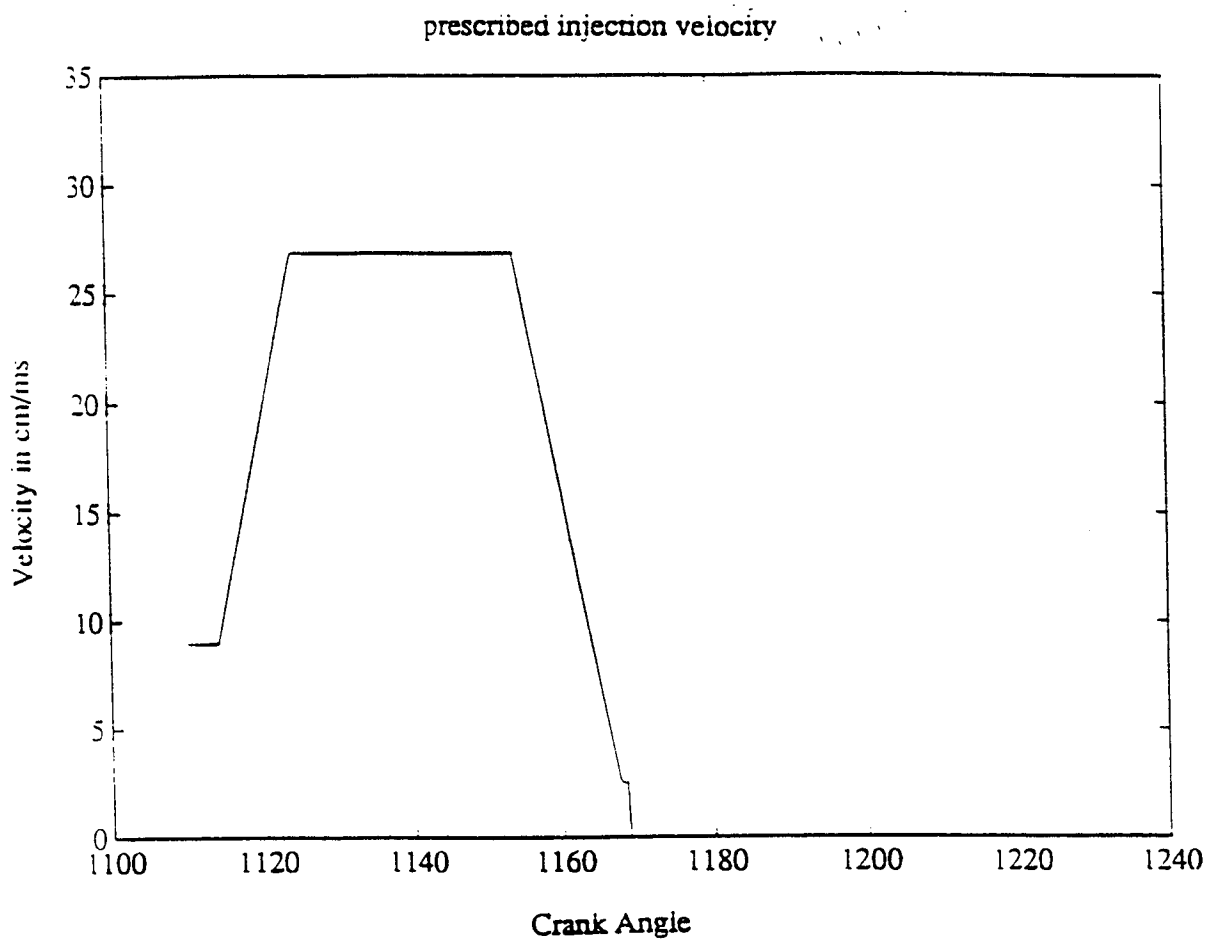


Fig. 35(a): Prescribed injection velocity for the AUI injection system

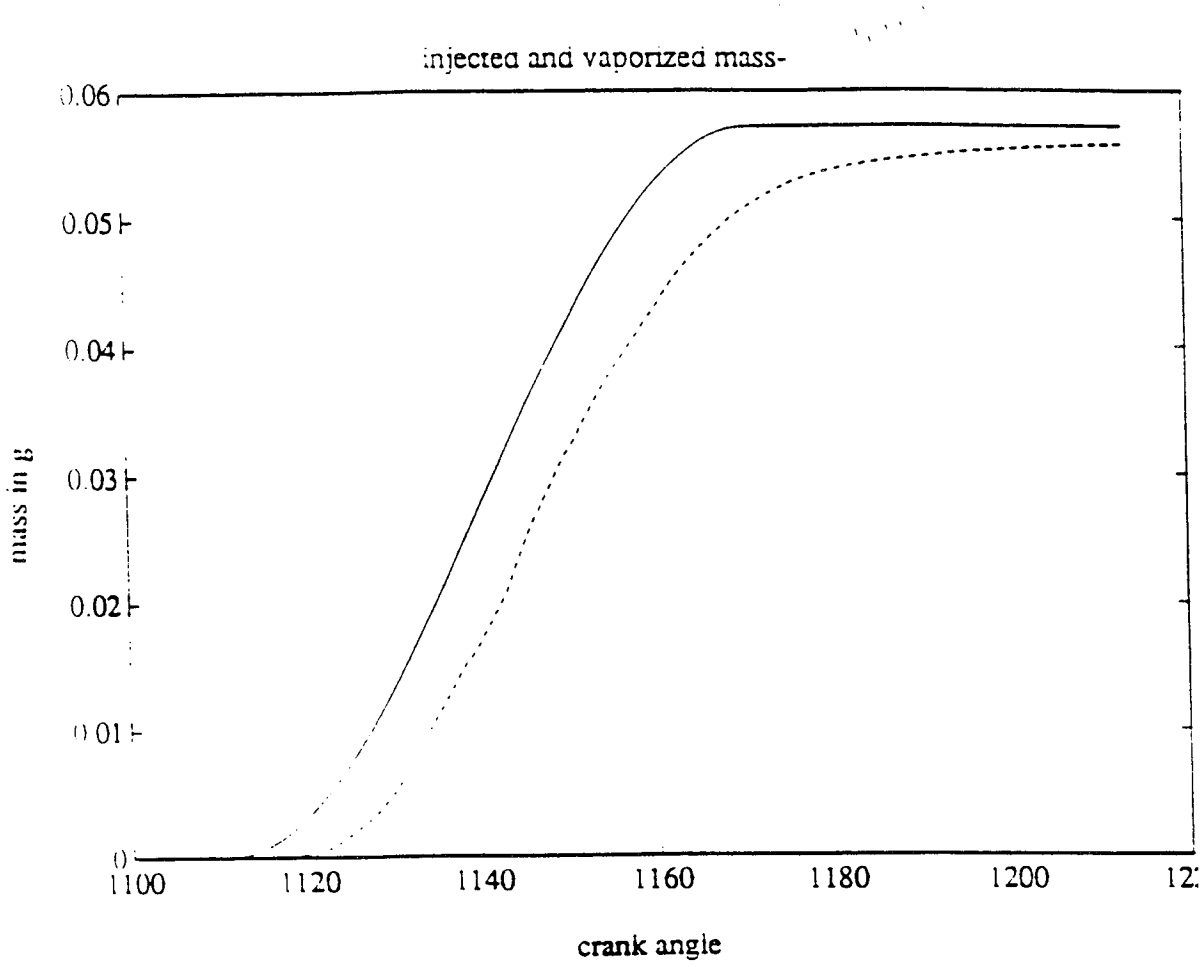


Fig. 36(a): Injected (------) and vaporized(-----) mass of fuel for the AUI system

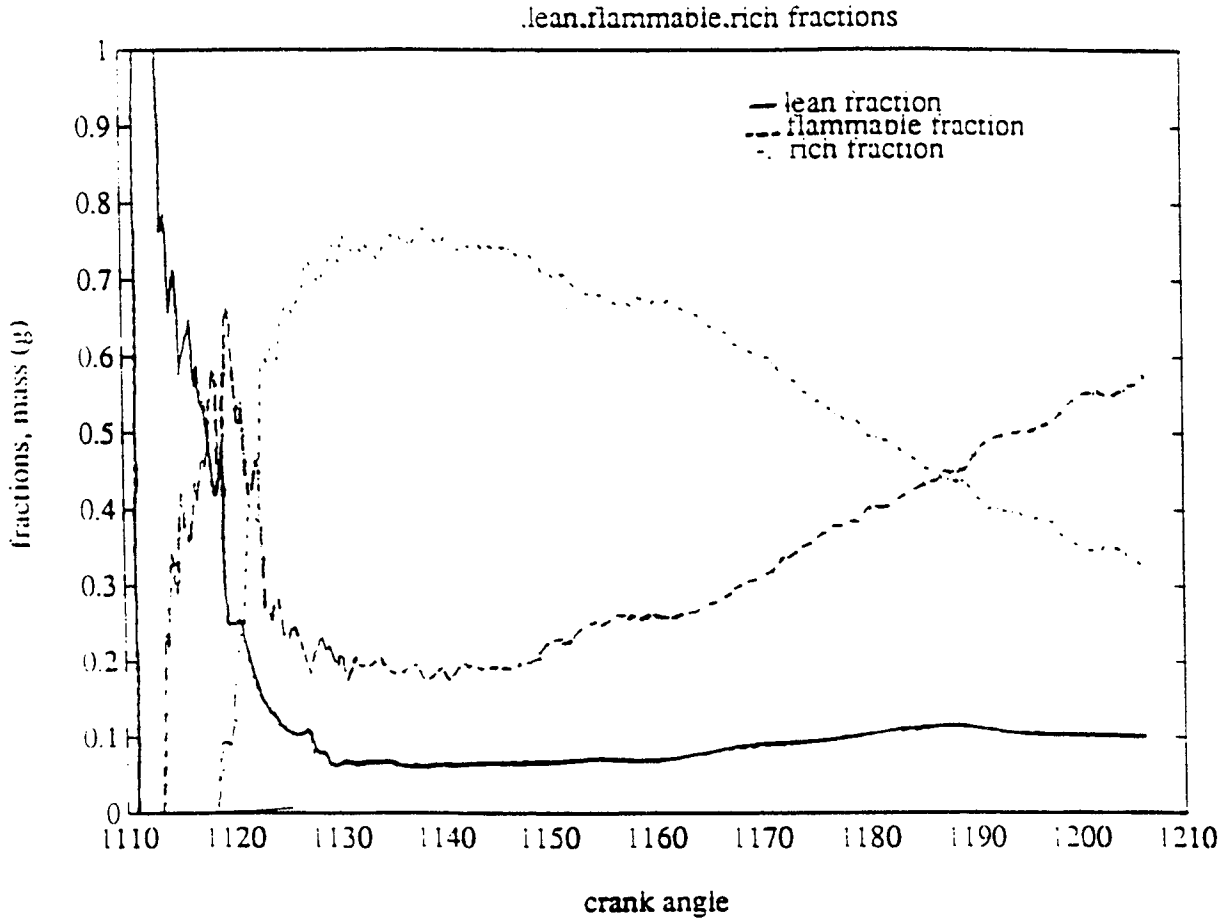


Fig. 38(a): Lean,Rich and Flammable fractions of vaporized fuel as a function of crank angle for the AUI system

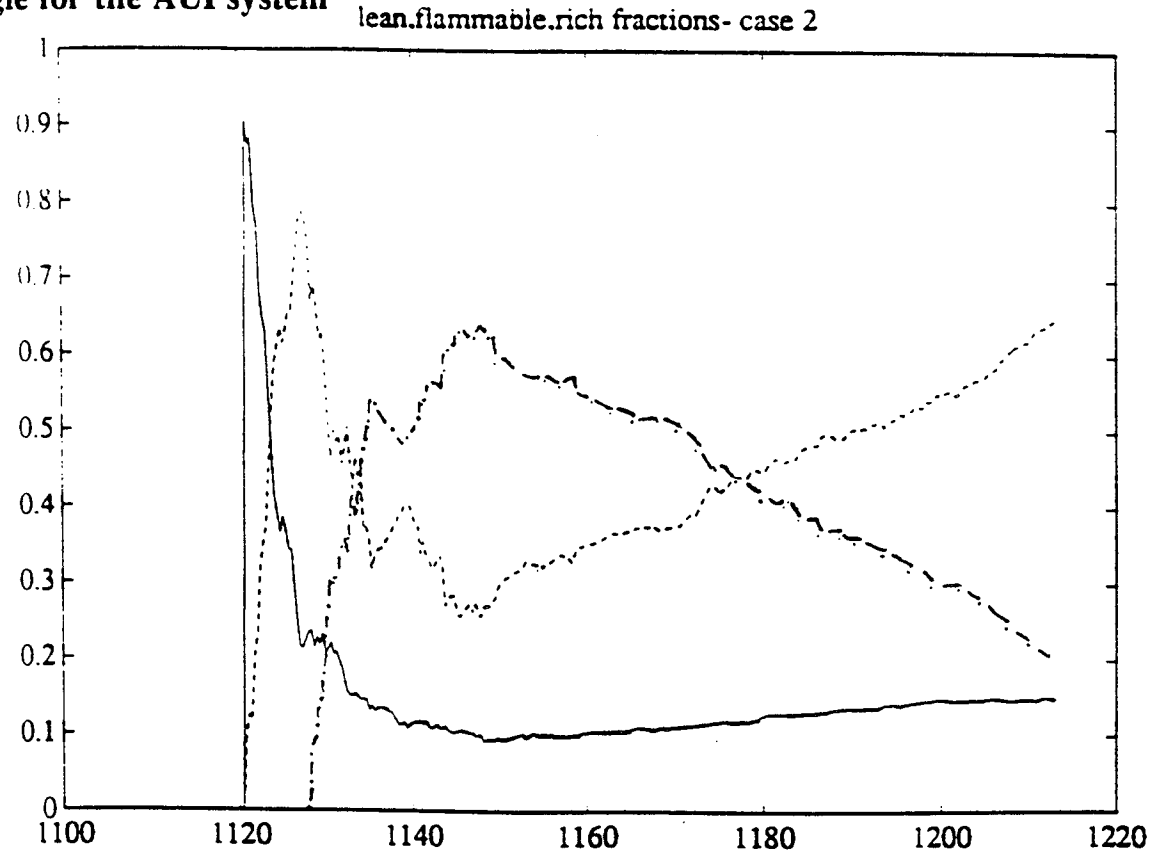
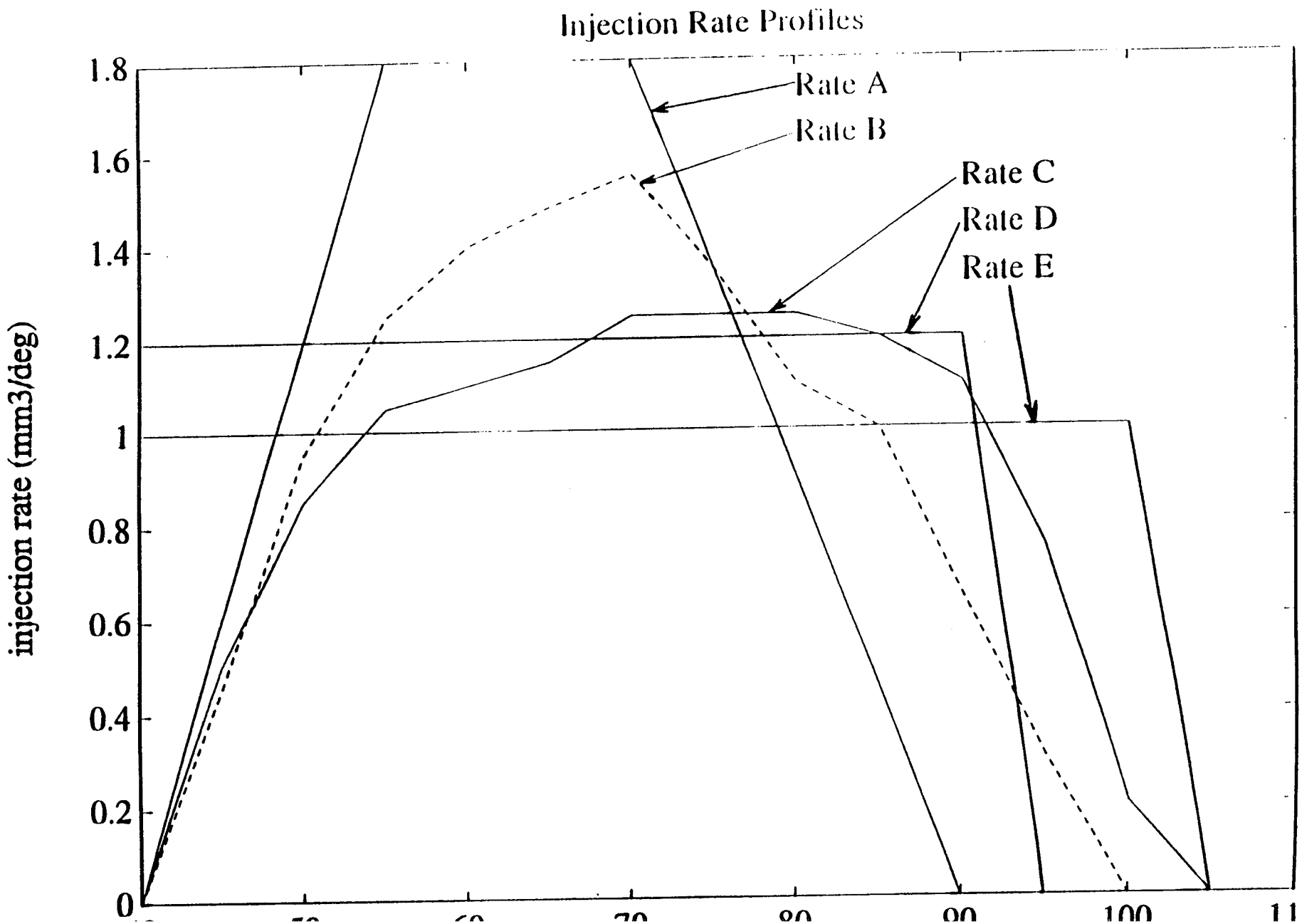


Fig. 38(b): Lean,Rich and Flammable fractions of vaporized fuel as a function of crank angle for the AUI system


Injection Rate Profiles
injection rate (mm3/deg)
Rate A
Rate B
Rate C
Rate D
Rate E
1.8
1.6
1.4
1.2
1
0.8
0.6
0.4
0.2
0
90
100
110

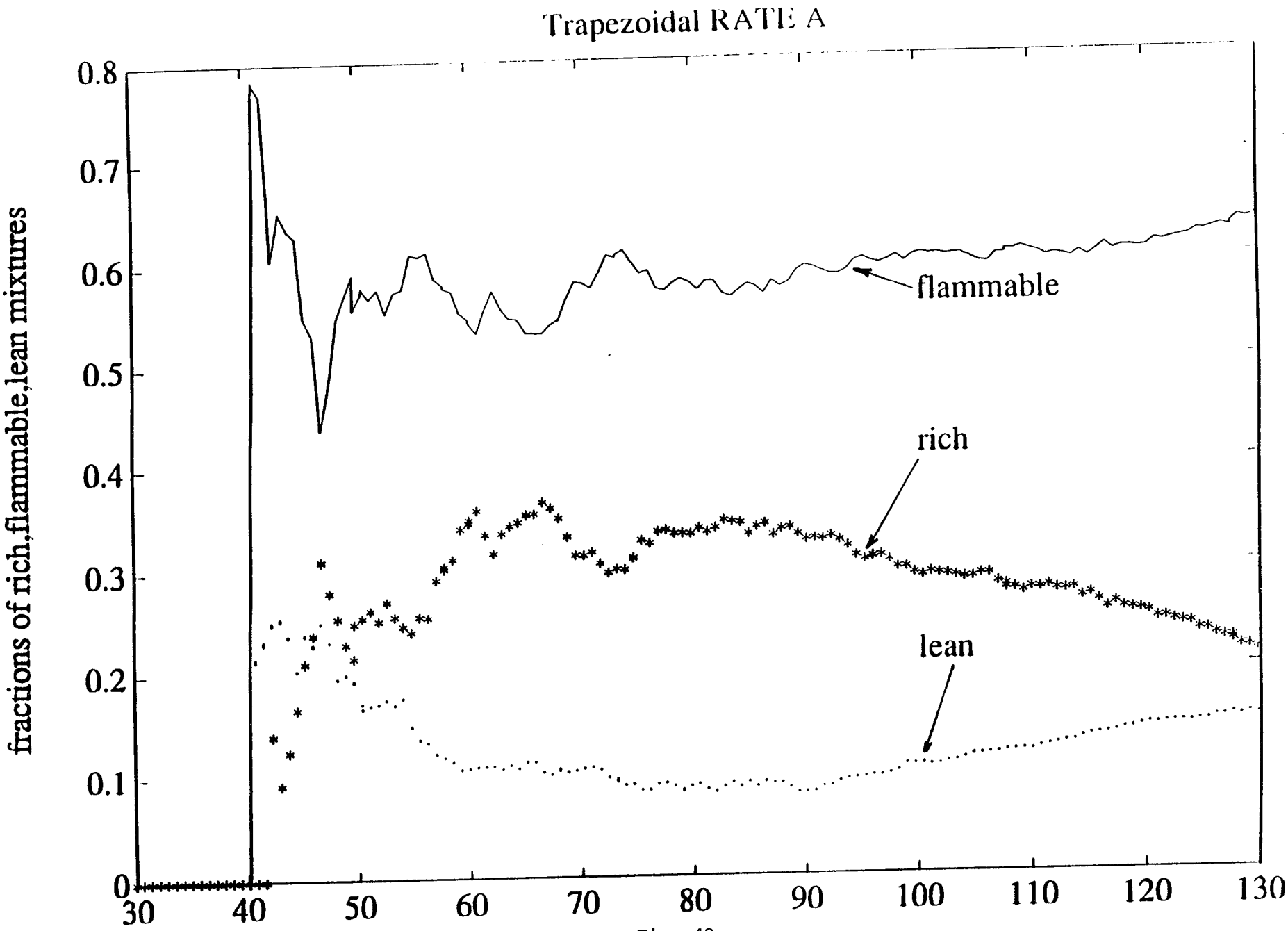

Trapezoidal RATE A
fractions of rich,flammable,lean mixtures
0.8
0.7
0.6
0.5
0.4
0.3
0.2
0.1
0
30
40
50
60
70
80
90
100
110
120
130
flammable
rich
lean

Fig. 42

fractions of rich,flammable,lean mixtures
0.8
0.7
0.6
0.5
0.4
0.3
0.2
0.1
0
flammable
rich
lean
AMBAC PUMP RATE B
100
90
80

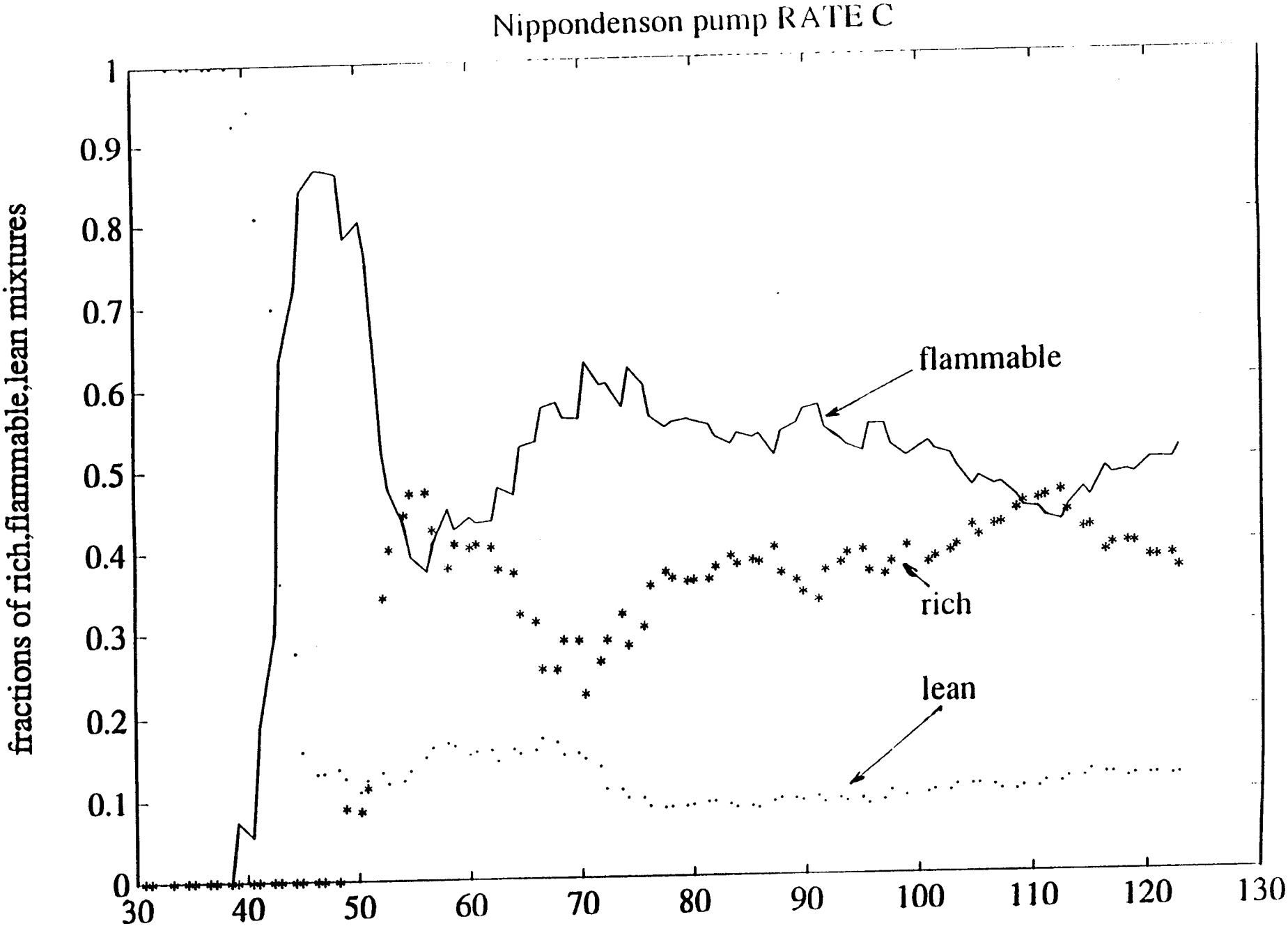
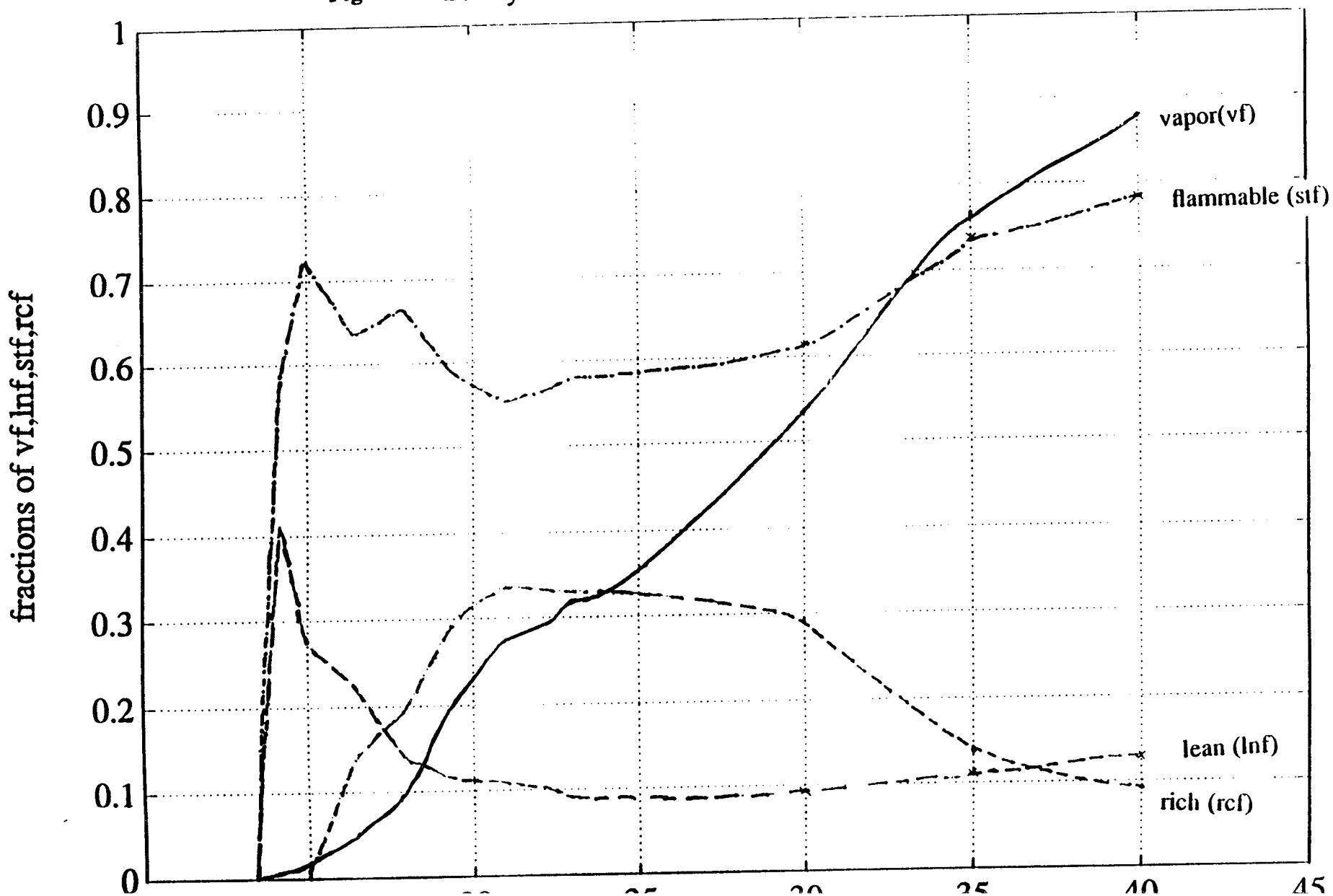

Nippondenson pump RATE C
fractions of rich,flammable,lean mixtures
flammable
rich
lean
0
0.1
0.2
0.3
0.4
0.5
0.6
0.7
0.8
0.9
1
30
40
50
60
70
80
90
100
110
120
130

Fig. 44

Fig.47: Study of Effect of L/D ,reference case 1



4.0 CRITICAL TECHNOLOGIES

PRECEDING PAGE BLANK NOT FILMED

4.1 ADVANCED FUEL INJECTION SYSTEMS

PRECEDING PAGE BLANK NOT FILMED

PAGE 96 INTENTIONALLY BLANK

4.1 ADVANCED FUEL INJECTION SYSTEMS

INTRODUCTION

Fuel injection system research focused on identifying candidate systems for operation at high engine speeds and on supporting engine development tests.

Fuel injection system developers were surveyed in an attempt to identify a candidate fuel injection system suitable for operation with the Stratified Charge Rotary Engine (SCRE) at engine speeds exceeding 8000 RPM. A new concept based on a rotating valve which has the capability of very high injection frequencies and great flexibility in injection timing and injection rate shaping was selected. A feasibility analysis of the concept revealed no major impediments to further design development.

Engine testing and development of existing fuel injection systems was supported with NDenso A-Pumps and AMBAC M100 pumps. Injection rates were measured and engine tests were performed which indicated that the SCRE is relatively insensitive to fuel injection rate shape. Injection durations were shortened for use with the re-entrant and dual rotor combustion pocket concept tests. The pilot injection system was retuned and nozzle cooling improved to allow further development and refinement of the dual orifice pilot injection system.

The power output of the 70 Series Stratified Charge Rotary Engine (SCRE) has historically been limited by the fuel injection system. The rotary engine is inherently balanced and engines of this size can operate easily at speeds up to 10,000 rpm--racing engines have been run even faster.

The fuel specified for this engine (Jet A) has very little resistance to combustion so the residence time of the fuel in the combustion chamber must be kept to a minimum. If the residence time of fuel is small, a rotary engine can theoretically be run on conventional diesel and jet fuels and gasoline. JDTI has considerable experience running rotaries on Diesel and Jet-A and limited experience with gasoline, JP- 4, and JP-8.

The low residence time requirement dictates direct injection of the fuel into the combustion chamber. In addition to merely providing the fuel to the combustion chamber, the fuel injection system must distribute the fuel appropriately in the combustion chamber to facilitate fuel/air mixing. The system must also be capable of supplying the fuel over appropriate time intervals in order to control engine pressure rise rate and peak combustion pressure.

Techniques for directly injecting fuel into the combustion chamber are highly developed because of their use in diesel engines. Unfortunately, diesel engines are slow by comparison to the rotary with the highest speed diesel engines operating around 5000 RPM on a four stroke cycle. From the fuel injection standpoint, the rotary engine operates like a two stroke engine, so that instead of one injection being supplied for every second revolution of the

engine crankshaft one injection is required for each revolution of the engine crankshaft. Figure 1 shows the speed and fuel delivery requirements of the rotary engine compared to those of production diesel engines. The injection frequency for the small rotary is 5 times the maximum injection frequency of a diesel engine requiring a similar quantity of fuel per injection. Conventional fuel injection systems must be highly modified in order to operate with this rotary engine.

Considerable progress has been made toward providing a fuel system for the SCRE during two previous NASA contracts, NAS3-23056 and NAS3-24628. The fuel systems for the first engines consisted of two modified Stanadyne DM fuel injection pumps. These pumps are of the distributor variety, where one set of pumping elements is used to supply the fuel to up to 8 cylinders of a conventional engine. The output from the pumping elements is directed to each cylinder in turn by a rotating distributor valve, which may be integral with the pumping element. By eliminating the distributor function so that all output goes to one injector, high speeds are easily attainable. The DM pumps are limited to relatively small fuel delivery quantities, so engine torque and power output were limited. A higher output fuel system was necessary.

The next fuel system used on a SCRE was an Accumulator Unit Injector system designed and fabricated by Stanadyne. It utilized a solenoid valve and hydraulic servo circuit to modulate fuel being delivered from a high pressure rail. This system provided adequate fuel delivery and complete flexibility of injection timing and average injection rate. No improvement in engine performance was observed even with this added fuel system flexibility. The system was a unique prototype and suffered problems with reliability and durability which interfered with running the engine.

A more reliable fuel system was needed to support engine testing. Previous experience with AMBAC M200 pumps showed the feasibility of running multi-plunger "jerk" pumps up to 8000 injections/minute. A version of Nippondenso's A-Pump capable of operating at speeds up to 8500 RPM was developed. This pump proved reliable and provided adequate performance in terms of injection frequency and fuel quantity delivered. The A-Pump is limited to peak injection pressures of 9000 psi (62.01 mPa), which may not be sufficient to obtain best engine performance with some combustion chamber configurations. The 9000 psi (62.01 mPa) pressure limit is most likely to be detrimental to high power operation. The injection rate shape of the A-Pump based system is difficult to modify.

The following tasks were initially planned for the current contract.

1) Perform injection rate measurements on the existing injection systems in order to understand the effects of fuel injection rate on performance.

2) Develop a system for testing the benefits of higher injection pressure on the single rotor rig engine early in the program.

3) Support two rotor rig testing with a two rotor version of the existing single rotor Jerk pumps. A system for testing higher injection pressures or modified injection rate on the two rotor engine is expected to require considerable effort and not to be available until very late in the program. It is expected that any air system test work can be performed on the two rotor rig without the optimum fuel injection system if necessary.

4) Study the available fuel injection concepts in order to determine the best candidate fuel system for the two rotor rig engine. Procure and engine test the best system during the course of the program.

As a result of the program redirection as discussed in Section 2.0, the fuel injection effort was reduced. Hence, Task 3 was reduced in scope with no two rotor testing and Task 4 studies were terminated.

OBJECTIVES

The performance objectives of a fuel system for the SCRE are

- Injection frequency of 8000 injections/minute minimum with growth to 10,000 injections/minute.
- Maximum main fuel delivery of 100 mm^3/injection minimum.
- Pilot fuel delivery of approximately 5 mm^3/injection.
- Minimum main fuel delivery of 5 mm^3/injection
- Useful life of 2000 hours.
- Not adversely affected by low temperatures and low pressures
- Multi-fuel capability
- Flexibility in injection timing, pressure, and rate shape. These parameters should be easily modified.
- Minimized drive power
- Lightweight
- Minimized peak drive torque
- Small intrusion into the rotor housing to simplify rotor housing cooling and improve rotor housing structural integrity.

- Failure modes which cause loss of engine control or loss of engine power must be minimized.

TECHNICAL APPROACH

Consideration and selection of the SCRE fuel injection system and the required characteristics of the system was divided into the four parts shown below:

1. Fuel System Survey

A survey of possible fuel injection systems for the SCRE was performed.

2. A-Pump Development

A-Pumps were used to support most of the engine development during the Phase III program. A two rotor A-Pump capable of 8000 injections/minute was developed for use with the 2 rotor engine. Fuel System configuration modifications were required in order to support improved engine configurations with enhanced combustion. Pilot fuel system development was required in order to obtain data with the dual orifice pilot nozzle system.

3. AMBAC M100 Injection System

An AMBAC M100 fuel system was procured in order to test the effect of higher injection pressure on engine performance and to provide shorter injection durations for some modified rotor configurations.

4. Injection Rate: Measurement and Shape

A long tube type injection rate measuring system was procured and utilized to measure the injection rates of the Stanadyne DM pumps, the AUI system, many configurations of the A-Pump, and the M100 pump.

Modifications were made to the A-pump to provide an injection rate shape matched to that of the Stanadyne DM pump in order to determine the effect of the rate shape on engine performance.

RESULTS

Fuel System Survey

Performance and packaging objectives for a fuel system for the SCRE were selected. Evaluation weights were applied to the objectives based on estimation of their importance in meeting the overall goals for an aircraft version of the SCRE (see Table 1). Six different fuel system candidates were considered for the future of this application.

The first system considered was the M100 pump with splitter valve described below. The major difficulty with this system for this study is the inability of the M100 to supply fuel to more than one rotor. There have been high speed M100 pumps tested in the past which could perhaps supply fuel to a 2 rotor engine at speeds up to 8000 injections/minute, but beyond that new designs with multiple hydraulic heads become necessary. These add considerable size and weight to the system. A secondary disadvantage of the M100 is the relative lack of timing and rate flexibility provided by this pump. For more details on the M100 system see below.

The second system considered was an improved jerk pump in which start and end of injection are controlled by a metering sleeve (See Figure 2). By moving the sleeve up and down the pumping position on the camshaft is altered and hence so are injection rate and timing (for details see section on injection rate below). A timing device added to the front of the injection pump allows independent control of injection timing. This system suffers from excessive size and weight, and some lack of timing flexibility depending upon the design of the timing device. The normal 10 degree advance timing device utilized on conventional diesel engines is not adequate for the rotary engine, which requires 40 degrees of advance in the current configuration. A fuel system used in combustion development benefits from additional timing flexibility until about 90 degrees of flexibility is achieved, since it is difficult to predict the proper timing for use with modified combustion chambers.

A third system considered was the use of conventional camshaft driven unit injectors (Figure 3). These are an improvement in capability over the previous systems, but still suffer from some limitation in timing capability. The packaging problem is considerable, since a camshaft would have to be designed into the hot side of the engine and sealed so as to contain oil. Fuel needs to be routed to the injector and leakage fuel returned to the tank. Any design would have to consider the necessity of frequent nozzle changes during engine development.

Fourth is a medium pressure common rail system (Figure 4). Fuel is supplied at an intermediate pressure in the range of 1000 to 5000 psi (6.89-34.45 mPa). The fuel charges an intensifier in the nozzle. When injection is required a solenoid is turned on which allows access to the low pressure side of the intensifier. The fuel charge is pressurized and fills an accumulator in the nozzle. The solenoid is de-energized, allowing the fuel in the low pressure side of the intensifier to bleed back to the tank. The pressure in the high pressure side of the intensifier is reduced, allowing the nozzle needle to lift and the fuel to be injected.

Weaknesses of this technique for use with the Rotary are the high fuel flow rates involved and the relatively inflexible injection rate shape.

The fifth system considered was a high pressure common rail system (See Figure 5). This system operates identically to the medium pressure common rail system except that the fuel is supplied at full injection pressure and the accumulator piston is not used. Direct solenoid control of the high pressure fuel allows both the start and end of injection to be controlled by the solenoid. A system like this was developed by Stanadyne and tested in an earlier program; details are provided in the section on injection rate.

The final system considered was a high pressure common rail system Appendix B, "Feasibility Analysis-Rotating Valve High Pressure Common Rail System" in which the fuel is turned on and off by a rotating metering valve, which is timed to the engine either mechanically or electronically. The metering valve eliminates the need for very high speed and precision solenoids. In addition, the depth of the slot in the metering valve can be controlled to facilitate injection rate shaping.

After rating each of the fuel systems for potential to meet the requirements of rotary engine fuel system (as defined in Table 1) a K-T analysis was performed. The results are as indicated in Figure 6. The rotating valve high pressure common rail fuel injection system appears to have the most potential for providing the best fuel injection for the SCRE.

A-Pump Development

Figure 7 shows a typical A-pump and its theory of operation. Pressurized fuel from the injection pump gallery fills the space above the plunger through the barrel port (1). The plunger moves upward until it closes off the barrel port for the start of injection (2). Further upward travel of the plunger causes fuel to be forced upward, lifting the delivery valve off of its seat and flowing outward through the injection line and nozzle (3). The plunger continues to move upward until a spill helix re-opens the barrel port. At this point the pressure above the plunger drops. The delivery valve returns to its seat, retracting a measured amount of fuel from the injection line and quickly dropping the pressure in the line (4). The quantity of fuel retracted by the delivery valve is determined experimentally to provide a residual pressure in the injection line when the delivery valve is seated, but not so much residual pressure as to force the injection nozzle to open a second time when the pressure wave from shutting the valve reaches it (a phenomenon known as a secondary injection).

In addition to the four single plunger pumps procured under the NASA Phase II program, three multi-plunger pumps have been procured which are capable of operating a two rotor engine at speeds up to 8000 RPM (slightly higher speeds can be obtained by simple governor modifications).

In order to make the multi plunger pump operate at the high speeds required for the rotary engine, we modified the camshaft to provide two lifts per cam lobe per revolution, installed a high force return spring, and increased the gallery pressure to 50 psi (0.344 mPa).

During the course of engine testing we experienced severe secondary injections at heavy loads with the four and five hole injection nozzles. The secondary injections are a consequence of increasing the injection line inner diameter (ID) from 1.2 mm to 1.5 mm, which was done in order to prevent exceeding the 9000 psi (62.01 mPa) pressure limit of the A-Pump. The solution used for this program was to increase the retraction of the delivery valve from 55 mm^3 to 80 mm^3. The increased retraction is not adequate at light loads and low speeds because the retraction is excessive and cavitation occurs. Flats cut on the delivery valve improved the situation, but did not solve it. Using large retraction volumes is inherently a poor solution because it lowers the efficiency of the pump--in order to inject 50 mm^3 of fuel we must now pump 130 mm^3.

Experience gained in the rate shaping test led to a means of eliminating the secondary injections. By changing the lift to port closing dimension on the pumping plunger (either by shimming the existing plunger or manufacturing new plungers) the rate of pumping can be decreased. A sufficient decrease in the rate of pumping allows using the original 1.2mm injection line diameter and using the original 55mm^3 retraction delivery valves without causing secondary injections.

The reduction in pumping rate also causes an undesirable effect of changing the shape of the injection rate versus crank angle curve. Test data indicates that the change in injection rate versus crank angle will not degrade engine combustion and the increased pumping efficiency may improve engine operating efficiency very slightly.

A dual orifice pilot nozzle was tested and found to be quite beneficial for reducing fuel consumption. On the first engine the fuel system developed a severe nozzle seat cavitation erosion problem which caused degradation of engine performance after as little as 30 minutes of operation. A secondary problem of excessive pilot nozzle tip temperature caused frequent plugging of the pilot nozzle orifices with carbon. These problems are discussed in more detail in a detailed test report submitted to NASA LeRC as part of the contractual reporting entitled "Investigation Into Changes in Engine Light-Off Performance Using the 2 Orifice 'Rabbit Ear' Pilot Configuration", 30 April 1991. The second engine which had a dual orifice pilot incorporated a re-tuned pilot injection system and decreased pilot nozzle tip clearance. The re-tuned pilot system was trouble free throughout the 14 hours of the engine test.

The fuel systems for the two rotor engines were designed using the technology available at the beginning of the contract. The fuel systems therefore do not include the two improvements discussed above.

The two rotor rig engine designed for the phase III program is based on existing production engine designs, and therefore has a gear train for driving one injection pump. The fuel

injection pump must supply both pilot and main injection for each of two rotors. This is achieved by installing two main plungers and two pilot plungers in the pump, and appropriately phasing the camshaft lobes. The pilot plungers have a flat helix, so the amount of pilot delivery is fixed for any given pump. The phasing between the pilot and main injections can be modified by shutting down the engine and changing the thickness of shim between the plunger and the tappet. The shim has the effect of changing the starting and ending lift of the pumping stroke and therefore the injection timing.

The limitations of fixed pilot fuel delivery and pilot to main phase angle are judged to be acceptable for the two rotor rig engine. The major portion of development work on this engine involves the air delivery system, where fuel injection changes make only a minimal amount of difference. Fuel system and combustion development will continue to be performed on the single rotor rig engine.

During development of the system several real world problems were discovered. The wide range of speeds and large turndown ratios cause some difficulty in avoiding secondary injections and delivered quantity variations throughout the operating range. These difficulties are an inherent part of the pump line nozzle injection system due to the large volumes of fuel between the pumping element and the nozzle spray orifice.

Figure 8 shows the range of pilot fuel deliveries where acceptable fuel injection quality is obtained as a function of engine speed. If too much pilot fuel is delivered at high engine speed secondary injections occur. These injections can accelerate pilot nozzle coking, degrade fuel consumption, and cause excessively smoky exhaust emissions. More fuel can be delivered by increasing the nozzle orifice area, but this has deleterious effects on combustion performance. Fortunately, the NASA rig engine seems to operate well on pilot quantities which can be delivered without secondary injections.

If slightly too little fuel is injected through the pilot injector vapor bubbles can be formed in the injection lines between injections. These bubbles collapse under injection pressure, causing cavitation erosion of the walls of the tubing. In severe cases the tubing wall can rupture in as little as ten hours of operation. This situation caused us some difficulty with the dual orifice pilot system as discussed above.

As the delivered quantity is reduced further the system becomes unstable, so that the injected quantity and timing no longer repeat accurately from one injection to the next.

It is noteworthy that the range of fuel deliveries at which acceptable injection is obtained narrows as the speed is increased. Fortunately, it is possible to select an injection quantity such that the pilot fuel delivery is within the acceptable range throughout the engine speed range. Figure 9 shows the pilot quantity delivered as a function of engine speed.

As seen in Figures 10 and 11 the same injection variation phenomena occur with the main injection system to a smaller degree. Comparing Figures 10 and 11 we see that the region

of secondary injections grows smaller as the nozzle orifice area is increased. We operate on the single rotor rig engine with much larger main delivery quantities by increasing the nozzle orifice area. This is undesirable because it sacrifices combustion performance at the lower speeds and loads in order to allow high speed and load operation. A loss of high speed and load performance is also likely.

Figures 12 and 13 show the injection timings achieved with the two rotor rig pump. Experience with our commercial engine development venture indicates that these timings will operate the engine successfully. We will need to retard the timings at lower speeds in order to obtain the best BSFC and highest torque capability. Conventional fuel injection timing devices are normally of limited range and have only speed dependence. A design layout of an oil pressure operated timing device capable of electronic control was completed early in this program (Reference Drawing LS34507).

AMBAC M100 Injection System

In order to facilitate high speed and power operation and to obtain test data with higher injection pressures, a contract was provided to AMBAC for development of a M100 injection pump capable of running at 8000 RPM on our existing gearbox. The M100 can operate at pressures of up to 15000 psi (103.35 mPa) for short periods of time. The M100 pump is expected to perform reliably at pressures around 12000 psi (82.68 mPa) using our current injection nozzles.

To provide higher speed capability a splitter valve was developed. This technology will allow us to operate the system at speeds up to 10000 injections/minute if such proves to be desirable. The splitter valve can significantly reduce the size and weight of future injection systems by allowing both pilot and main injection from one injection pump outlet. The pilot injection was demonstrated to be repeatable for a wide range of main fuel delivery. The splitter valve is, however, sensitive to the residual pressure in the injection line and requires re-tuning of the system each time main injection nozzles are changed.

A schematic of the splitter valve system is shown in figure 14. The system currently requires a separate pilot supply circuit from the boost pump, but techniques for eliminating this circuit are under consideration.

Figure 15 shows a cross section of the pilot injector with attached splitter valve. Fuel is supplied to the nozzle at 80 psi (0.551 mPa) through a check valve in the fuel supply duct. This fuel charges the pilot pumping cavity to the left of the pilot piston. When the injection pulse is received through the pump inlet, the pilot piston is forced left, pressurizing the fuel in the pilot injector and causing pilot injection. After a sufficient quantity of fuel has been ejected from the pilot nozzle, the main piston is far enough left to open the ports to the main injector and main injection starts. Pilot injection ends when the pilot piston closes off the pilot fill port and comes to rest against the fuel remaining in the pilot pumping cavity. At

the end of main injection the spring returns the pilot piston to the left, and the whole process starts over again.

Figure 16 shows the experimentally determined main and pilot fuel flows as a function of engine speed. This fuel flow data is at full load; similar data taken at 25, 50, and 75 percent load indicate that the pilot delivery is not affected by the main injection quantity.

The pilot fuel injection quantity is affected by residual pressure in the injection lines. If the residual pressure in the injection line is too large the spring force is not able to overcome the pressure force on the main piston, and pilot injection ceases. This sensitivity to residual pressure may make the system difficult to use in an experimental situation.

Figure 17 shows the timing lead of the pilot injection before the main injection. These timings are almost ideal by our current estimate of fuel system requirements with conventional rotor pockets and pilot nozzles. While the lead of the pilot injection over the main injection is smaller than that provided by our current systems at low speeds, we believe this reduction in pilot to main lead will actually improve engine performance at in the lower speed range.

Additional data were taken using the main injection pump alone. This data shows the M100 injection pump to be capable of supplying 125 mm^3/injection of fuel at around 12000 psi (82.68 mPa) with an acceptable 60 degree duration at 8000 RPM. This is adequate for us to obtain further information on the effect of injection pressure on engine combustion at high power.

A brief test of the M100 pump was performed on engine 0706-1 to evaluate the effect of the M100 injection rate, which is somewhat different from the injection rate of the A-Pumps. In general, performance with the M100 pump was found to be almost identical to performance with the A-Pumps. For details see the section on injection rate below.

The M100 pump was used as the main fuel injection pump for the last two rig engines run on this program. The primary reason for this was the higher rate of injection which allowed sufficient quantities of fuel to be injected in short durations for the experimental rotor pocket configurations. Performance data for Engine 0707-1, Leading Rectangular Pocket and Engine 0707-2, Leading Standard Pocket is provided in Section 12.0.

Injection Rate Measurement

Differences in performance have been observed between Rotary engines with various fuel injection systems.

The DM pumps showed better engine performance than data taken with the AUI injector system. This data is obscured somewhat by a difference in exhaust back-pressure between the two engines. See Figure 18.

The DM pumps showed better performance than was obtained with the A-Pumps. See Figure 19.

Fuel consumption was shown to decrease 6 percent on engine 0705-3 simply by changing the fuel injection line ID from 1.5 mm to 1.0 mm. See Figure 20.

Combustion modeling suggests the different fuel injection systems will provide different combustion efficiencies. Figure 21a shows five fuel injection rates for which performance was calculated. Rate A is a hypothetical injection system capable of producing a trapezoidal injection rate with a peak pressure around 14000 psi (96.46 mPa). Rate B is the AMBAC M100 fuel injection rate. Rate C is the Nippondenso A- Pump fuel injection rate. Rates D and E are hypothetical square wave injection rates. Figure 21b shows the rich, lean, and flammable fractions of the mixture in the combustion chamber as a function of engine crank angle degrees. For all these figures 90 degrees is engine minimum volume (TDC). The flammable mixture fraction calculates to be around 60% throughout the time of combustion with the trapezoidal rate injection system. Figure 21c shows similar results for the AMBAC M100 injection rate shape, except that the flammable portion is around 50% of the fuel in the combustion chamber. Figure 21d shows the same results for the Nippondenso A-pump injection rate shape. In this case the flammable portion of the fuel is between 45 and 55% depending upon the crank angle. From these modeling results one would expect the M100 and A-Pump systems to have similar engine performance, a result which was in fact obtained as discussed below.

Several schemes for measuring injection rate were evaluated. The long line technique described by Robert Bosch in SAE Paper 660749 was selected because of it's simplicity and wide acceptance.

A contract was provided to Adiabatics Inc. of Columbus, Indiana to design and fabricate an injection rate measuring device and perform measurements at a variety of speeds and fuel deliveries on both the Stanadyne DM pumps and the Stanadyne AUI system. The full results are published in Adiabatics Technical Report "Injection Rate Measurement Stanadyne DM fuel Pump and AUI Injection System". Excerpts of relevant data are provided here.

After rate measurements were completed at Adiabatics, all of the hardware was returned to JDTI. The rate measuring equipment was set up in our fuel lab and utilized to measure the injection rate of various fuel injection systems which were used in engine testing during this program.

Measurement of the instantaneous rate of injection for the different fuel systems was performed. Figure 22 shows the difference in injection rate shape between the DM and AUI

systems. It is noteworthy that the injection rate trace from the AUI system is very clean. There is no indication of after-dribble, slow needle closing, or other deleterious injection effects which would explain the performance difference observed between the DM and the AUI injection systems.

Figure 23 shows similar data for the DM and A-Pump systems. One difference is that the A-Pump injection rate is somewhat higher than the injection rate of the DM pump. Some of the performance difference between the DM and the A-pumps may be attributed to differences in pump power requirements. The injection lines used with the A-pump are considerably longer than those used with the DM system. The injection rate at the end of injection is higher with the A-pump than with the DM system. These two factors make the A-pump hydraulically less efficient than the DM pumps were and may perhaps account for as much as two horsepower difference in pump drive power at these speeds and loads. The performance difference seen is on the order of 10 HP (7.5 kw), however, so this explanation is not sufficient. Motoring frictions of the two engines are within two horsepower of each other throughout the speed range where data were taken. Some difference in combustion efficiency between the two engines is necessary to explain the data. The engine with the DM pump on it has 5% lower airflow which experience indicates would be detrimental to performance.

Figure 24 shows the results from the A-Pump with 1.5 mm injection line versus the A-Pump with 1.0 mm injection line. The pump used had a 7.5 mm plunger, an 80 mm^3 retraction delivery valve, and a snubber valve with a .7 mm diameter orifice. The nozzle was a Stanadyne slim tip pencil nozzle with four .009" diameter orifices. The major difference is a decreased peak injection rate and longer duration of injection for the better performing 1.0 mm ID system. In addition, the injection rate seems to be relatively constant compared to the injection rate of the 1.5 mm ID system.

Since the best performance obtained to date using a 6 hole shadowing spray pattern was obtained with the Stanadyne DM pumps, it was desirable to test the improved Non-Shadowing patterns using pumps with a similar injection rate shape. Unfortunately, the DM pumps can not deliver sufficient fuel for the power now being produced. It was therefore decided to reconfigure a Nippondenso A-Pump in order to match the Stanadyne injection rate shape.

Figure 25 shows the operating principle of the Stanadyne fuel injection pump. Pressurized fuel is metered through the metering valve and allowed to partially fill the cavity between the two plungers. As the distributor rotates, the inlet port connecting to the metering valve is closed and a discharge port leading to a fuel injector is opened. Further rotation causes the plungers to be driven inward by the cam lobes and deliver fuel into the engine. Start of injection occurs when the pumping elements first contact the cam. End of injection occurs when the pumping elements pass the cam nose.

Some consequences of this metering technique are:

1) The injection rate at the beginning of injection is higher than the injection rate at the end of injection because the injection is occurring over the cam nose.

2) The injection rate and timing of the start of injection vary with fuel delivery. Smaller quantities of fuel are injected at a lower rate.

In contrast, the pumping principle of a jerk pump (in this case the A-Pump) is shown in Figures 7-1 to 7-4. Fuel fills the space above the plunger when the plunger is below the fill port (7-1). The plunger is pushed up by the cam until the fill port is closed (7-2). The distance from the bottom of the plunger stroke to the position at which the port is closed is termed "lift to port closing" or LPC. The plunger continues to be pushed upward, pumping fuel (7-3). Finally, the plunger travels far enough so that the spill helix on the plunger lines up with the spill port, ending injection (7-4). In theory, this technique gives control over the timing and rate of both the beginning and the end of injection as a function of load. In practice, the beginning of injection is usually constant and the end of injection is varied.

Figure 26 shows the lift vs velocity curve for the A-pump camshaft. The pump was initially designed with LPC of 3 mm. This means that pumping occurred over range A. In order to match the pumping rate of the Stanadyne pump, it is desirable to set the LPC dimension to approximately 7 mm, so that pumping occurs over range B. It can be seen that the average pumping rate over range A is much higher than the rate over range B. This can be compensated for by increasing the plunger diameter as well as the LPC dimension.

A 10mm upper helix plunger was modified to obtain 7 mm LPC by grinding the fill port, grinding the top of the plunger, and placing a 1.5 mm shim under the barrel when installing the plunger in the pump. Grinding the plunger and fill port reduces the maximum fuel delivery available, but because the original 10mm plunger was capable of delivering 250 mm^3/injection this was not a problem.

Figure 27 shows the injection rate curve achieved at 60 mm^3/injection with the A pump compared with the injection rate achieved with the Stanadyne DM pump. As can be seen, the match is within the error band of measurement capability. Figure 28 shows the injection rate curves of the modified pump at a variety of fuel deliveries. It is seen that the A- Pump injection rate is somewhat higher at light loads than that of the DM pump. This is a consequence of the use of a lower helix plunger in the A-pump so that the beginning of injection stays at the same place on the camshaft. If further engine test data shows it to be desirable, a plunger could be manufactured with an upper helix so that the end of injection stayed constant; this would make the injection rates more similar at all fuel deliveries.

Engine testing of the modified Nippondenso A-Pump showed some performance improvement at light loads and a possible small loss in performance at heavy loads (See Figure 29). The differences are quite small and the performance may be the same within the accuracy of measurements.

Performance did not improve with the non-shadowing spray patterns (Figure 30). There is some question regarding the accuracy of this data because the performance of the engine degraded during this test; at the end of the test the performance with the N1 nozzle was .42 lb/hp-hr at best. The test cell gearbox broke before the cause of this performance loss was isolated.

Figure 31 shows a comparison of the injection rates for the baseline A-Pump configuration and the M100 fuel injection pump.

Figures 32 A and B show a comparison of the performance data obtained with the A-Pump and the data taken with the M100 pump. Figure 32a illustrates the significant shortening of injection duration with the M100 pump. The shortening of injection duration was directly applicable for use within the strict injection time constraints of the Leading Rectangular Pocket Rotor in Engine 0707-1. Only a limited amount of engine operation data with the pump was obtained. Figure 32b shows a comparison of the fuel consumption between the M100 and the A-Pump. Based on these 6 data points at 6000 RPM and the simulation predictions discussed above, it may be conjectured that there is no difference in engine performance between the A-Pump and the M100 injection systems.

CONCLUSIONS

A dual orifice pilot nozzle and fuel system configuration which will provide adequate life and reliability is feasible.

The rotating valve type high pressure common rail system has potential to provide the best fuel injection characteristics for the Stratified Charge Rotary Engine.

The SCRE with our conventional rotor pocket as described in drawing 617001N2 is relatively insensitive to changes in fuel system injection rate.

RECOMMENDATIONS

Pursue development of a rotary valve type high pressure common rail system for future aircraft type stratified charge rotary engines.

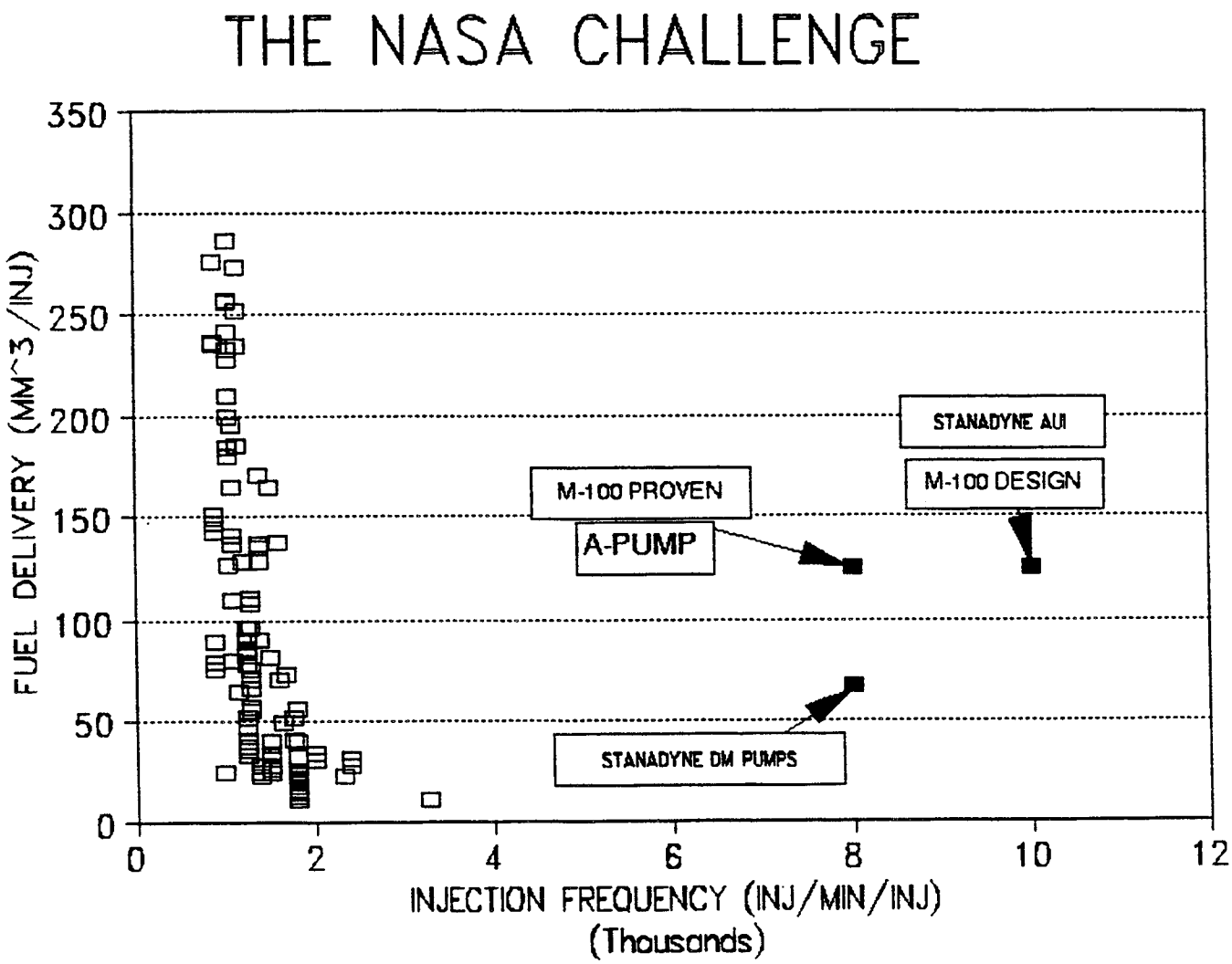
TABLE I

TECHNOLOGY REVIEW

K-T ANALYSIS OF EXISTING & ADVANCED
FUEL INJECTION SYSTEM TECHNOLOGY

CRITERIA	WEIGHT
INJECTION FREQUENCY	10
ADEQUATE FLOW	10*
TIMING FLEXIBILITY (90 BTC TO TC)	10
MULTI-ROTOR CAPABILITY	9
INJECTION RATE CONTROL	8
MAXIMUM PRESSURE CAPABILITY	8
REPEATABILITY INJECTION TO INJECTION	7
ESTIMATED WEIGHT	7
PACKAGABILITY	7
PEAK DRIVE TORQUE	7
SAFE FAILURE MODES**	7
INDEPENDENT CONTROL OF EACH INJECTOR	5
ROTOR HOUSING INTRUSION	4
DRIVE POWER	3
DURABILITY	2
MULTI FUEL CAPABILITY	*

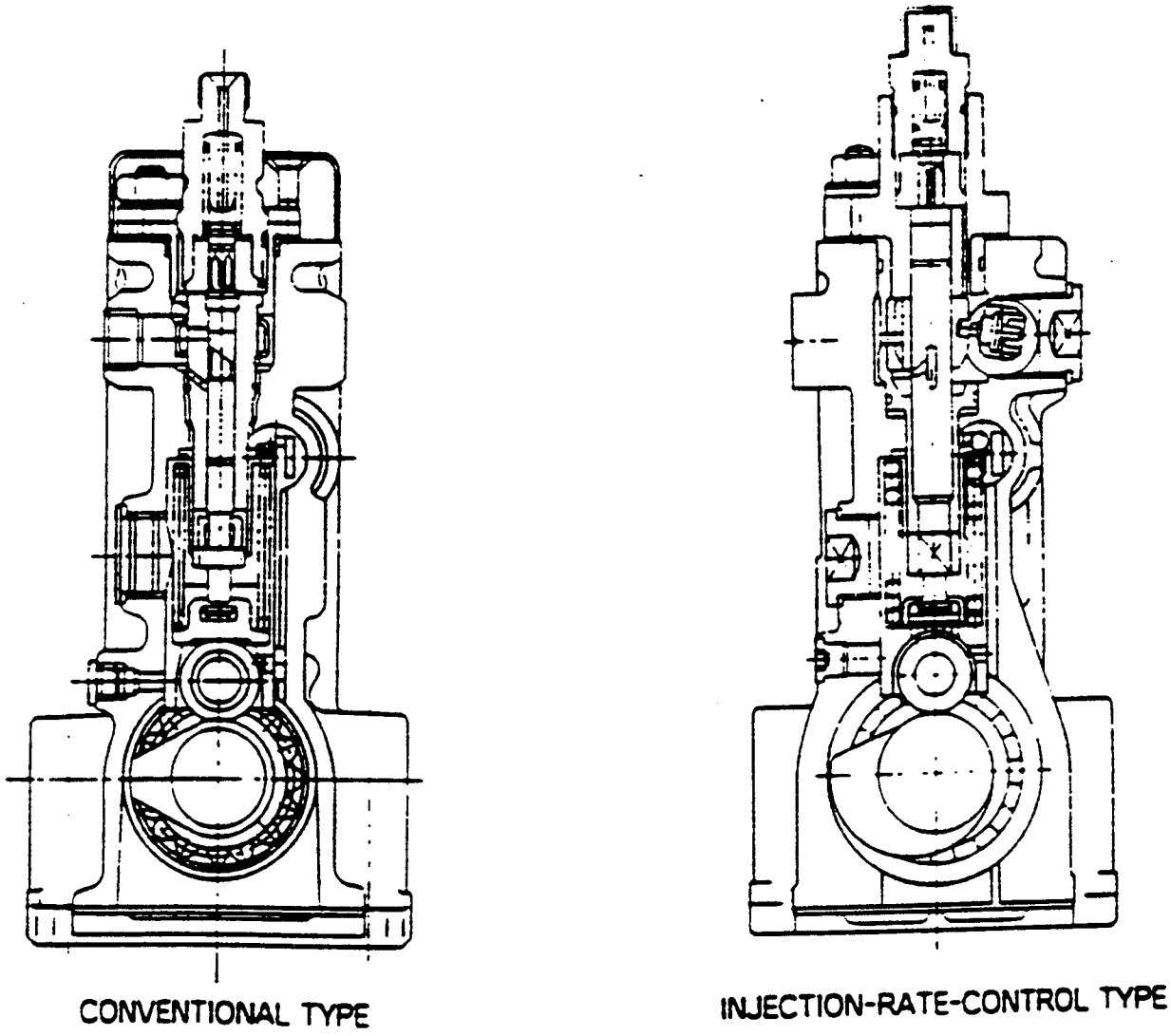
* SYSTEMS WERE ALL CONSIDERED TO BE EQUAL
** SYSTEMS WITHOUT SAFE FAILURE MODES CAN BE MADE SAFE BY THE ADDITION OF EXTRA DEVICES



COMPARISON OF INJECTION FREQUENCY

Figure No. 1

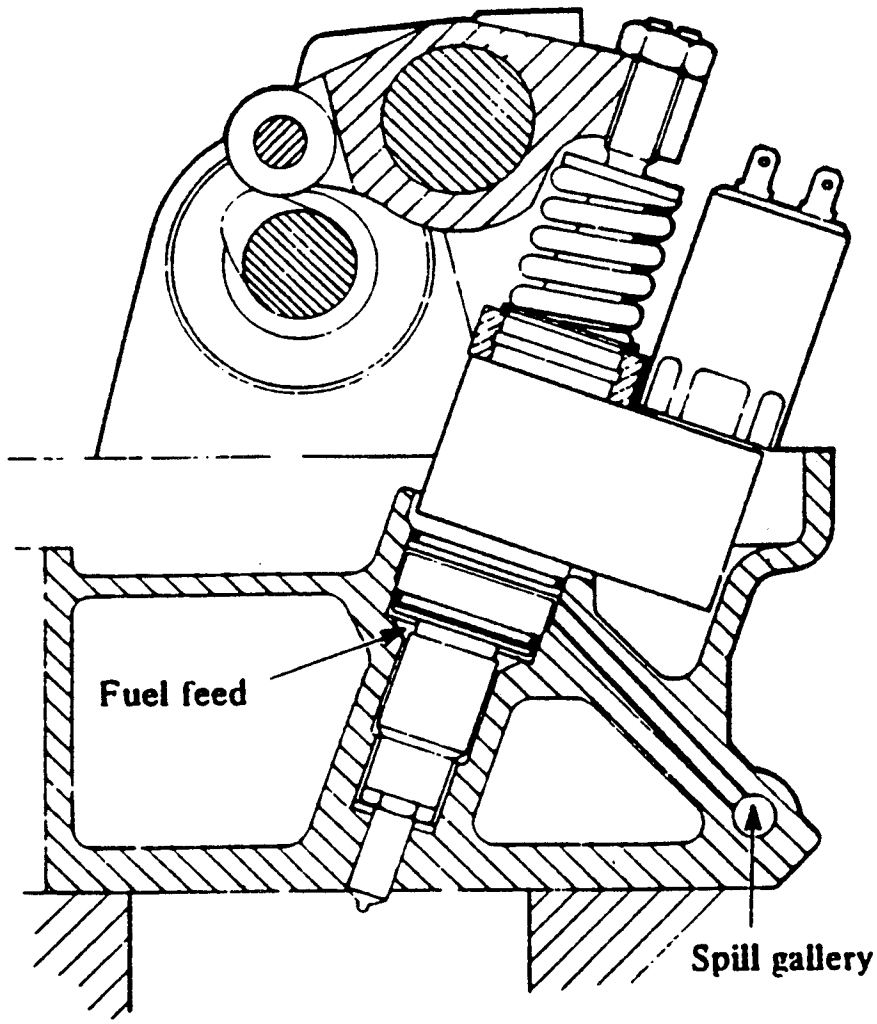
RATE CONTROL JERK PUMP



INJECTION RATE CONTROL

Figure No. 2

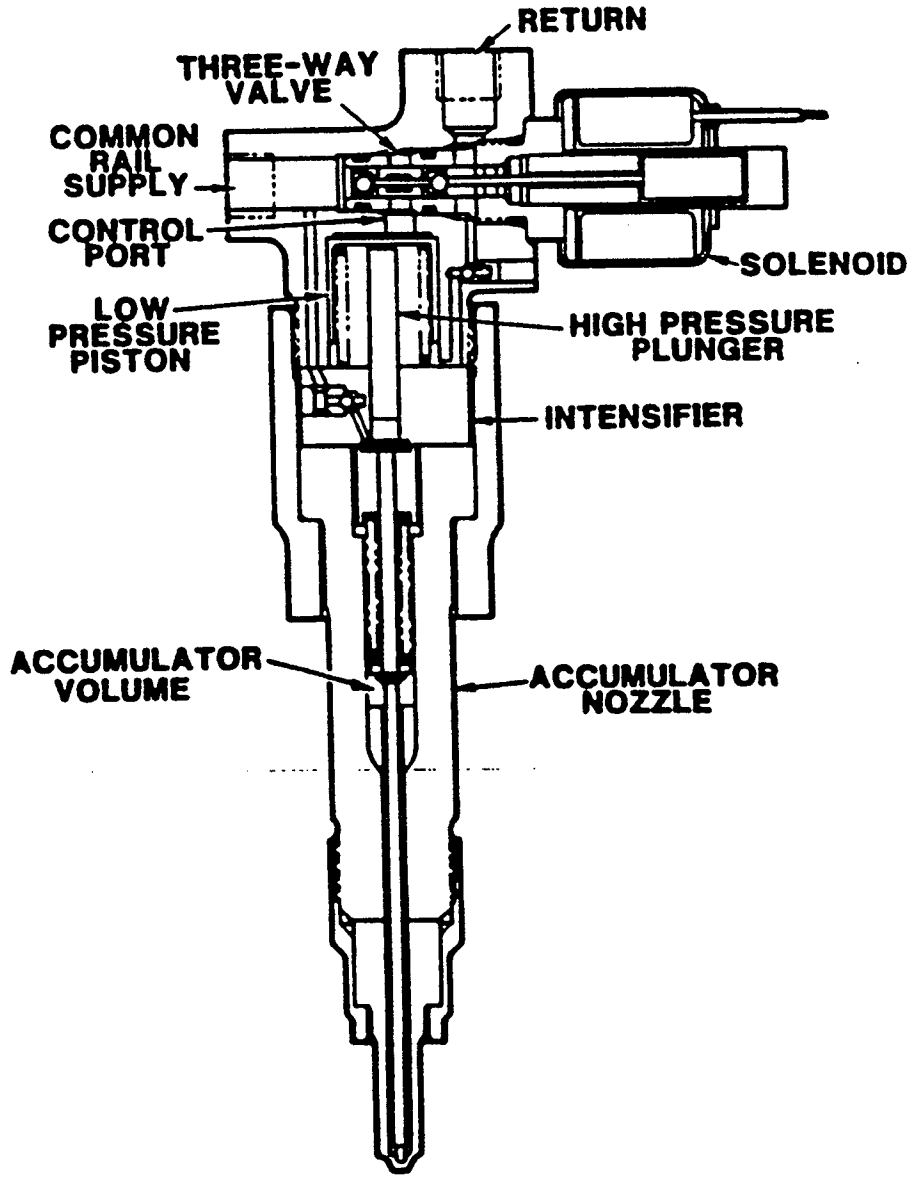
UNIT INJECTORS



CAMSHAFT DRIVEN INJECTORS

Figure No. 3

MEDIUM PRESSURE COMMON RAIL



HIGH PRESSURE COMMON RAIL
(REMOVE AMPLIFIER PISTON)

Figure No. 4

STANADYNE ACCUMULATOR INJECTOR OPERATION

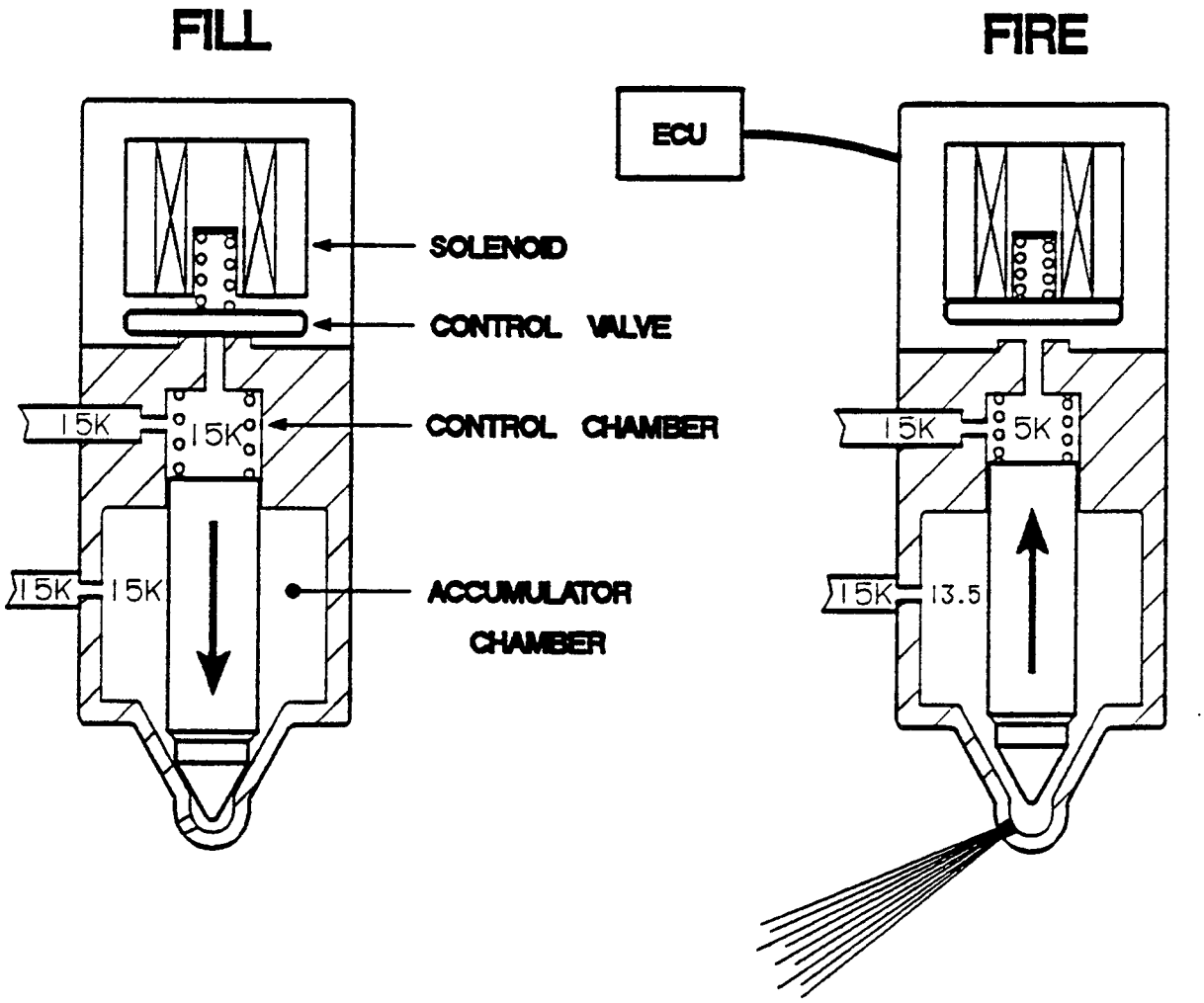


Figure No. 5

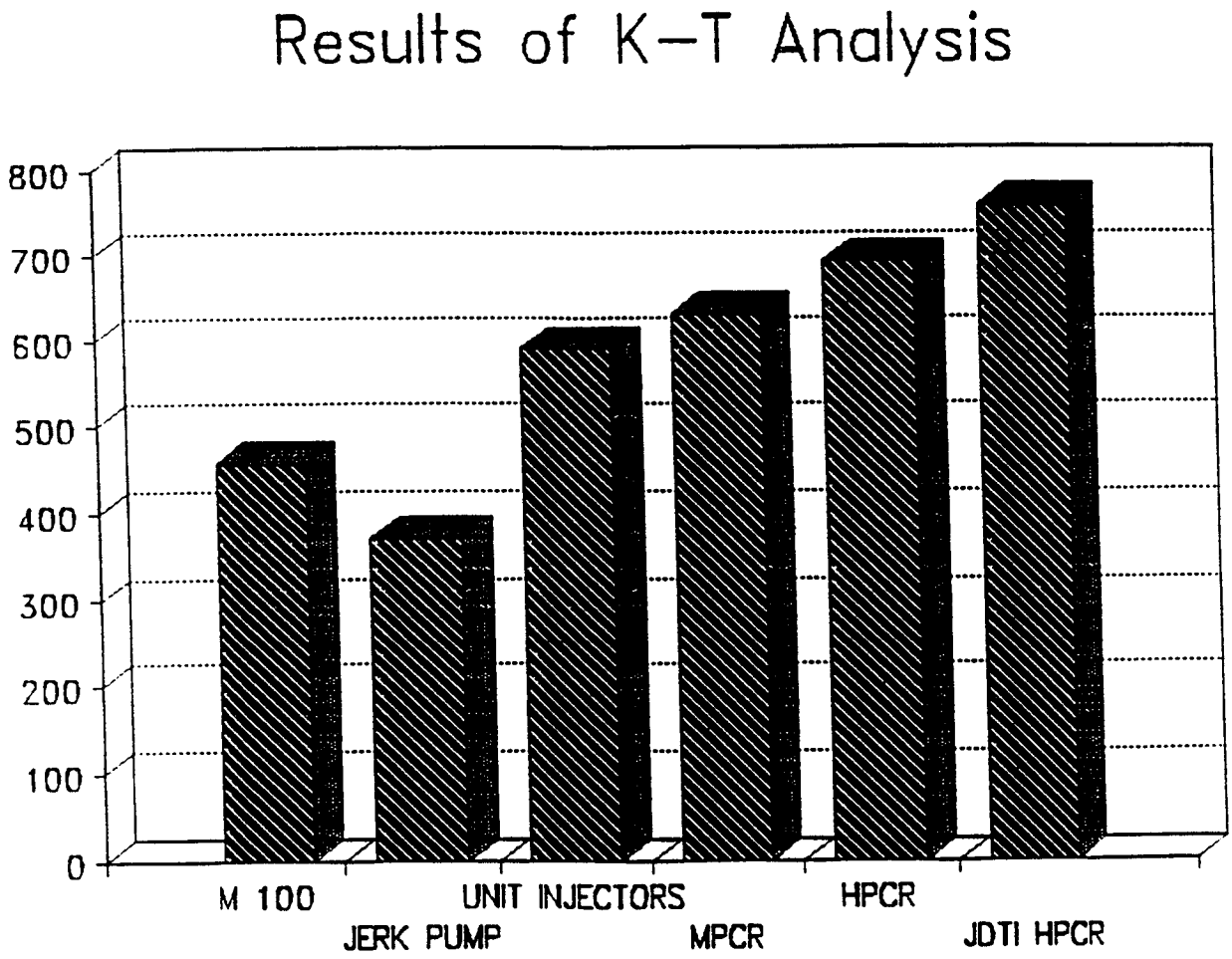
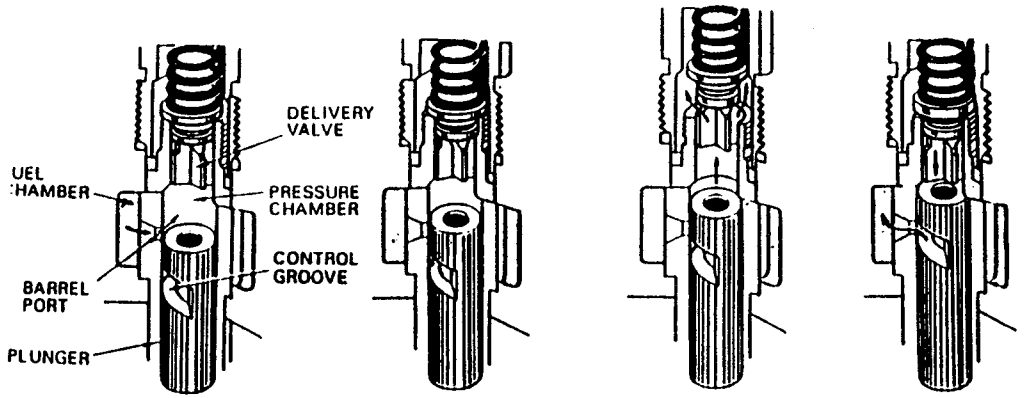
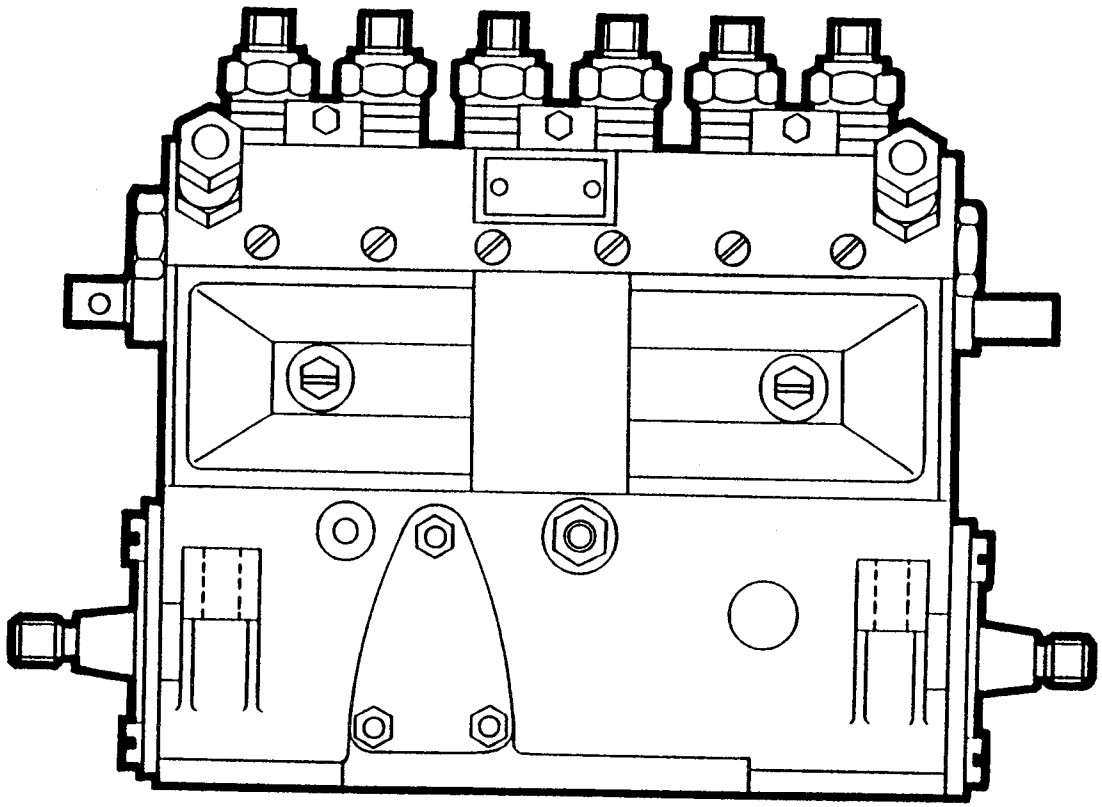

Results of K–T Analysis
800
700
600
500
400
300
200
100
0
M 100
JERK PUMP
UNIT INJECTORS
MPCR
HPCR
JDTI HPCR

Figure No. 6

CURRENT SYSTEM (A PUMP)



(1) Bottom dead center (2) Commencement of fuel delivery (3) Delivery (4) End of fuel delivery



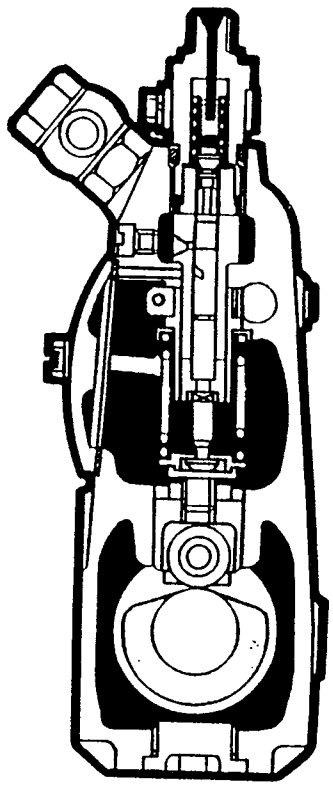


Figure No. 7

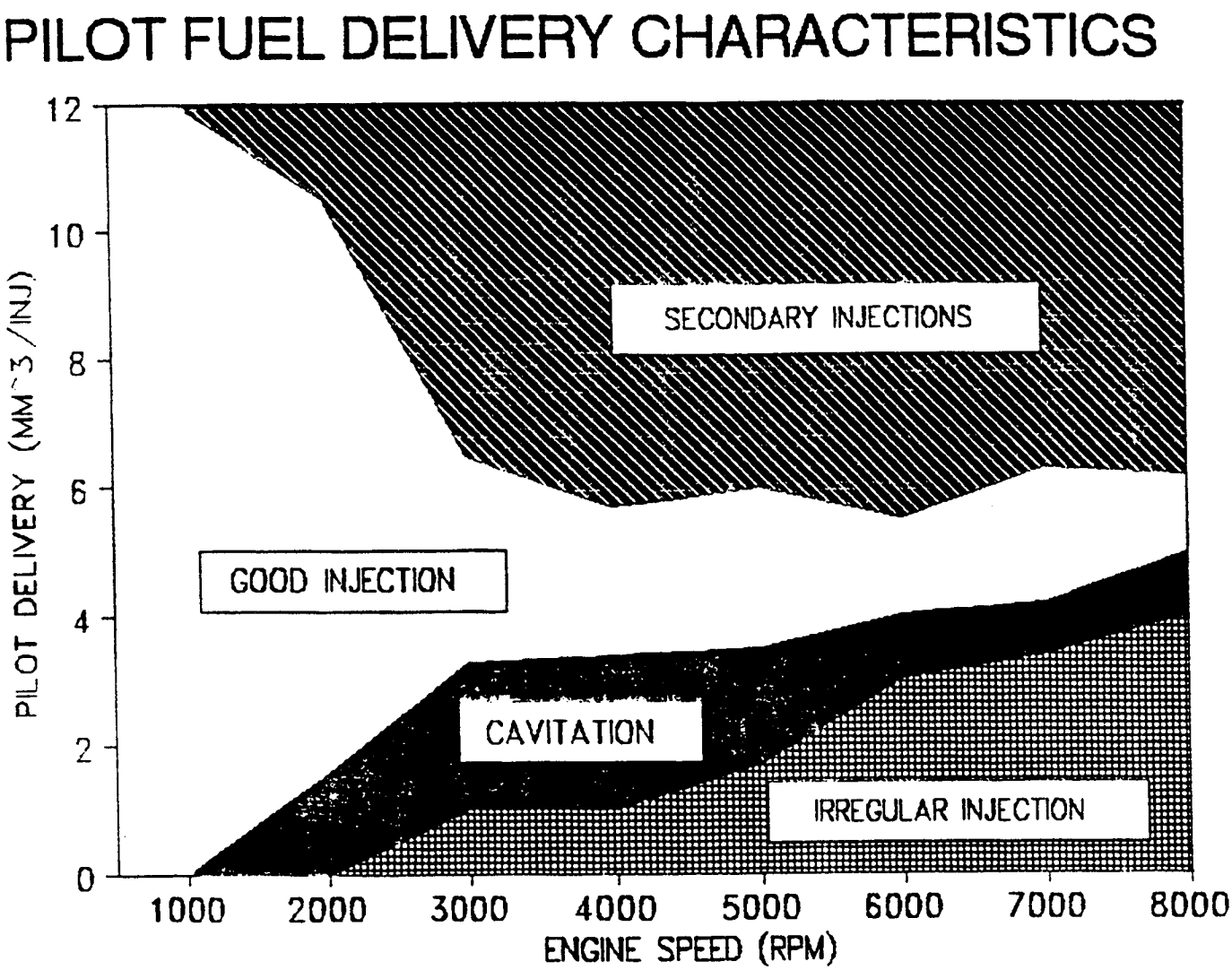

PILOT FUEL DELIVERY CHARACTERISTICS
PILOT DELIVERY (MM^3/INJ)
12
10
8
6
4
2
0
SECONDARY INJECTIONS
GOOD INJECTION
CAVITATION
IRREGULAR INJECTION
1000
2000
3000
4000
5000
6000
7000
8000
ENGINE SPEED (RPM)

Figure No. 8

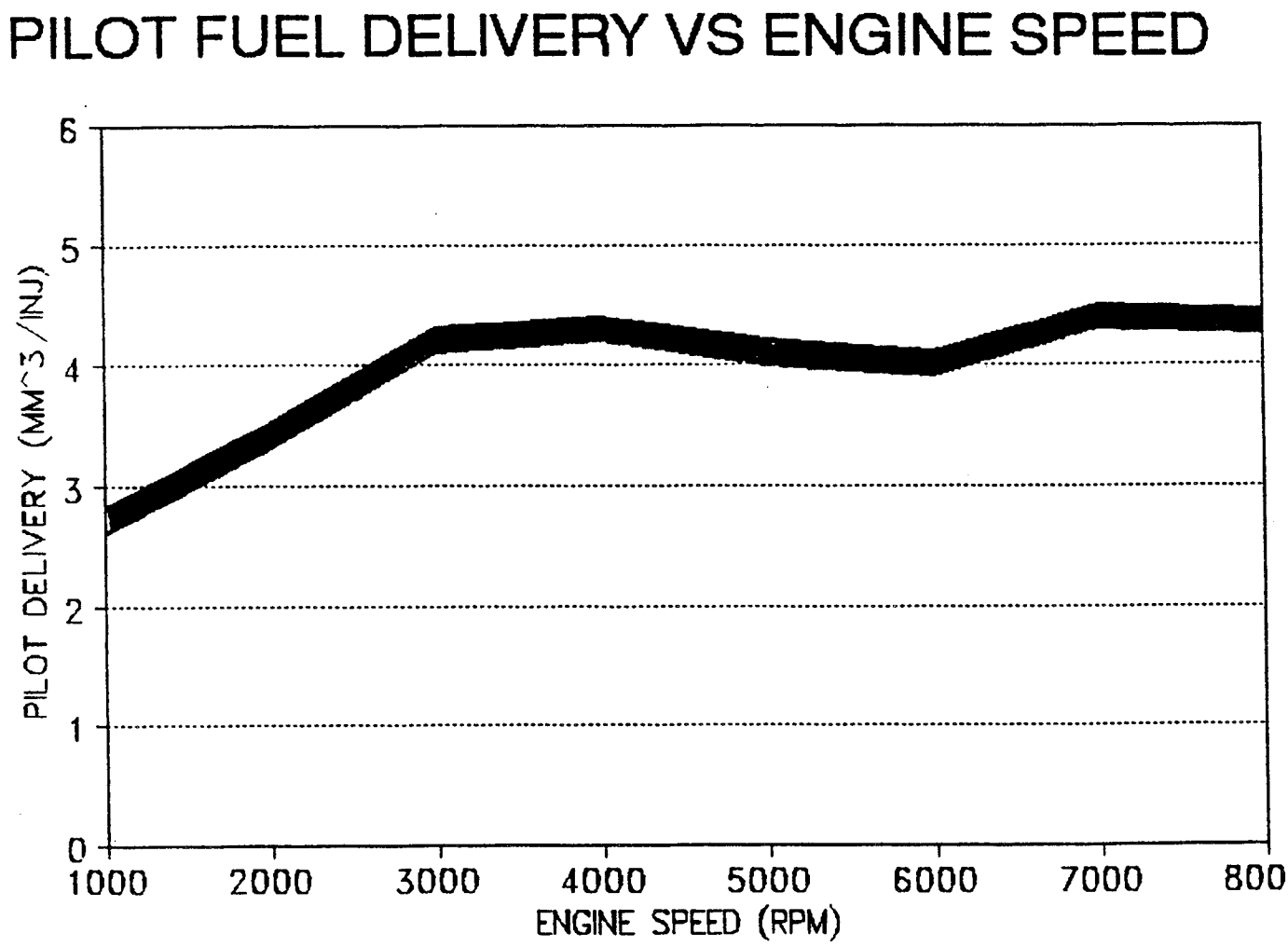

PILOT FUEL DELIVERY VS ENGINE SPEED
PILOT DELIVERY (MM^3/INJ)
0
1
2
3
4
5
6
1000
2000
3000
4000
5000
6000
7000
800
ENGINE SPEED (RPM)

Figure No. 9

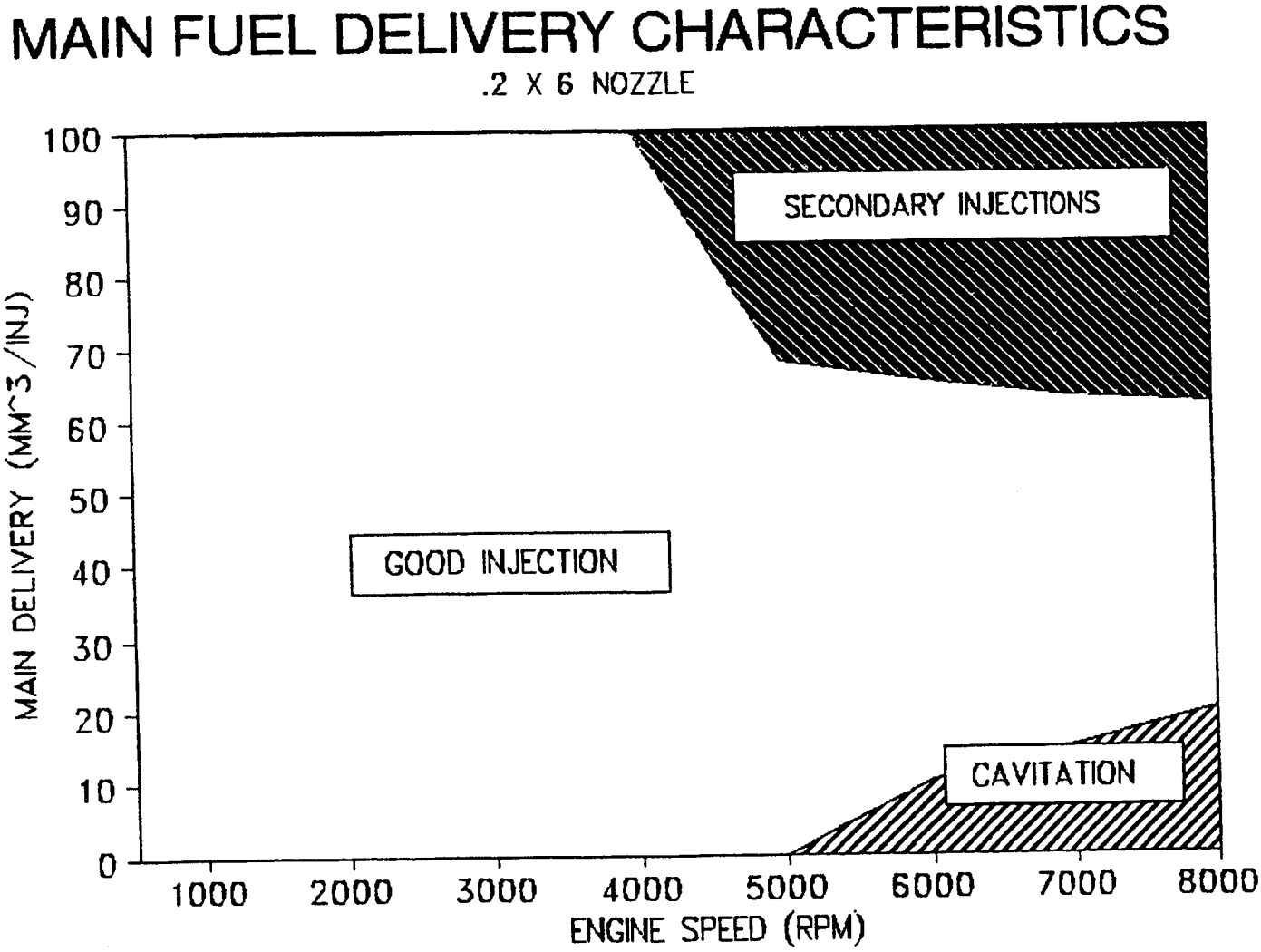

MAIN FUEL DELIVERY CHARACTERISTICS
.2 X 6 NOZZLE
MAIN DELIVERY (MM^3/INJ)
100
90
80
70
60
50
40
30
20
10
0
1000
2000
3000
4000
5000
6000
7000
8000
ENGINE SPEED (RPM)
SECONDARY INJECTIONS
GOOD INJECTION
CAVITATION

Figure No. 10

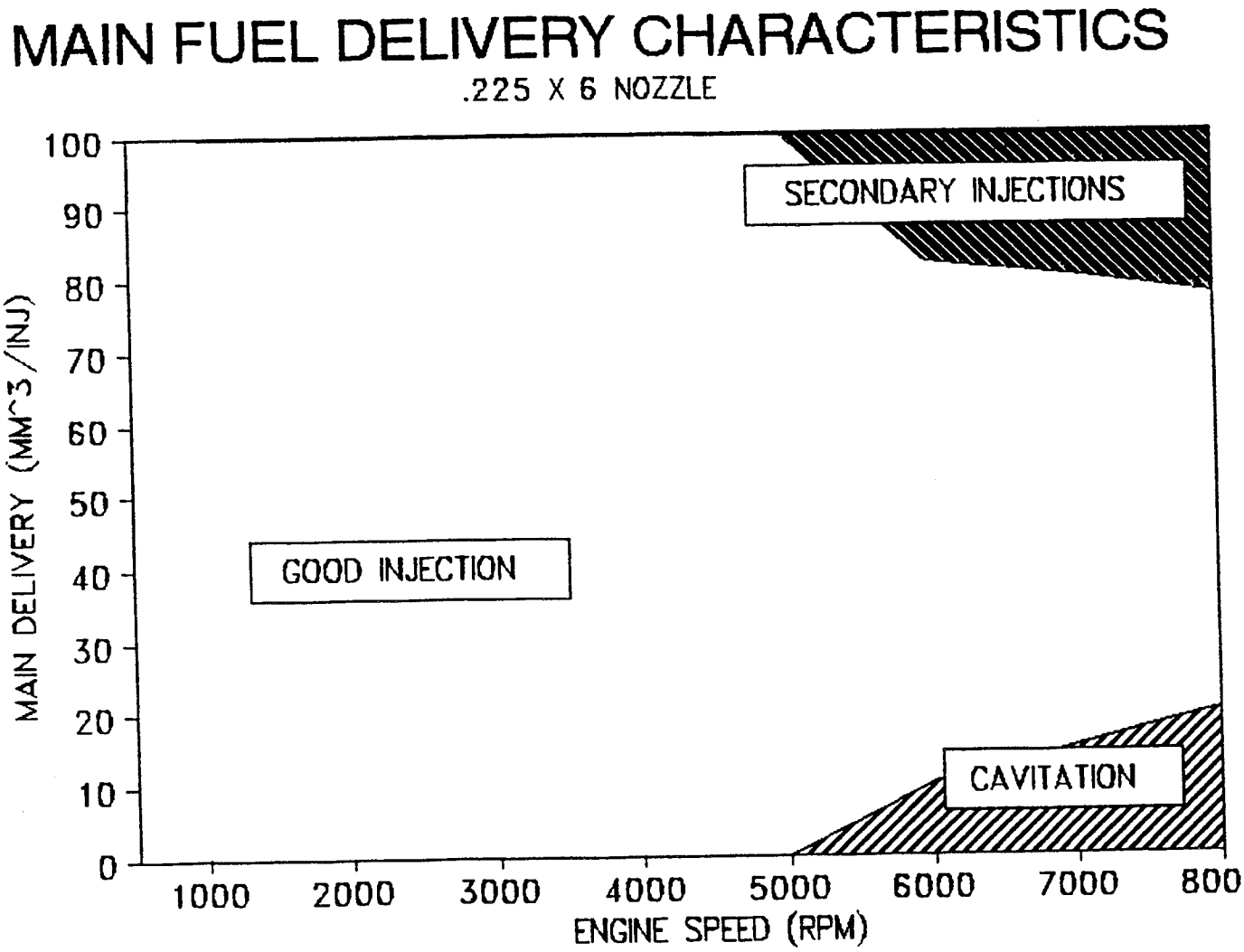

MAIN FUEL DELIVERY CHARACTERISTICS
.225 X 6 NOZZLE
MAIN DELIVERY (MM^3/INJ)
100
90
80
70
60
50
40
30
20
10
0
1000
2000
3000
4000
5000
6000
7000
800
ENGINE SPEED (RPM)
SECONDARY INJECTIONS
GOOD INJECTION
CAVITATION

Figure No. 11

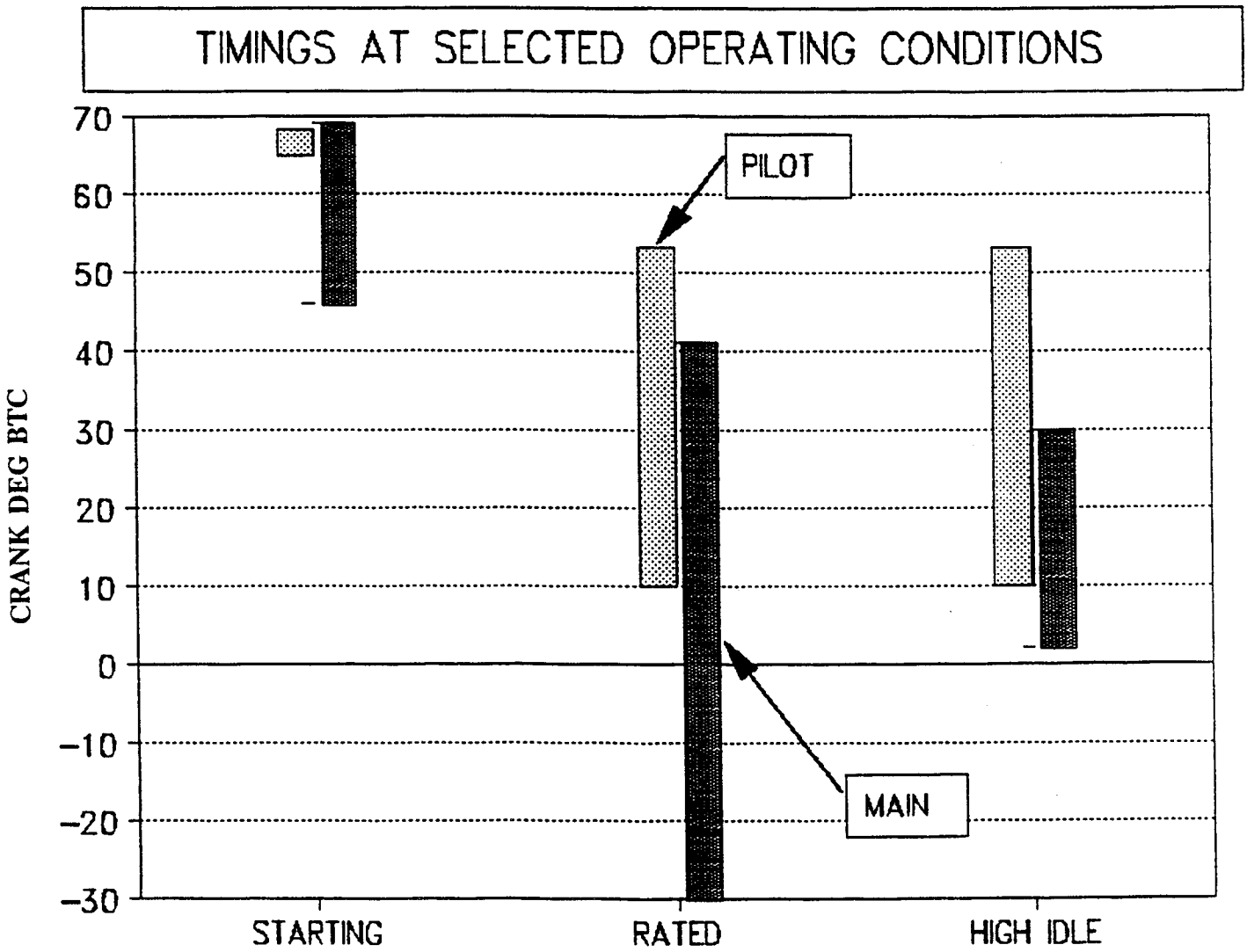

TIMINGS AT SELECTED OPERATING CONDITIONS
CRANK DEG BTC
70
60
50
40
30
20
10
0
-10
-20
-30
PILOT
MAIN
STARTING
RATED
HIGH IDLE

Figure No. 12

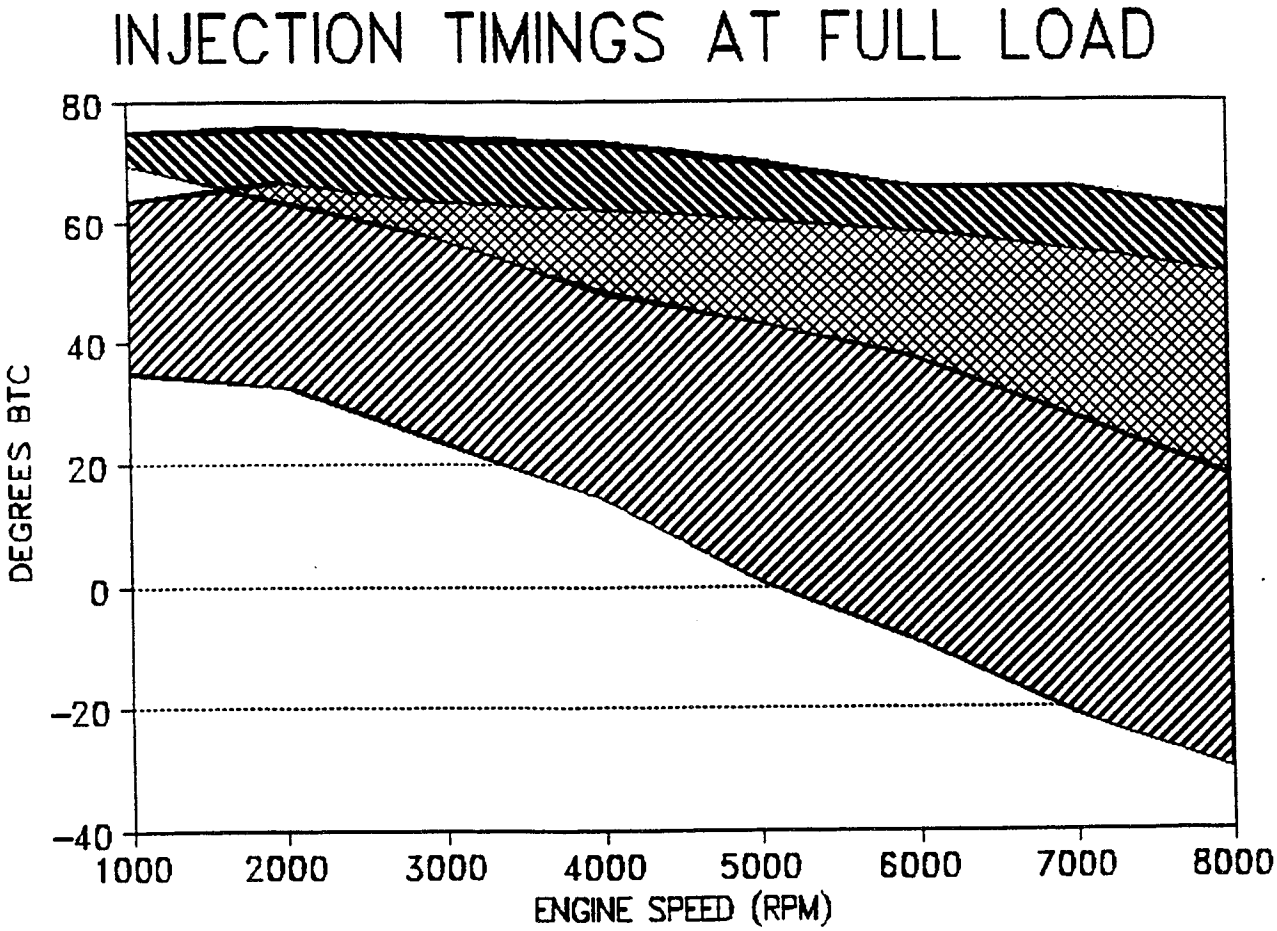
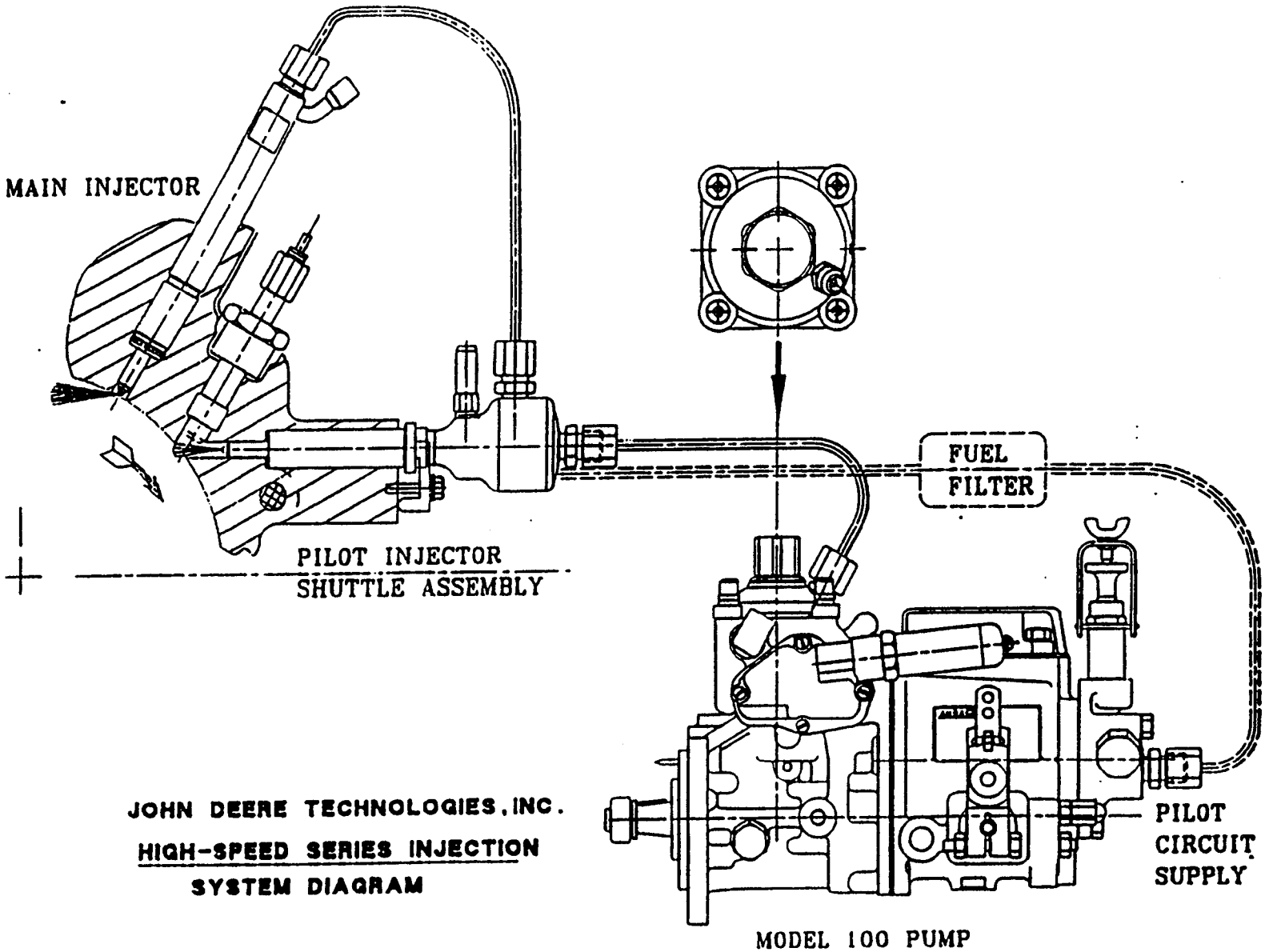

INJECTION TIMINGS AT FULL LOAD
80
60
40
20
0
-20
-40
DEGREES BTC
1000
2000
3000
4000
5000
6000
7000
8000
ENGINE SPEED (RPM)

Figure No. 13



JOHN DEERE TECHNOLOGIES, INC.

HIGH-SPEED SERIES INJECTION SYSTEM DIAGRAM

Figure No. 14

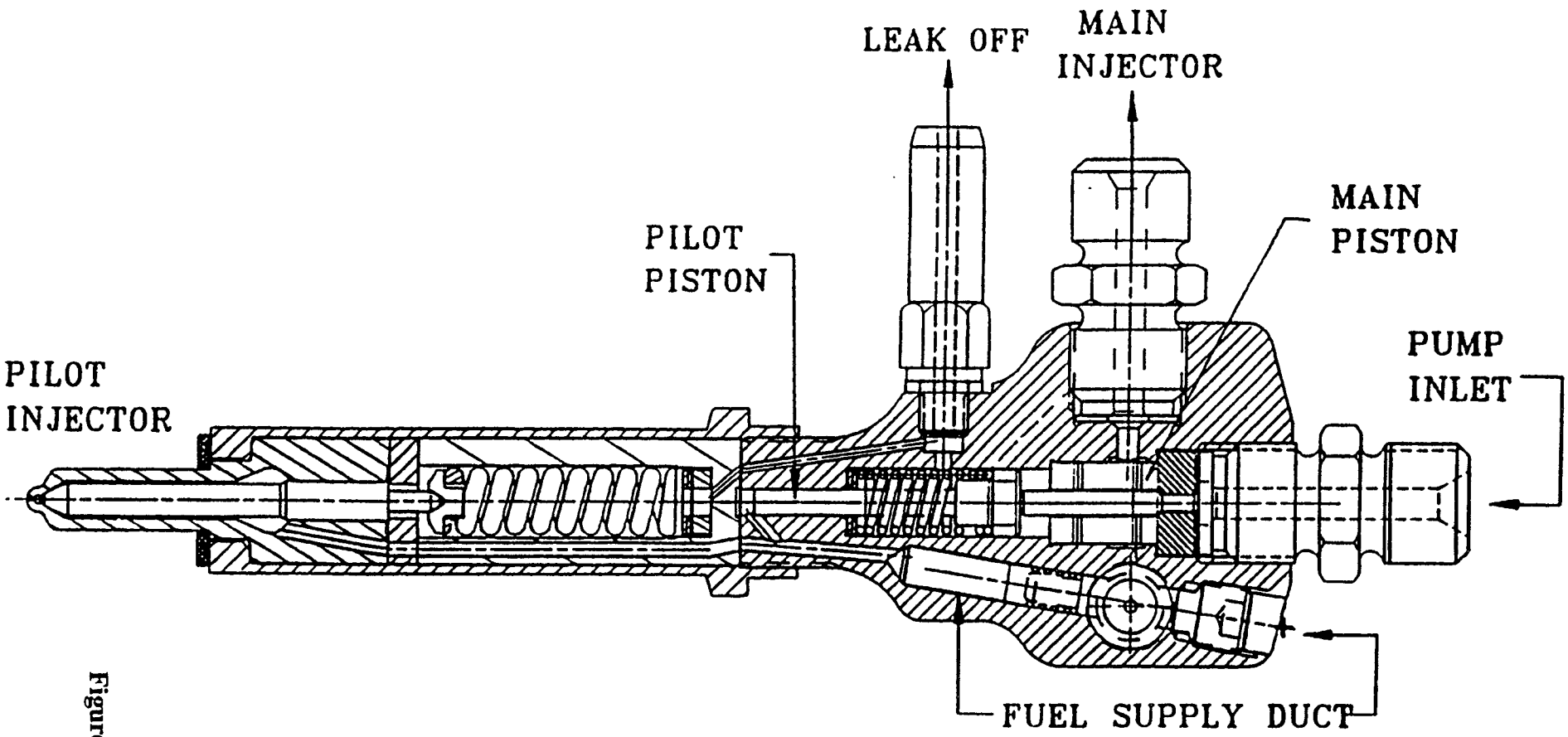


Figure No. 15

Detail of Pilot Splitter Valve

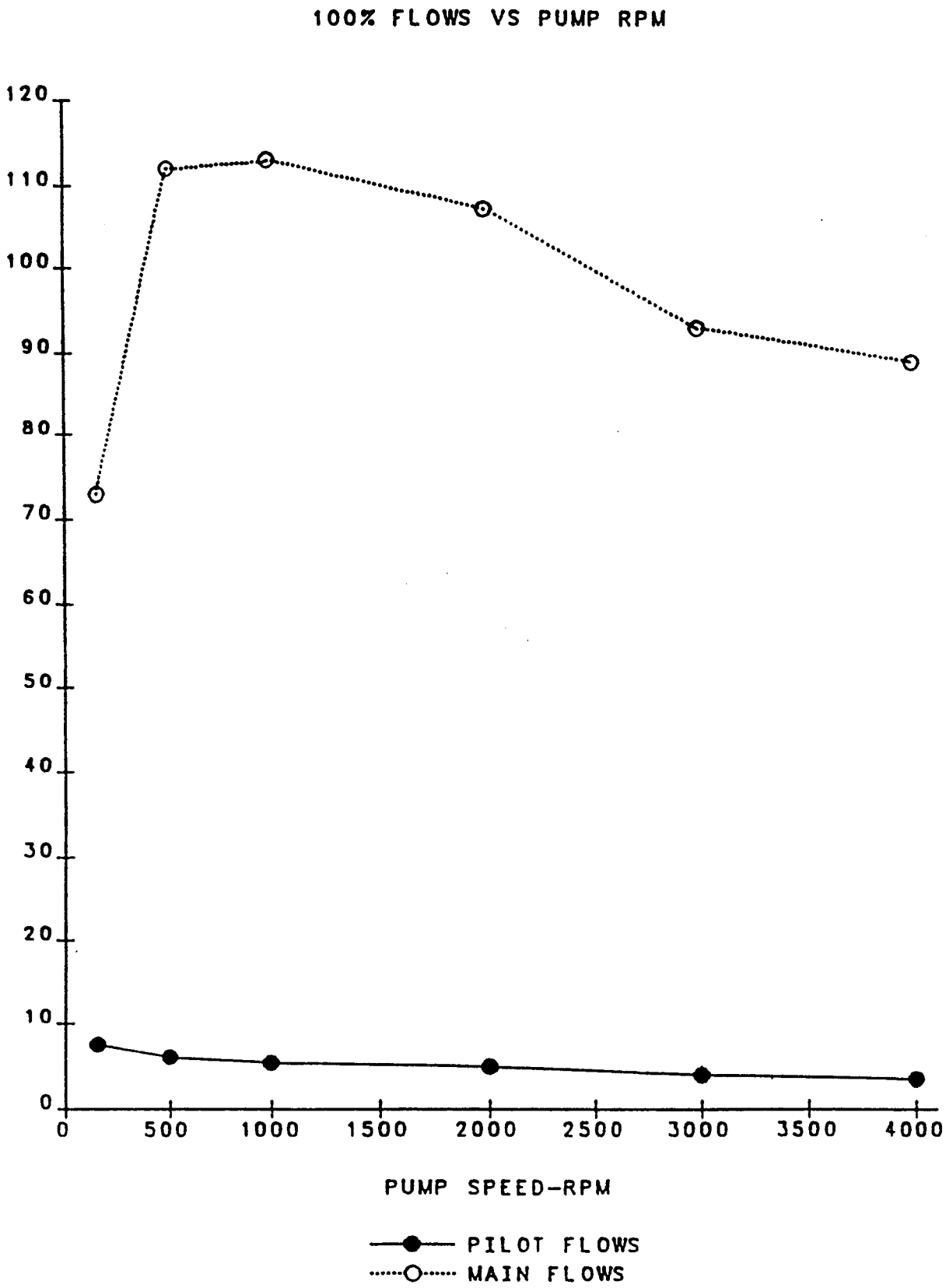

100% FLOWS VS PUMP RPM
120
110
100
90
80
70
60
50
40
30
20
10
0
0
500
1000
1500
2000
2500
3000
3500
4000
PUMP SPEED-RPM
PILOT FLOWS
MAIN FLOWS

Figure No. 16

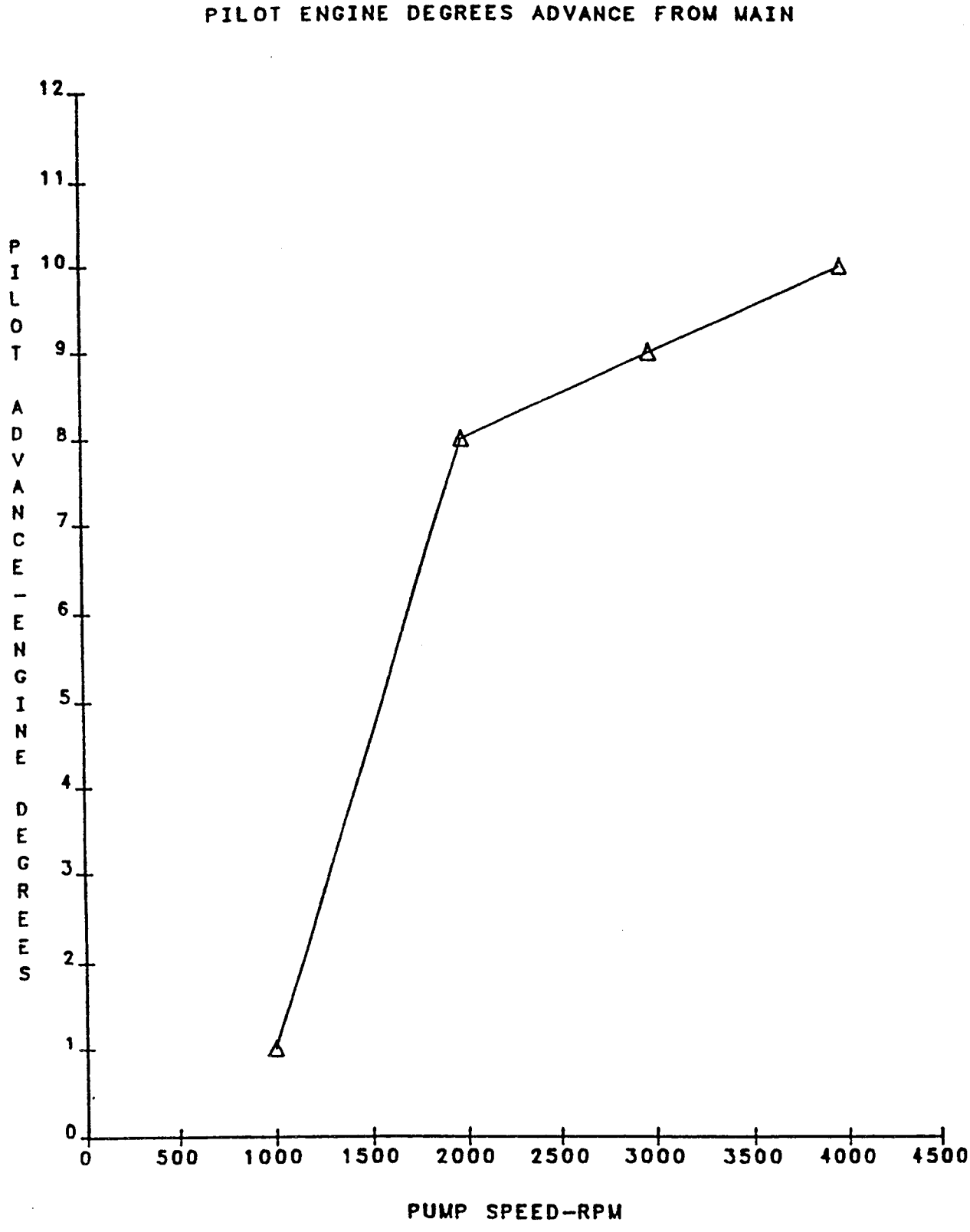

PILOT ENGINE DEGREES ADVANCE FROM MAIN
PILOT ADVANCE-ENGINE DEGREES
0
1
2
3
4
5
6
7
8
9
10
11
12
0
500
1000
1500
2000
2500
3000
3500
4000
4500
PUMP SPEED-RPM

Figure No. 17

ESTIMATE OF INDICATED FUEL CONSUMPTION OF THE 70 SERIES ENGINE
CORRECTED FOR BACK-PRESSURE; NOT CORRECTED FOR F/A RATIO

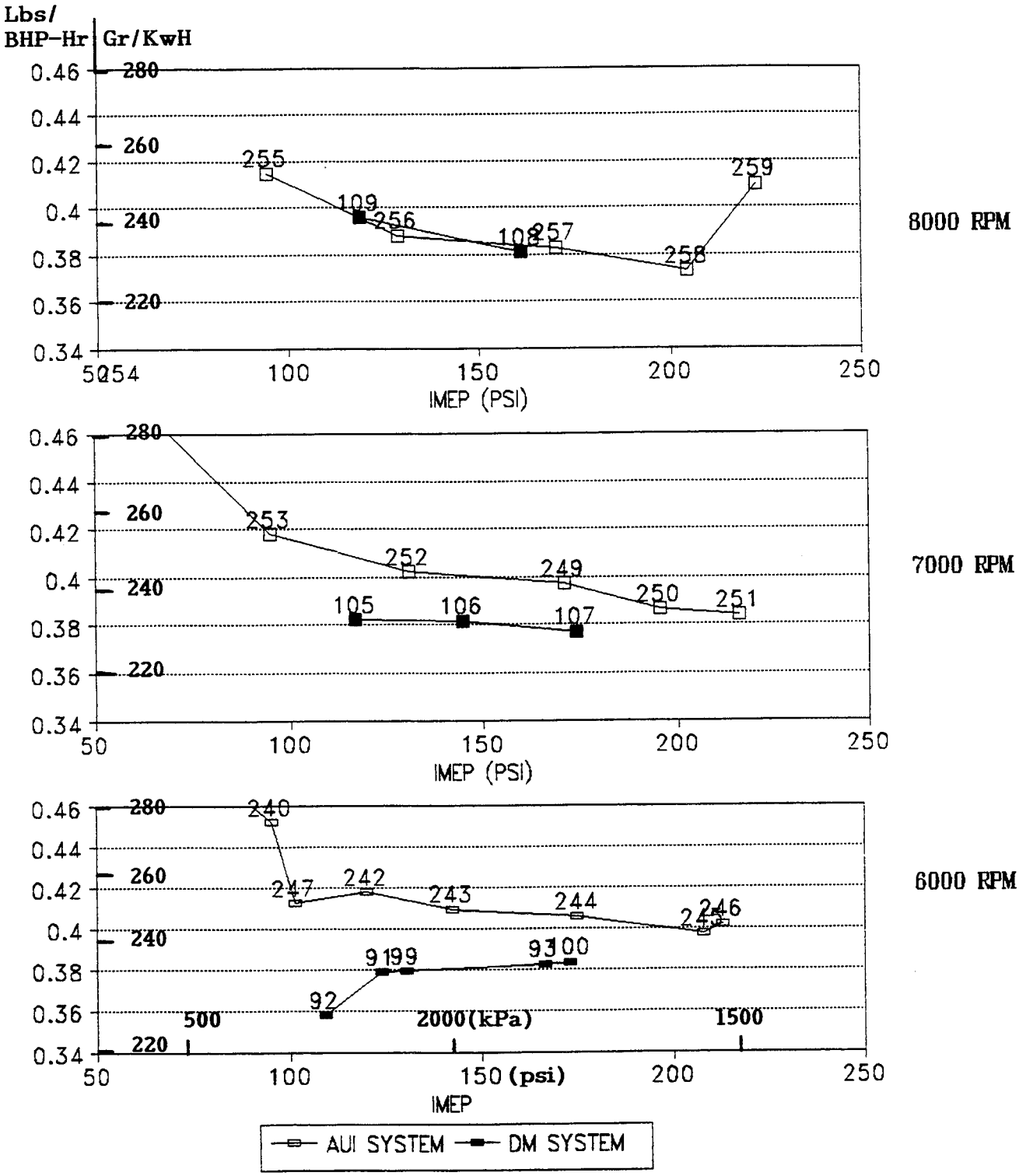


Figure No. 18

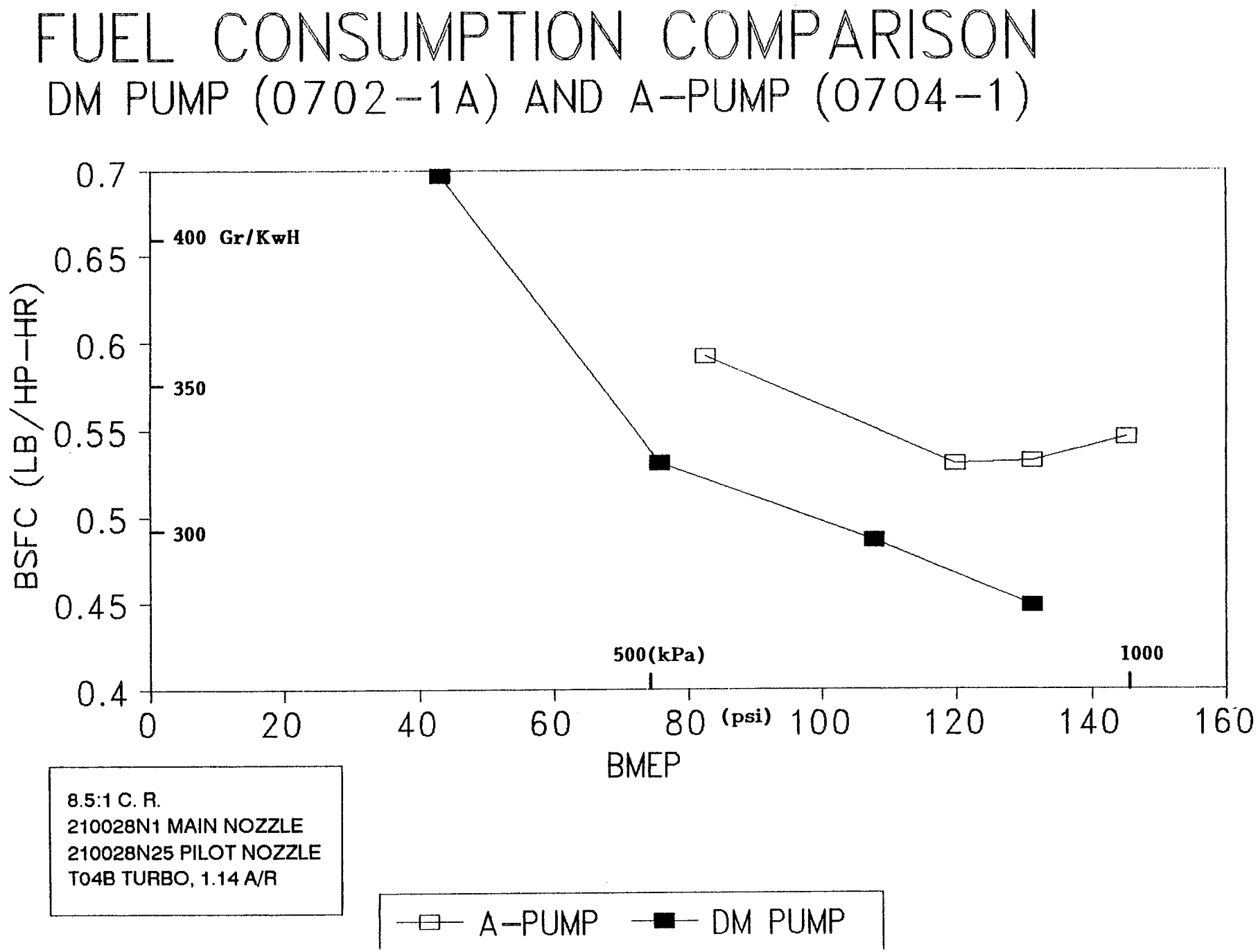

FUEL CONSUMPTION COMPARISON
DM PUMP (0702-1A) AND A-PUMP (0704-1)
BSFC (LB/HP-HR)
0.7
0.65
0.6
0.55
0.5
0.45
0.4
400 Gr/KwH
350
300
500(kPa)
1000
0
20
40
60
80
(psi)
100
120
140
160
BMEP
8.5:1 C. R.
210028N1 MAIN NOZZLE
210028N25 PILOT NOZZLE
T04B TURBO, 1.14 A/R
A-PUMP
DM PUMP

Figure No. 19

EFFECT OF INJECTION LINE ON PERFORMANCE
ENGINE 0705-2, 5500 RPM

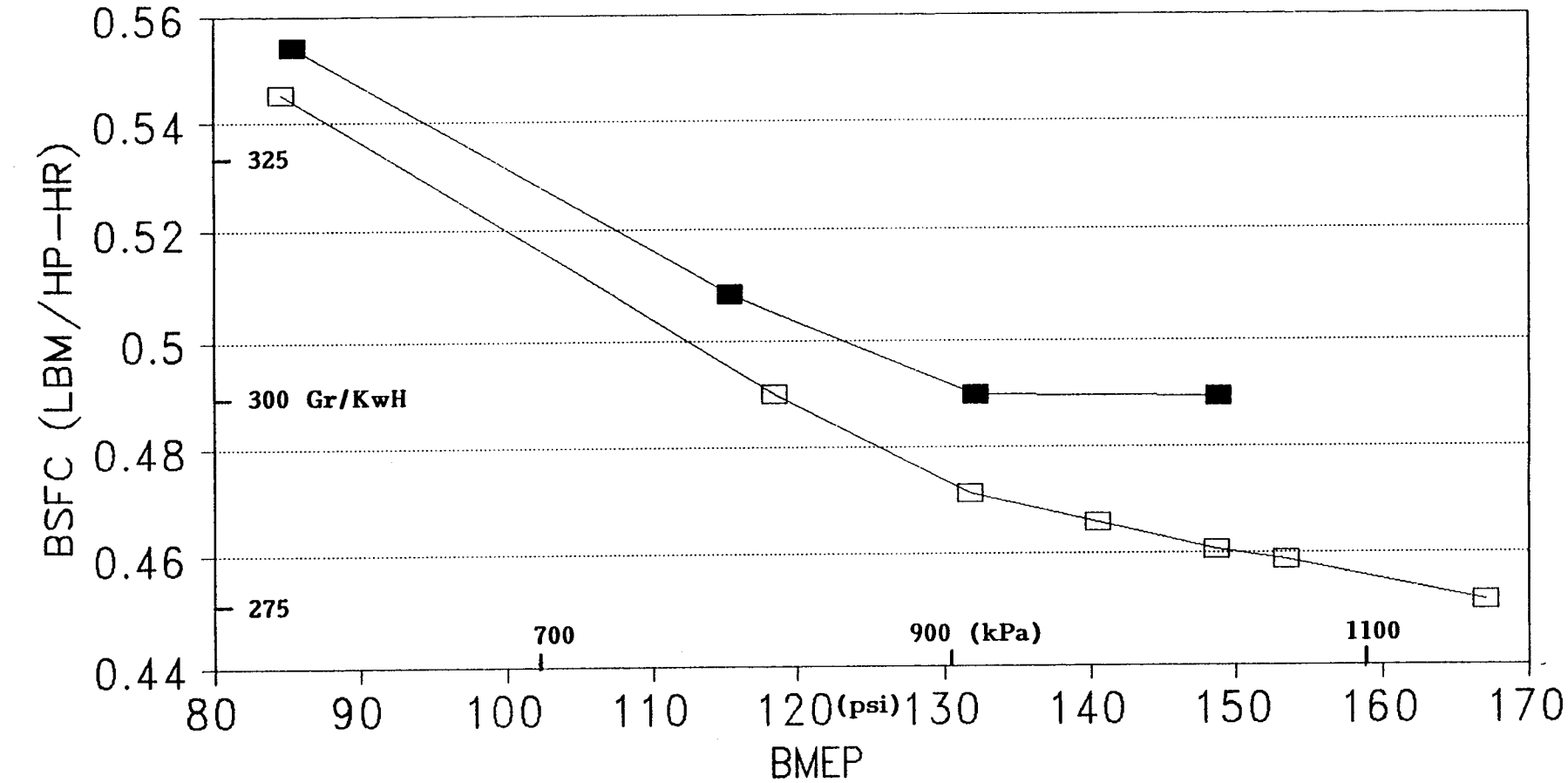


Figure No. 20

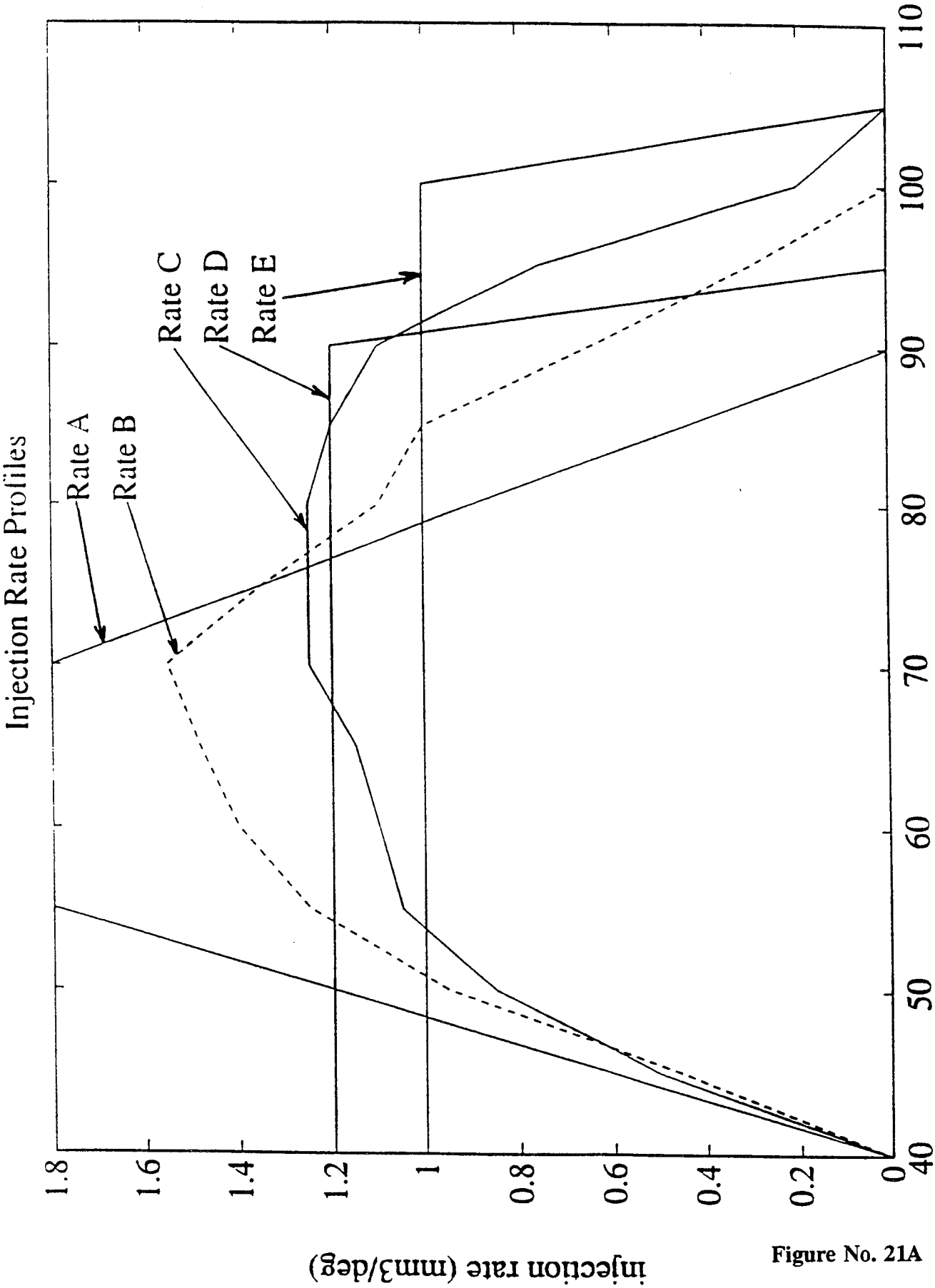


Figure No. 21A

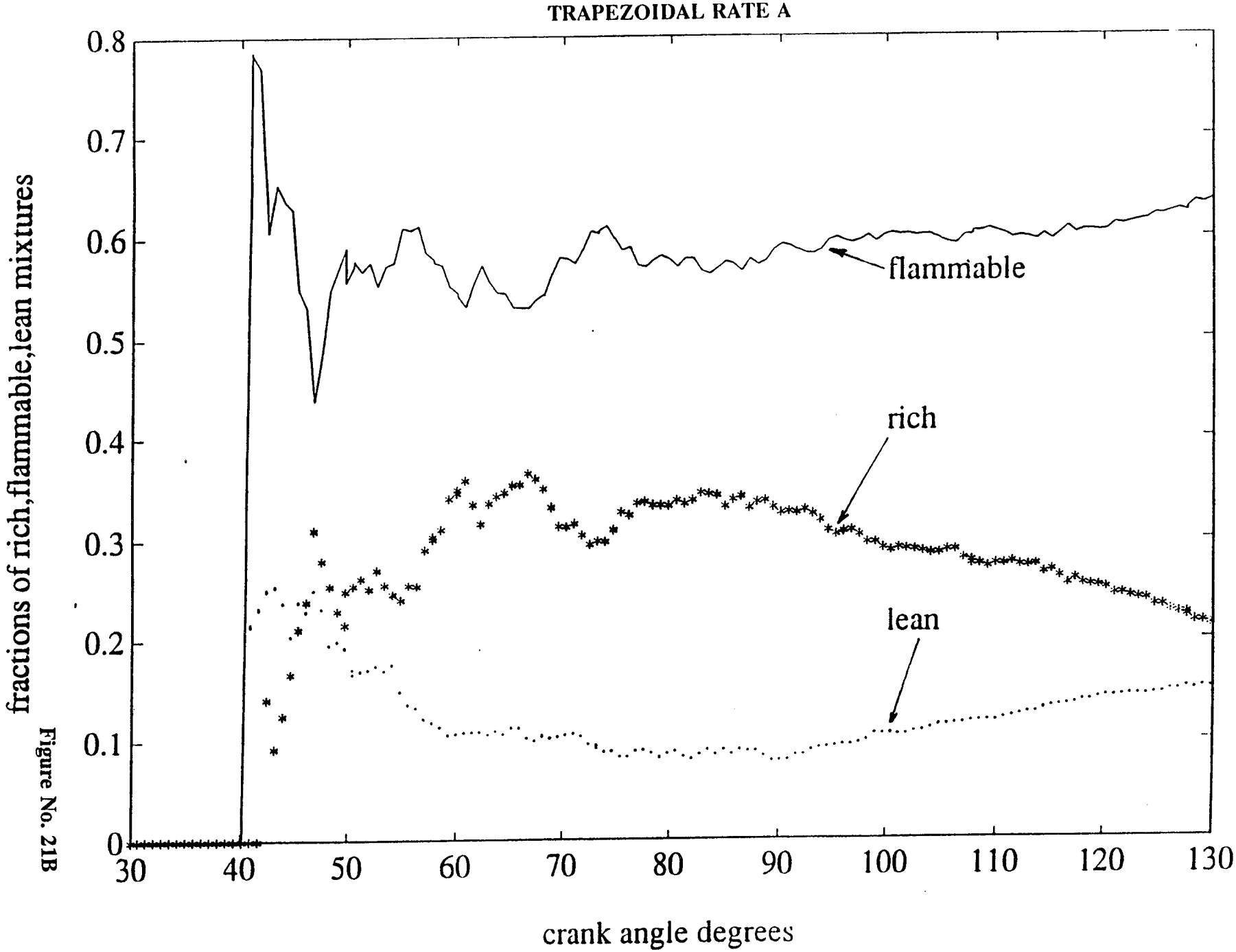


Figure No. 21B

Computed fractions of rich, flammable and lean mixtures in the combustion chamber as a function of crank angle degrees for rate 'A'

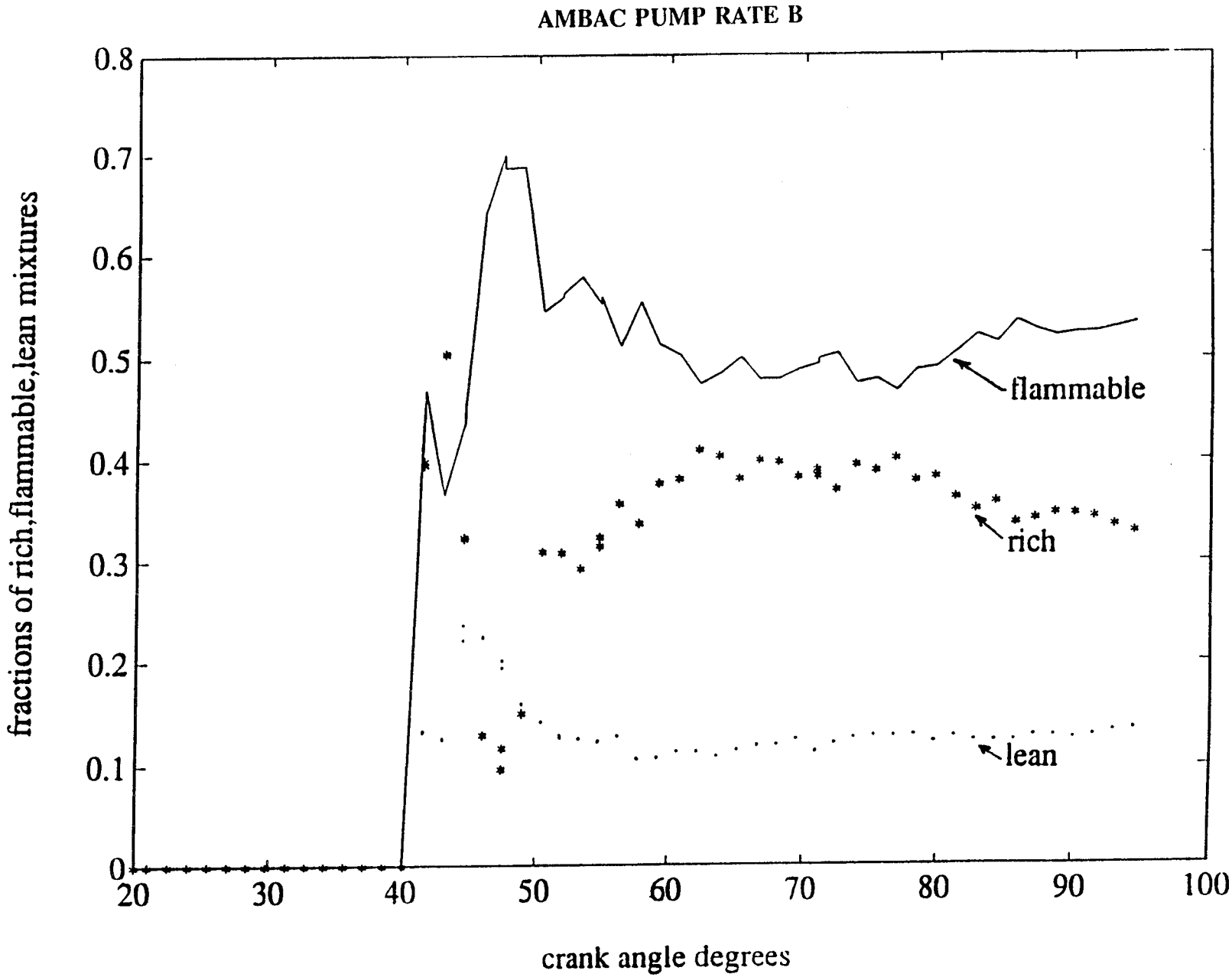


Figure No. 21C

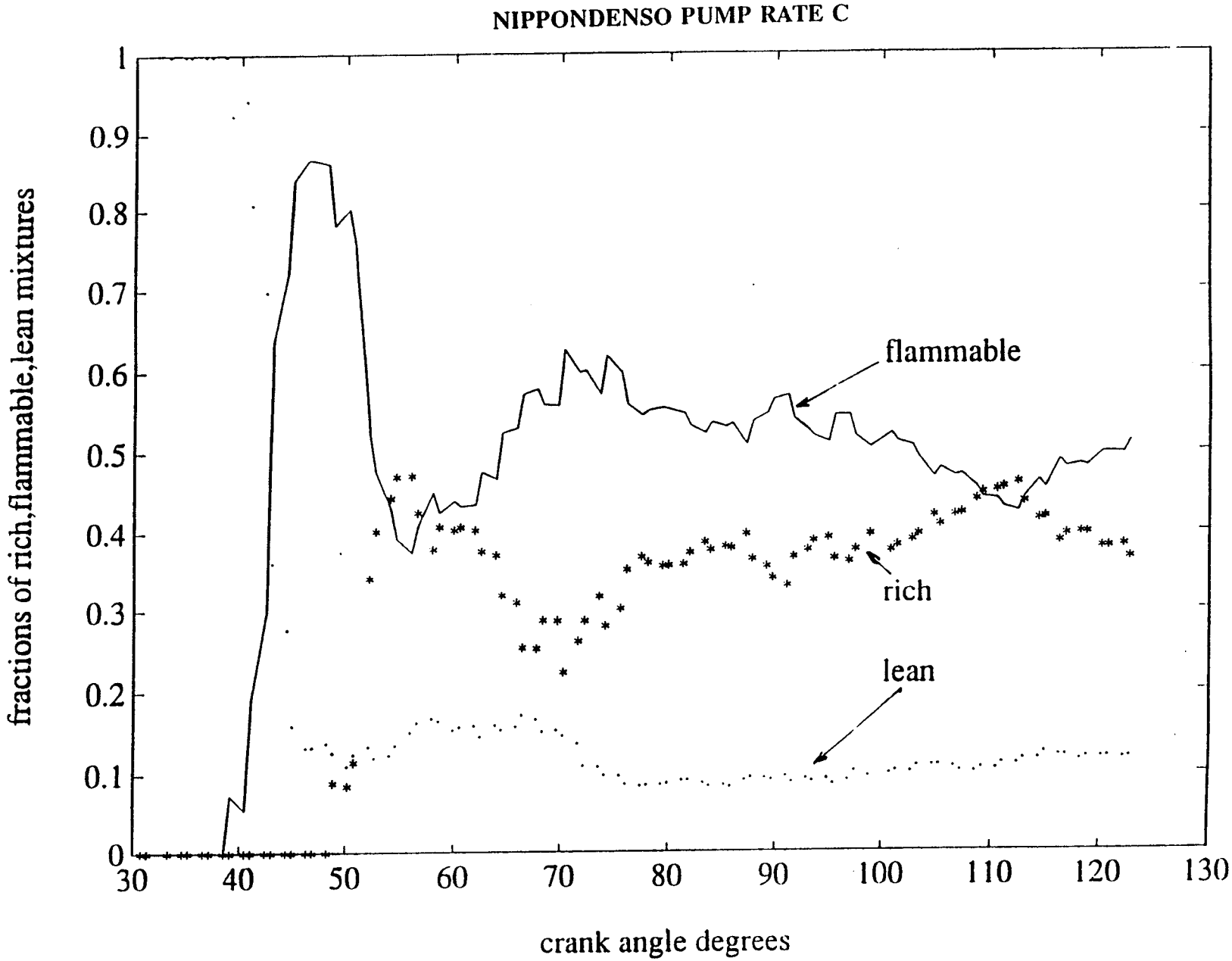


Figure No. 21D

Computed fractions of rich, flammable and lean mixtures in the combustion chamber as a function of crank angle degrees for rate 'C'

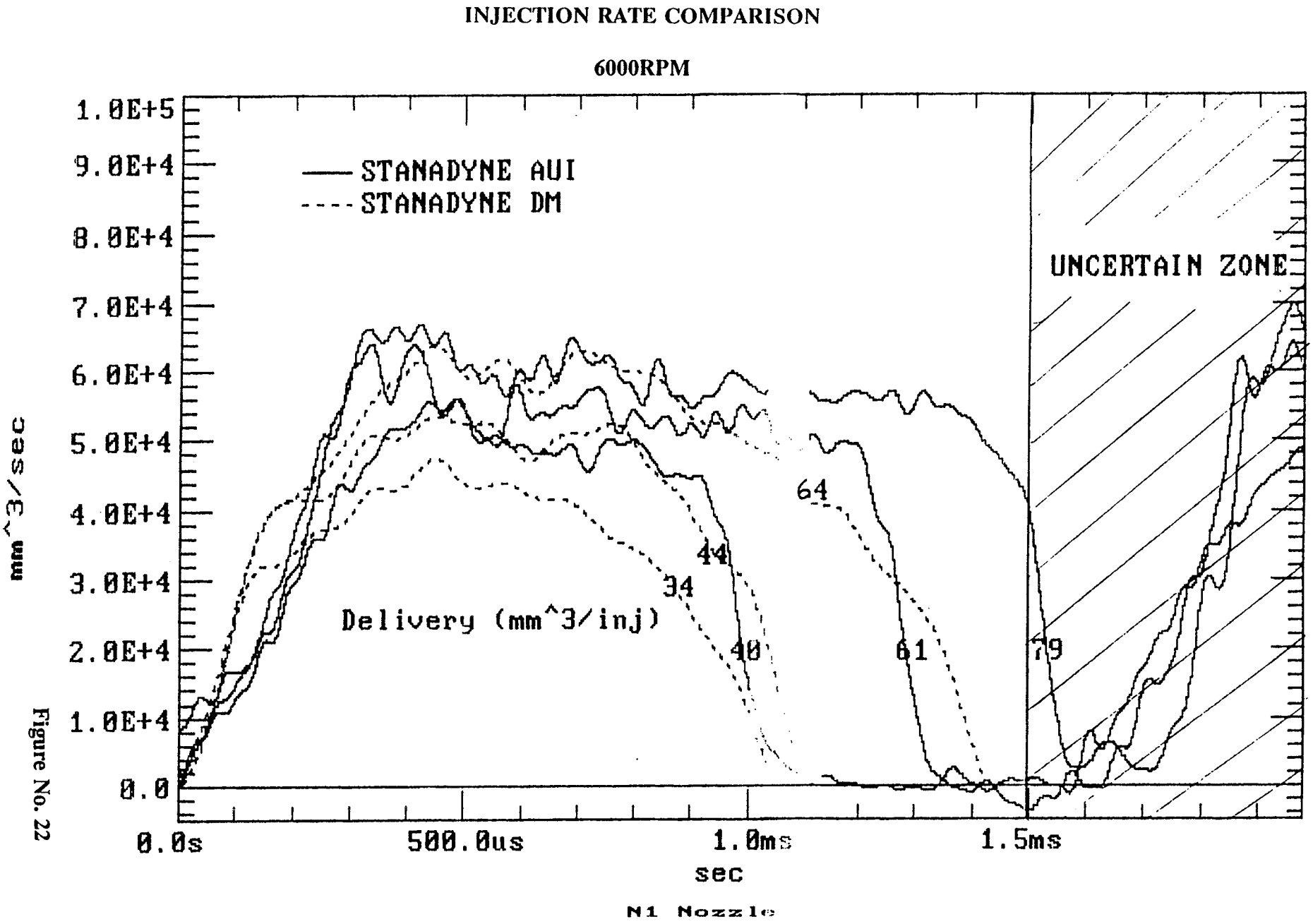

INJECTION RATE COMPARISON
6000RPM
STANADYNE AUI
STANADYNE DM
UNCERTAIN ZONE
Delivery (mm^3/inj)
64
44
34
40
61
79
1.0E+5
9.0E+4
8.0E+4
7.0E+4
6.0E+4
5.0E+4
4.0E+4
3.0E+4
2.0E+4
1.0E+4
0.0
mm^3/sec
0.0s
500.0us
1.0ms
1.5ms
sec
N1 Nozzle

Figure No. 22

COMPARISON OF A-PUMP AND DM-PUMP INJECTION RATES

6000RPM

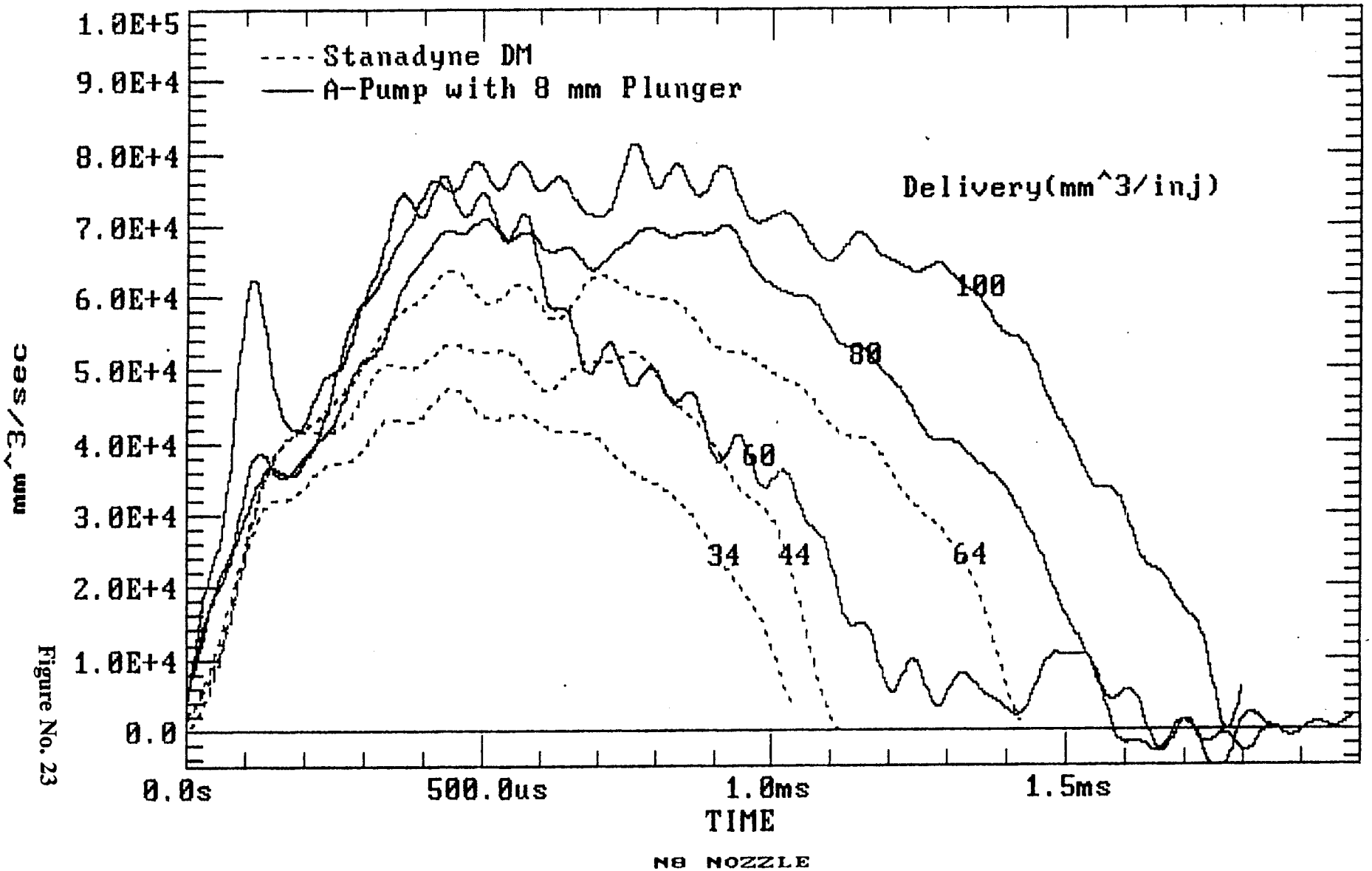


Figure No. 23

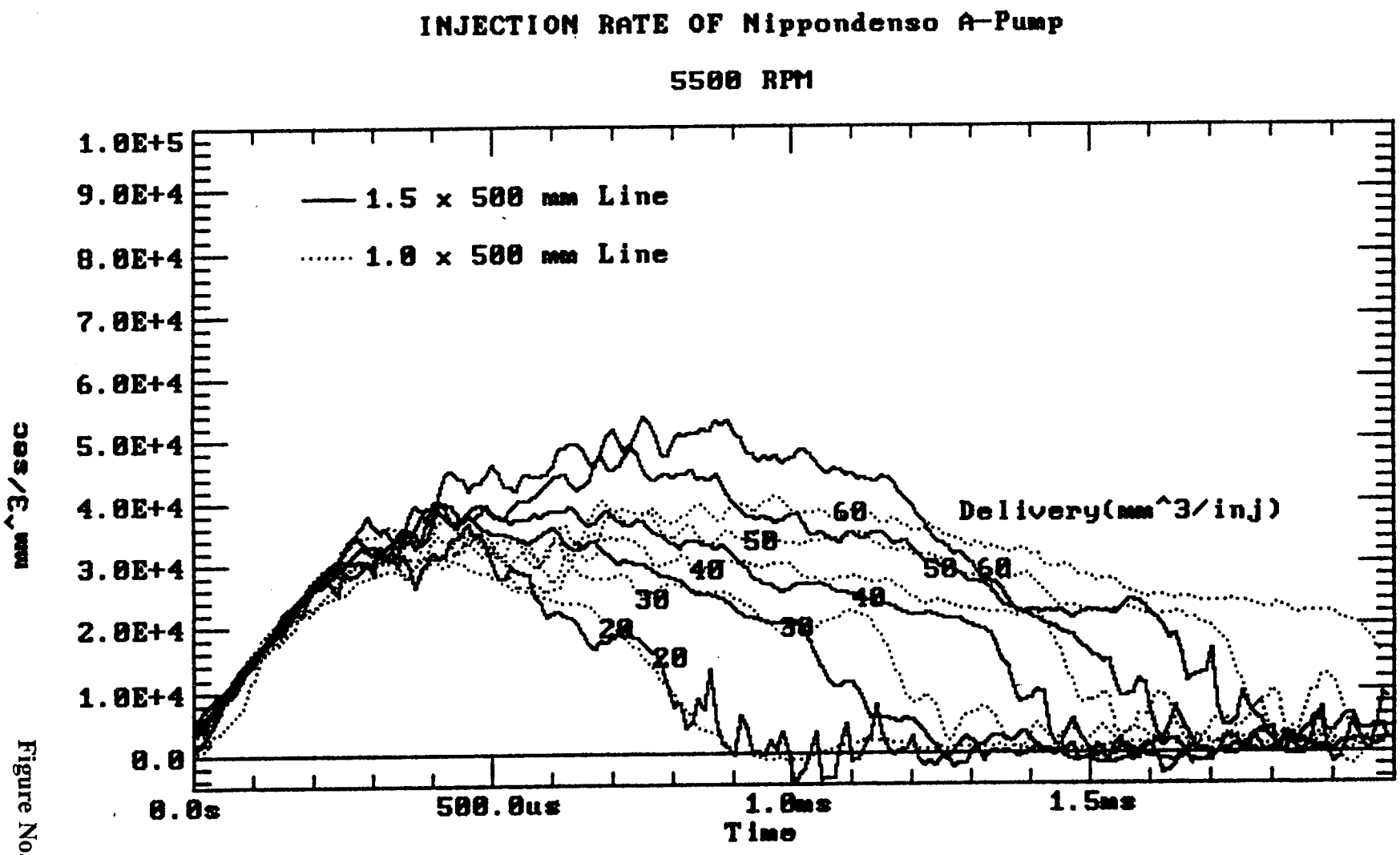
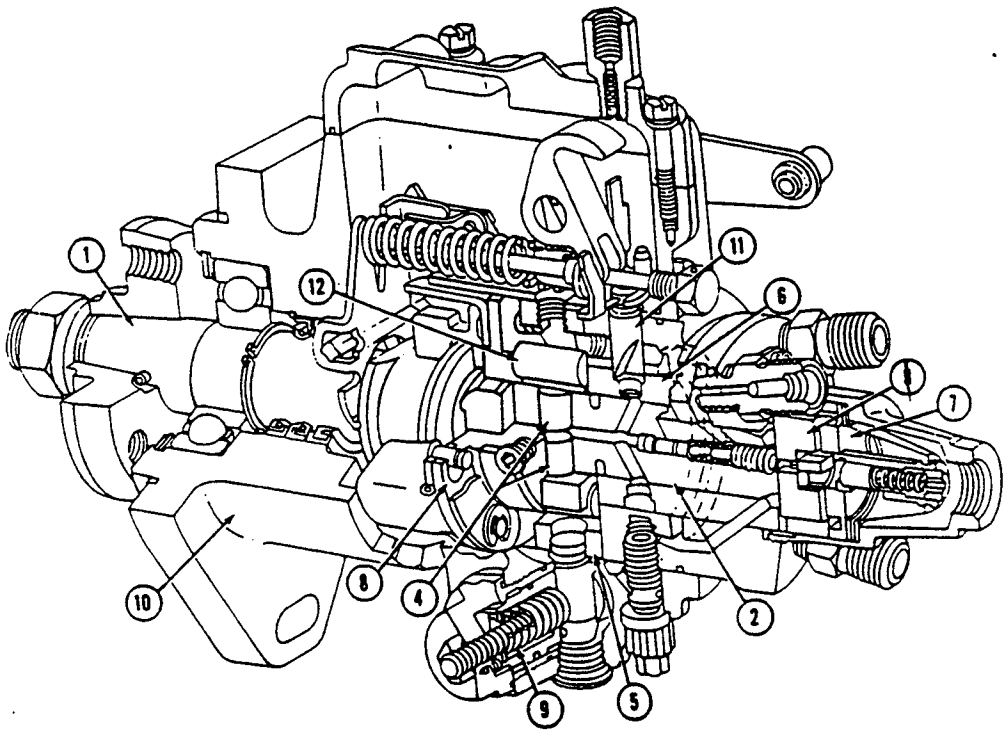
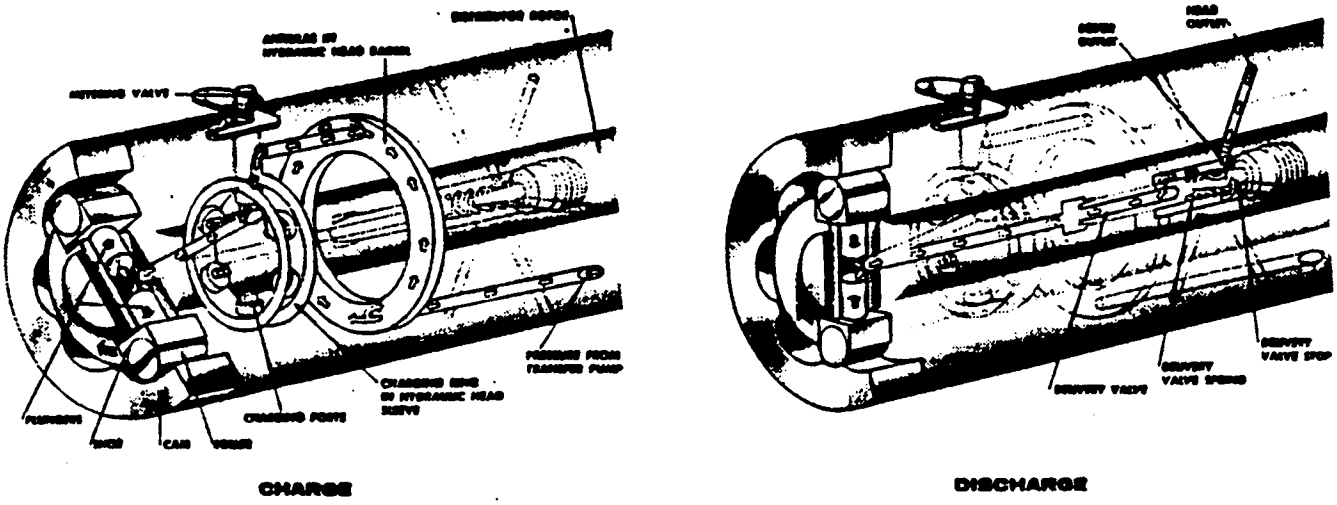

INJECTION RATE OF Nippondenso A-Pump
5500 RPM
1.0E+5
9.0E+4
8.0E+4
7.0E+4
6.0E+4
5.0E+4
4.0E+4
3.0E+4
2.0E+4
1.0E+4
0.0
mm^3/sec
1.5 x 500 mm Line
1.0 x 500 mm Line
Delivery(mm^3/inj)
60
50
40
30
20
0.0s
500.0us
1.0ms
1.5ms
Time
4 x .009 NOZZLE
7.5 mm PLUNGER, 5-290 DELIVERY VALVE

Figure No. 24

10000 INJECTIONS/MINUTE





Stanadyne DM Fuel Injection Pump

Figure No. 25

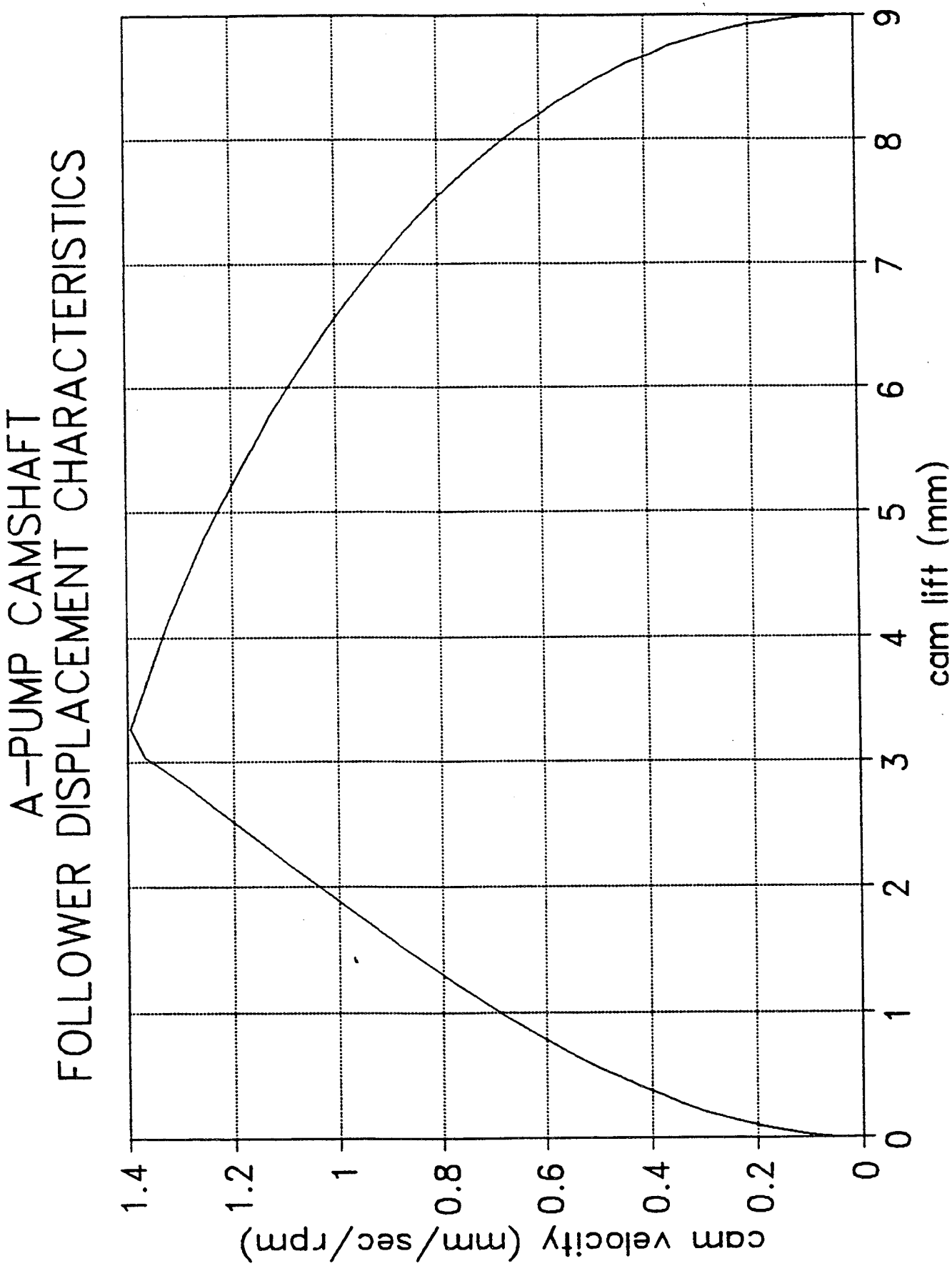

A-PUMP CAMSHAFT
FOLLOWER DISPLACEMENT CHARACTERISTICS
cam velocity (mm/sec/rpm)
1.4
1.2
1
0.8
0.6
0.4
0.2
0
cam lift (mm)
0
1
2
3
4
5
6
7
8
9

Figure No. 26

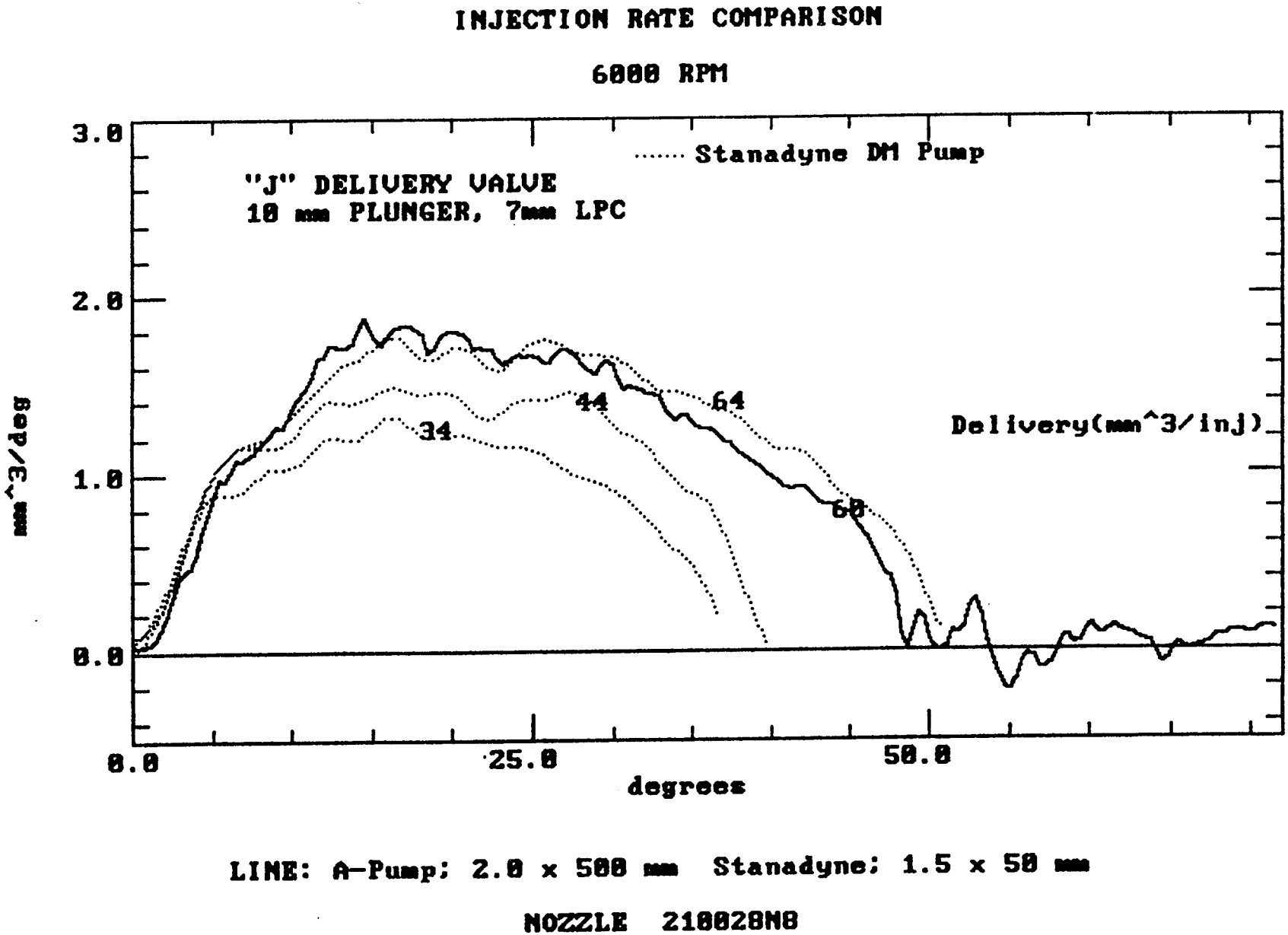

INJECTION RATE COMPARISON
6000 RPM
Stanadyne DM Pump
"J" DELIVERY VALVE
10 mm PLUNGER, 7mm LPC
3.0
2.0
1.0
0.0
mm^3/deg
34
44
64
60
Delivery(mm^3/inj)
0.0
25.0
50.0
degrees
LINE: A-Pump: 2.0 x 500 mm Stanadyne: 1.5 x 50 mm
NOZZLE 210028N8

Figure No. 27

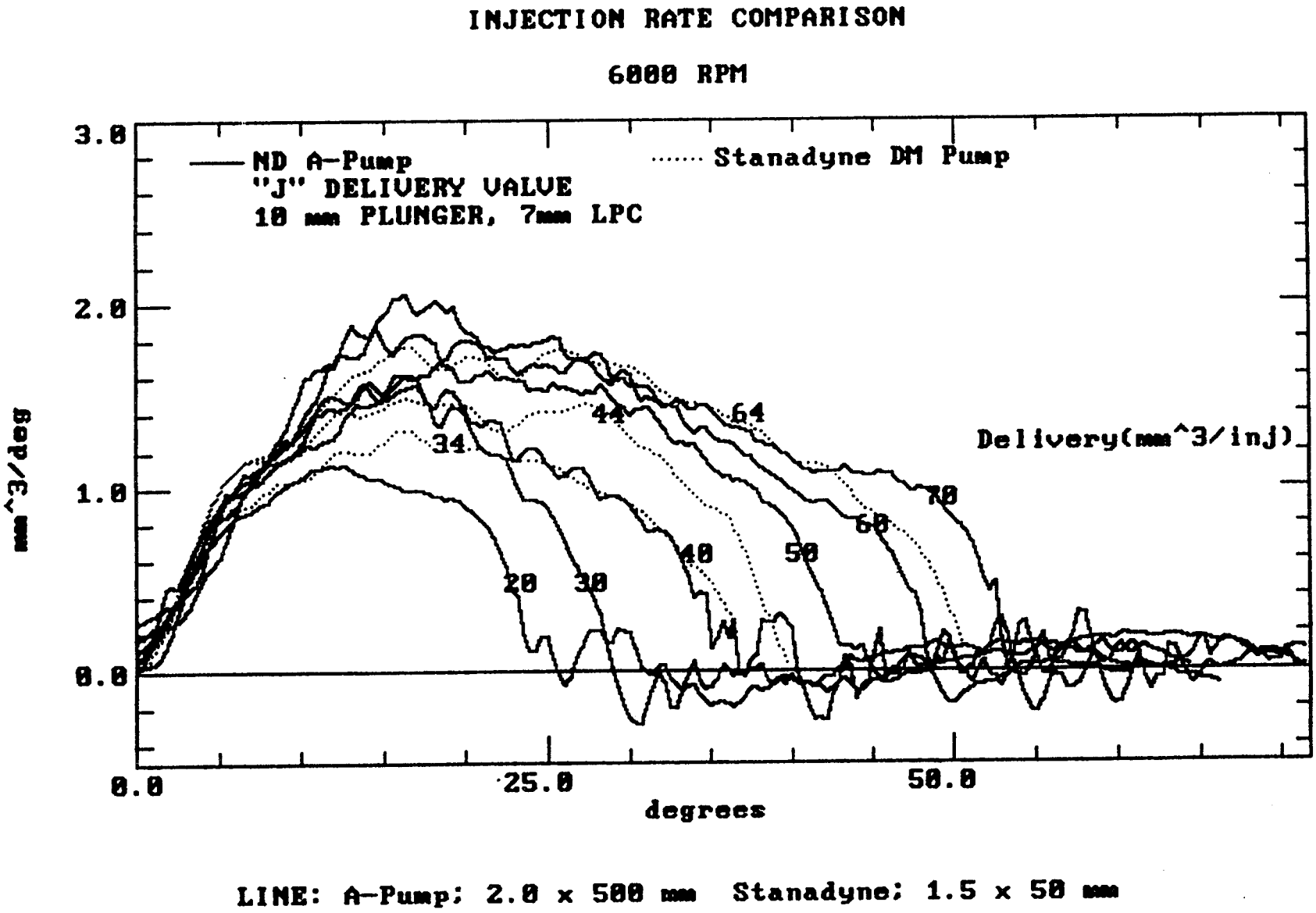

INJECTION RATE COMPARISON
6000 RPM
ND A-Pump
"J" DELIVERY VALVE
10 mm PLUNGER, 7mm LPC
Stanadyne DM Pump
Delivery(mm^3/inj)
20
30
34
40
44
50
60
64
70
3.0
2.0
1.0
0.0
mm^3/deg
0.0
25.0
50.0
degrees
LINE: A-Pump: 2.0 x 500 mm Stanadyne: 1.5 x 50 mm
NOZZLE 210028N8

Figure No. 28

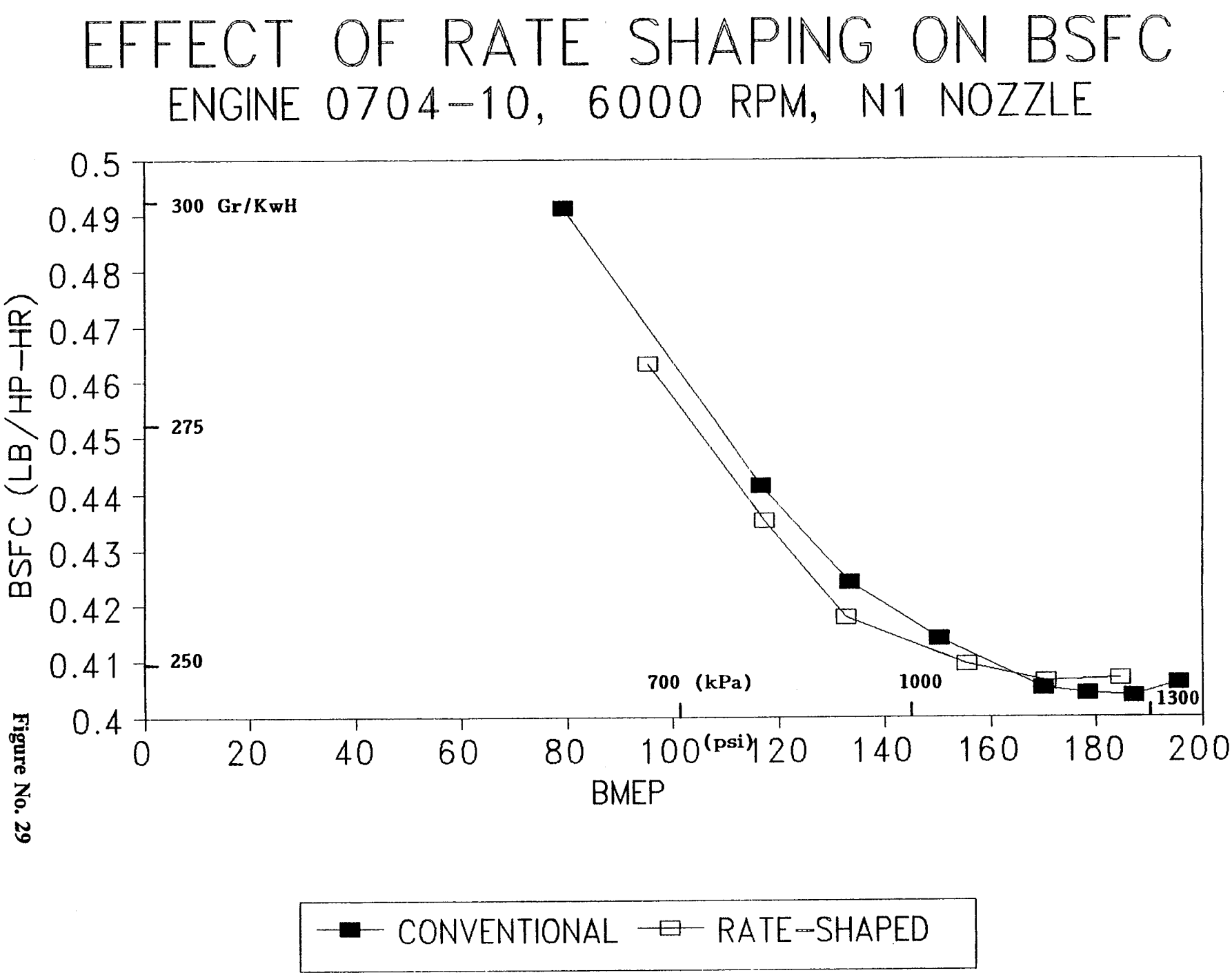

EFFECT OF RATE SHAPING ON BSFC
ENGINE 0704-10, 6000 RPM, N1 NOZZLE
BSFC (LB/HP-HR)
0.5
0.49
0.48
0.47
0.46
0.45
0.44
0.43
0.42
0.41
0.4
300 Gr/KwH
275
250
0
20
40
60
80
100
120
140
160
180
200
700 (kPa)
1000
1300
(psi)
BMEP
CONVENTIONAL
RATE-SHAPED

Figure No. 29

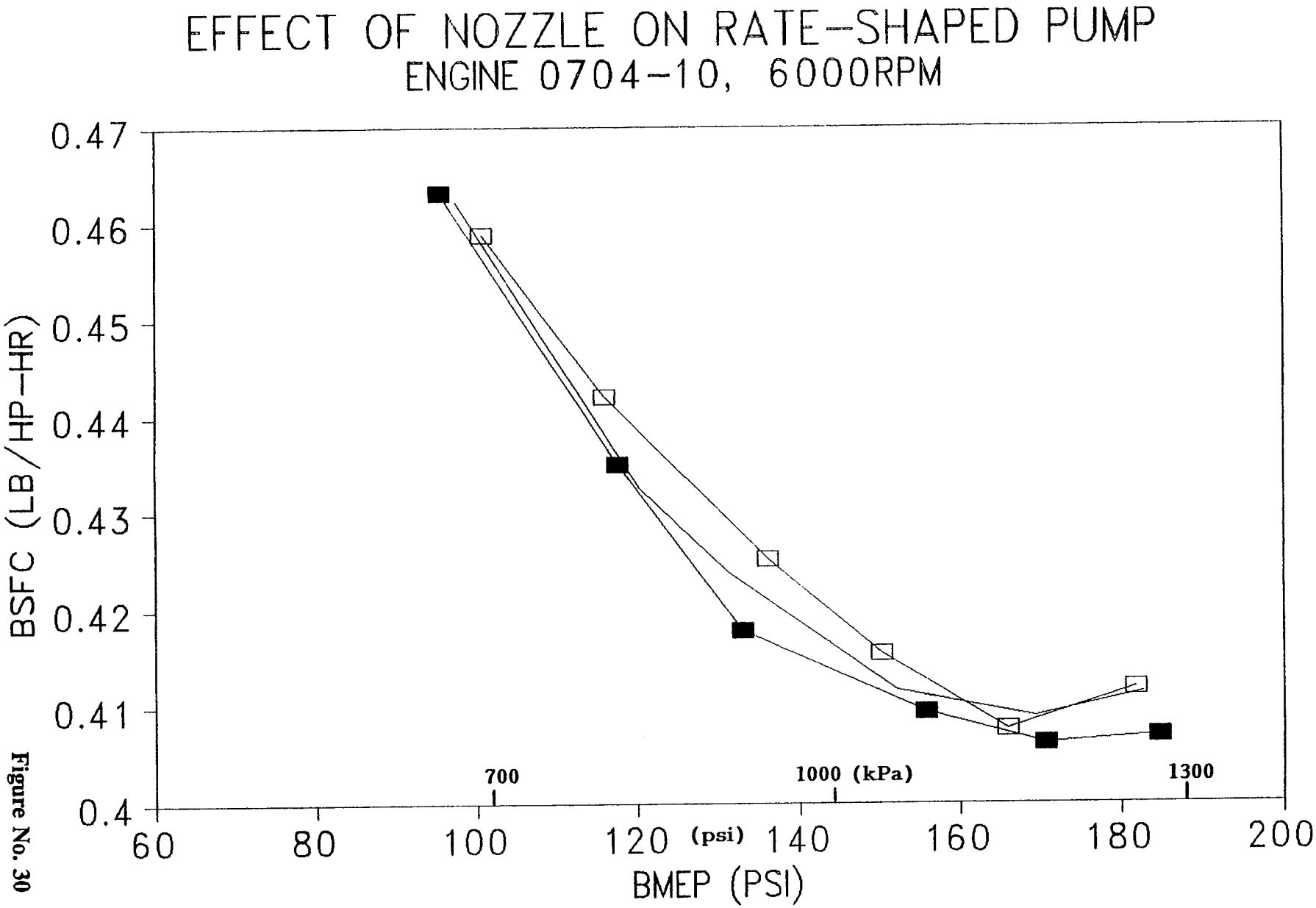

EFFECT OF NOZZLE ON RATE-SHAPED PUMP
ENGINE 0704-10, 6000RPM
BSFC (LB/HP-HR)
0.47
0.46
0.45
0.44
0.43
0.42
0.41
0.4
60
80
100
120
140
160
180
200
BMEP (PSI)
700
1000 (kPa)
1300
(psi)

Figure No. 30

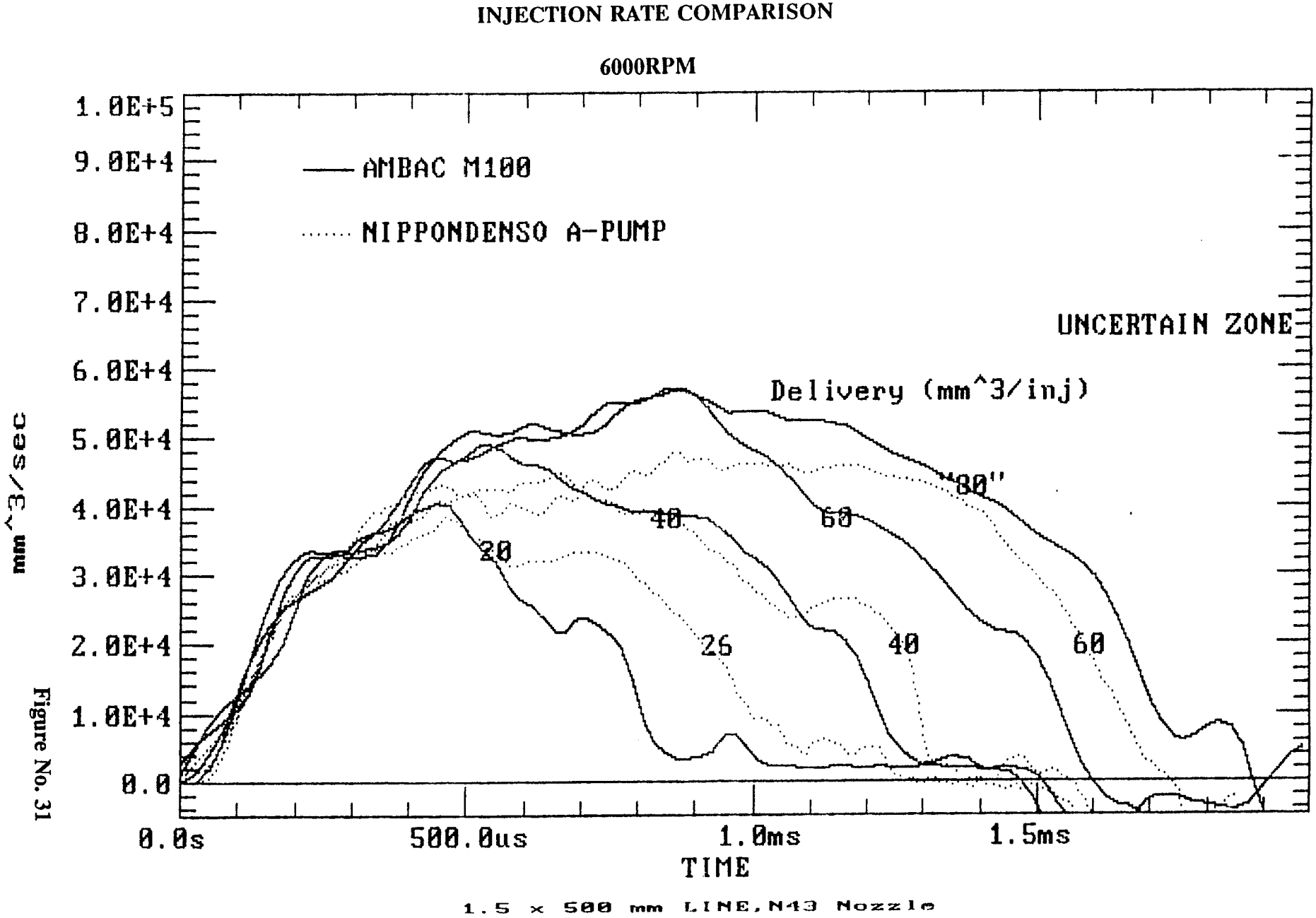

INJECTION RATE COMPARISON
6000RPM
AMBAC M100
NIPPONDENSO A-PUMP
UNCERTAIN ZONE
Delivery (mm^3/inj)
mm^3/sec
TIME
1.0E+5
9.0E+4
8.0E+4
7.0E+4
6.0E+4
5.0E+4
4.0E+4
3.0E+4
2.0E+4
1.0E+4
0.0
0.0s
500.0us
1.0ms
1.5ms
80"
60
40
20
60
40
26
1.5 x 500 mm LINE,N43 Nozzle

Figure No. 31